A STUDY OF THE SEISMIC STRUCTURE OF UPPER OCEANIC CRUST USING WIDE-ANGLE REFLECTIONS

by

Kristin Marie Michener Rohr

B.A., Brown University
(1977)

SUBMITTED IN PARTIAL FULFILLMENT
OF THE REQUIREMENTS FOR THE DEGREE OF
DOCTOR OF PHILOSOPHY

at the

MASSACHUSETTS INSTITUTE OF TECHNOLOGY
and the
WOODS HOLE OCEANOGRAPHIC INSTITUTION

January, 1983

Signature of Author.....
Department of Earth and Planetary Sciences, Massachusetts Institute of Technology and the Joint Program in Oceanography, Massachusetts Institute of Technology/Woods Hole Oceanographic Institution, January, 1983.

Certified by.....
Thesis Supervisor

Accepted by.....
Chairman, Joint Committee for Marine Geology and Geophysics, Massachusetts Institute of Technology / Woods Hole Oceanographic Institution

A STUDY OF THE SEISMIC STRUCTURE OF UPPER OCEANIC CRUST USING WIDE-ANGLE REFLECTIONS

by

Kristin Marie Michener Rohr
Submitted to the Department of Earth and Planetary Sciences,
Massachusetts Institute of Technology
and
the Department of Geology and Geophysics,
Woods Hole Oceanographic Institution
on January 21, 1983,
in partial fulfillment of the requirements
for the degree of Doctor of Philosophy.

ABSTRACT

The lateral homogeneity of oceanic crust on the scale of a seismic experiment is a condition that most methods of seismic interpretation depend on. Whether this condition is in fact true is largely unknown and only recently have efforts been made to test this hypothesis. This thesis is part of that effort and is focussed on determining with as much resolution as possible the seismic structure of upper oceanic crust, i.e. Layer 1 and the uppermost part of Layer 2. This portion of the crust is of interest, because of the effect of the sediment-basement interface on the transmission and conversion of seismic energy, also because of the possibility of detecting lateral heterogeneities in upper Layer 2 caused by faulting, hydrothermal circulation etc. The data employed are a set of wide-angle reflections from oceanic crust 130 m.y. old in the western North Atlantic Ocean southwest of Bermuda. First, the sedimentary structure is determined by stacking the data along hyperbolae and interpreting the stacking velocities and two-way normal incidence travel-times for interval velocities. This method has not been applied to deep sea marine data before; it gives a more detailed velocity structure of the sediments than does a traditional study of the basement reflections' travel-times. Second, the same data are mapped into tau-p space in order to measure the velocity gradient in oceanic basement; unfortunately the scatter in the tau-p picks caused by the topography of the basement reflector combine with the properties of the tau-sum inversion to make such a measurement impossible. Third, the amplitudes of the basement reflections observed on three seismic lines are modelled by synthetic seismograms; each can be matched by velocity-depth models which contain a transition zone between the sediments and the basement. The different thicknesses of this transition zone near the three receivers is an indication that the top few hundred meters of Layer 2 are laterally heterogeneous on a scale of 3 to 8 km.

ACKNOWLEDGEMENTS

This work was supported by NSF Grant OCE-7909464 and partial support was supplied by a fellowship from the Phillips Petroleum Foundation.

I would like to present my thanks in chronological order:

First of all thanks are due to my mother who wouldn't let me use coloring books, but insisted that I draw my own pictures, and to my father who gave me a telescope for Christmas twenty years ago after I'd expressed an interest in astronomy.

My most inspired teacher has to be Mrs. Mickey Wright; she has a respect for the scientific method and never fails to have fun with it. It was in a term project for her earth sciences class in 1968 that I first came across the wonders of plate tectonics.

My thanks are extended to the entire Brown Geological Sciences Department who gave me a thorough education in the earth sciences, especially Dr.s Chapple, Imbrie and Forsythe.

In W.H.O.I.'s Summer Student Fellow program I worked with my present advisor, G.M. Purdy, on some refraction data and fell for the bait; i.e. I applied to the Joint Program the following semester.

Many have helped in my tenure here; let me count the ways.

First and foremost is G.M. Purdy without whose organisational expertise the data would never have been collected, and whose criticism has always been useful. His example will always be remembered.

Thanks are due to the trusty VAX 11/780 and HP 2100 that

patiently performed hour after hour of tedious processing. M.D. Allison and L. Gove helped when either I or the system balked at a particular task. I might have been better off had I followed M.D.A.'s example in ranting and raving and L.G.'s example in being laid-back. D.Dubois (better known as DOMDD) provided much assistance negotiating the processing.

H. Schouten has long been a friend and scientific critic. Through him I enjoyed a tour on a Dutch research/cruise vessel, as well as numerous superb potluck suppers; his help as a committee member is appreciated.

C. Denham has also been a friend and shown an interest in my work; his ability to always have time to listen is rare.

R.A. Stephen has provided discussions on various aspects of theoretical seismology, and constructive remarks on my writing.

J.I. Ewing has provided guidance through the years and especially as a committe member, his encouragement has meant much.

E.T. Bunce was the first person I met at W.H.O.I., she tried to steer me away from reflection work to refraction, but in the long run, it didn't work. She has been most encouraging, especially as my thesis committee chairman.

S. Solomon and W.B. Bryan have been long suffering and patient by serving on both my general exam and thesis committees; they have given valuable time and thought towards my efforts.

Jake, Abbie, Dixie, and Connie have been kind and patient all the times I registered late, lost my waiver, and most recently when

I forgot my thesis title.

The guards at W.H.O.I. have always had cheerful words on Sunday afternoons when I was not.

The following people and things have contributed to my sanity and insanity over the last few years: Robert J., the Black Duck, the Market Bookshop, E. Costello, the Nickelodeon, and the Village Voice. Without the following friends life would not have been the same: M.L. Bremer, L.Tear, R. Jaffe, A. Eisen, J. Traschen, L. Rohr, D. Faibes, S. and A. Swift, L. Shure, S. Pfirman, P. Speer and all the J. P. students.

The place of honor, the last mention, is for J.A. Collins; he has put up with everything. Even more amazing he is still smiling. It may be a cliche, but without him, this thesis would not have been finished.

TABLE OF CONTENTS

Chapter 1

Introduction

Methods of interpreting the seismic structure of oceanic Layers 1 and 2 (Raitt, 1963) from wide-angle reflections are investigated in detail in this thesis. As technical and tectonic knowledge have increased, seismic experiments of increasing resolution and sophistication have been performed in order to investigate the structure and evolution of oceanic crust. The travel times of wide-angle reflections recorded on sonobuoys have been used extensively in the investigation of the velocity structure of Layer 1, yet in many regions our knowledge of the sediments' velocity structure is limited to an average value of their velocities (Houtz, 1980). In chapter 2 an analytic technique (Taner and Koehler, 1969) widely and successfully used on multi-channel data collected on continental shelves is adapted to data collected by an ocean-bottom hydrophone in the deep sea in order to resolve the velocity structure within Layer 1. Another question being addressed in marine seismology is the scale of lateral homogeneity of oceanic crust (Purdy, 1982). Lateral heterogeneity of the uppermost Layer 2 on the scale of a few km is examined by interpreting wide-angle reflections from the sediment-basement interface. In chapter 3 the reflections are mapped into tau-p space in order to interpret the velocity gradient in Layer 2. In chapter 4 the amplitudes of basement reflections are modelled in order to interpet the velocity structure of the sediment-basement interface.

An aim of seismic studies is to investigate the seismic velocity structure of the earth. The end result of many studies is a

velocity-depth function which characterises the earth or a specific region of the earth, and an interpretation of this structure's relation to geophysical or geological data and processes. The methods of interpreting velocity structures from seismic data vary; most involve the travel-times of seismic waves (Kennett, 1977), and more recently their amplitudes have been used (Helmberger and Morris, 1970). In any case, some understanding or physical model of how energy propagates through the earth must exist in order to model or invert seismic data. Additionally, one must be able to implement these models mathematically and numerically. Many geologic structures are so complicated that either adequate physical models do not exist or we do not yet have the ability to implement them.

While geologists and geophysicists have been studying the structure of continental crust for at least one hundred years, the structure of oceanic crust has only been studied in the last few decades and is comparatively poorly known. Technological advances coupled with military interest in the ocean basins led to many marine seismic refraction experiments being performed in the 1950's (e.g. Ewing et al., 1952; Katz and Ewing, 1956; Hersey et al., 1959). Large shot spacing and the interpretation of the travel-times in terms of homogeneous layers resulted in a view of oceanic crust which seemed to be uniform in all ocean basins (Raitt, 1964). Four layers were discerned; the highest standard deviation of the velocities occur in Layer 2. In the 1960's widespread use of disposable sonobuoys (Houtz, Ewing and LePichon, 1968) led to

increased detail measured in the structure of Layer 1; these interpretations were based on the travel-times of wide-angle reflections from reflectors within Layer 1 and the top of Layer 2.

Since the formulation of the plate tectonics paradigm for the earth sciences, studies of oceanic crust have largely been directed towards investigating the implications of plate tectonics. Experiments to determine the structure of plate boundaries, how crust ages once it has been formed and whether the spreading center creates crust of uniform structure both in time and space have all been carried out in the past few decades. Once a map (Fig. 1.1) of the age of oceanic crust and its present and fossil plate boundaries had been constructed, it became apparent that the seismic refraction experiments of the 1950's had been performed at random with respect to age and direction of structure and over several features which plate tectonics predicts should have different structures. Thus our picture of oceanic crustal structure is highly generalised and averaged.

Seismic experiments with increasing resolution are now being carried out. The four layer model of oceanic crust has been subdivided into many more layers (Houtz and Ewing, 1976) and the ability to model the amplitudes of seismic arrivals has resulted in a model of oceanic crust based on velocity gradients rather than single velocity layers. The question of lateral heterogeneity, however, remains unresolved. The scale of these heterogeneities may

occur over a thousand kilometers as in the aging of Layer 2 (Houtz and Ewing, 1976) and may well occur over the space of a few km (Spudich and Orcutt, 1980; Purdy and Rohr, 1979). This latter scale is important in the interpretation of seismic data since most inversion and modelling methods assume that the oceanic crust covered by the experiment is homogeneous. The difficulty in measuring heterogeneities, if they exist, lies in the resolution of the seismic energy (wavelengths used are typically 0.5 to 1.0 km) and the lack of ablilty to model waves travelling through heterogeneous media.

Other developments in seismology include the examination of the data in spaces other than the time-distance space. Seismic data have been mapped into amplitude-frequency space (Dorman et al., 1960), stacking velocity-two-way normal incidence travel-time space (Taner and Koehler, 1969) and tau-p space (Stoffa et al., 1980) for additional insights into the velocity structure through which the seismic energy has travelled.

*

This thesis is part of an experiment designed to measure the lateral homogeneity of oceanic crust formed at a spreading center. Here the focus is on the resolution of the structure of upper oceanic crust, Layers 1 and 2. Measurements of deeper crust are limited by knowledge of the structure of the crust that lies above it; variability in the amplitides or travel-times of refractions from Layer 3 or Moho could be caused by variability in the structure

of Layer 1 or Layer 2. The experiment was carefully located south of a fracture zone on crust ~140 my old (Fig. 1.1) which had been formed during an episode of constant velocity spreading at ~1.0 cm/yr (Schouten and Klitgord, 1982). Eight ocean-bottom hydrophones were deployed in a 10 x 15 km cross-shaped pattern and a variety of seismic experiments were performed (Purdy, 1982b). In each of the three following chapters the wide-angle reflections produced by a 0.66L (40 in^3) airgun are interpreted by different methods, and these methods' properties and ability to resolve seismic structure are discussed.

In the second chapter the structure of Layer 1 is resolved by mapping wide-angle reflections from sedimentary reflectors and the sediment-basement interface into stacking velocity-two way normal incidence travel-time. Working in this domain has been of great help to exploration seismologists interpreting data from continental shelves, but has not previously been used to investigate the velocity structure of deep-sea sediments. Here, instead of using just the semblance function, the stack and semblance functions are combined in the manner suggested by Stoffa et al. (1980) for mapping data into tau-p space. In this region sonobuoy studies (Houtz, 1980) have measured an average velocity of sound in the sediments but have not been able to resolve the seismic structure associated with reflectors A^c, A* and Beta. These reflectors are observed on the normal incidence seismic reflection records (Tucholke, 1981) and elsewhere are associated with increases in seismic velocity (Houtz,

LePichon, and Ewing, 1968).

In the third chapter the data are mapped into tau-p space (Stoffa et al., 1980) in order to measure the velocity gradient in the uppermost Layer 2. Here, the mapping is designed to preserve the amplitude of the stack in the most coherent subarray in the final tau-p map so that postcritical events can be distinguished from precritical events. In tau-p space one can distinguish seismic arrivals reflecting off a sharp velocity discontinuity from arrivals which have turned in a velocity gradient by the positive curvature of the former and the negative curvature of the latter. Once the arrivals have been identified, they can be inverted for a velocity-depth function.

Chapter 4 investigates the structure of the uppermost Layer 2 by modelling the amplitudes of reflections from the sediment-basement interface. Igneous crust (Layers 2 and 3) is most often interpreted from seismic refractions; unfortunately refractions from the uppermost Layer 2 are rarely observed except by instruments, such as borehole seismometers (Stephen, 1980), located within or below this structure. Earlier arrivals tend to interfere with the first refracted arrivals (Stephen, 1982). Alternatively, the velocity structure in the uppermost Layer 2 can be inferred from refractions which have passed through it deeper into the crust (Ewing and Purdy, 1982). Wide-angle reflections from the interface between Layer 1 and 2 respond to structure approximately a wavelength in scale at

the interface and hence are a direct measurement of the velocity structure in the top few hundred meters of Layer 2.

Figure 1.1 Location of seismic refraction experiments carried out before 1970 plotted on schematic map of magnetic anomalies (after Shouten and Klitgord, (1977). Articles describing the experiments are Ewing et al., 1952; Officer et al, 1952; Katz and Ewing, 1956; Ewing and Ewing, 1959; Hersey et al., 1959; Houtz and Ewing, 1963; Houtz and Ewing, 1964; Sheridan et al., 1966. Small black box indicates the location of the experiment discussed here.

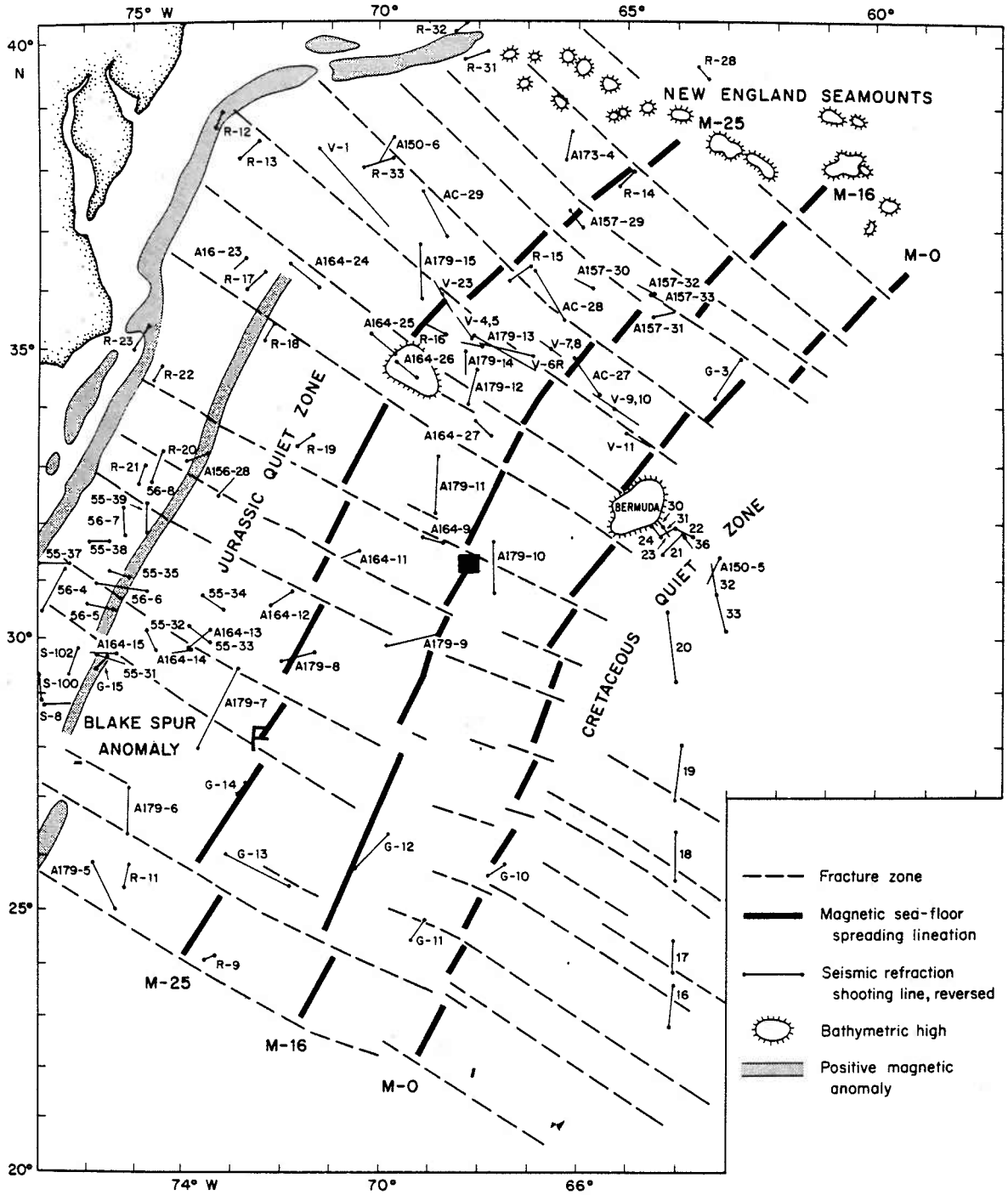
75° W
70°
65°
60°
40° N
35°
30°
25°
20°
74° W
70°
66°
NEW ENGLAND SEAMOUNTS
M-25
M-16
M-0
JURASSIC QUIET ZONE
CRETACEOUS QUIET ZONE
BERMUDA
BLAKE SPUR ANOMALY
Fracture zone
Magnetic sea-floor spreading lineation
Seismic refraction shooting line, reversed
Bathymetric high
Positive magnetic anomaly

BIBLIOGRAPHY

Dorman, J., J. Ewing and J. Oliver, Study of shear-velocity distribution in the upper mantle by mantle Raleigh waves, Bull. Seism. Soc. Amer., 50, 87-115, 1960.

Ewing, M. and J. Ewing, Seismic refraction measurements in the Atlantic Ocean basins, in the Mediterranean Sea, on the Mid-Atlantic Ridge, and in the Norwegian Sea, Geol. Soc. Amer. Bull., 70, 291-318, 1959.

Ewing, J.I. and G.M. Purdy, Upper crustal velocity structure in the ROSE area of the East Pacific Rise, J. Geophys. Res., 87, 8397-8402, 1982.

Helmberger, D.V. and G.B. Morris, A travel time and amplitude interpretation of a marine refraction profile: Transformed shear waves, Bull. Seism. Soc. Am., 60, 593-611, 1970.

Hersey, J.B., E.T. Bunce, R.F. Wyrick, and F.T. Dietz, Geophysical investigation of the continental margin between Cape Henry, Virginia, and Jacksonville, Florida, Geol. Soc. Am. Bull., 70, 437-466, 1959.

Houtz, R. E., Comparison of velocity characteristics in western North Atlantic and Norwegian Sea sediments, J. Acoust. Soc. Amer., 68, 1409-1414, 1980.

Houtz, R. E., J. Ewing, and X. LePichon, Velocity of Deep Sea Sediments from Sonobuoy Data, J. Geophys. Res., 73, 2615-2641, 1968.

Houtz, R. E. and J. Ewing, Detailed sedimentary velocities of the western North Atlantic Margin, J. Geophys. Res., 68, 5235-5258,

1963.

Houtz, R.E. and J.I. Ewing, Sedimentary velocities of the western North Atlantic margin, Bull. Seism. Soc. Am., 54, 867-895, 1964.

Katz, S. and M. Ewing, Seismic refraction measurements in the Atlantic Ocean, 7, Bull. Seism. Soc. Amer., 67, 475-510, 1956.

Kennett, B.L.N., Towards a more detailed seismic picture of the oceanic crust and mantle, Mar. Geophys. Res., 3, 7-42, 1977.

Koelsch, D.E. and G.M. Purdy, An ocean bottom hydrophone instrument for seismic refraction experiments on the deep ocean, Mar. Geophys. Res., 4, 115-125, 1979.

Purdy, G.M., The variability in seismic structure of Layer 2 near the East Pacific Rise at 12^{o} N, J. Geophys. Res., 87, 8403-8416, 1982a.

Purdy, G.M., The seismic structure of 140 my old crust in the western central North Atlantic Ocean, subm. to Geophys. J. Roy. Astr. Soc., 1982.

Purdy, G.M. and K. Rohr, A geophysical survey within the Mesozoic magnetic anomaly sequence south of Bermuda, J. Geophys. Res., 84, 5487-5496, 1979.

Raitt, R.W., The crustal rocks, in M.N. Hill (ed.), The Sea, v.3, Interscience, N.Y., 1963.

Schouten, H. and K. Klitgord, Map showing Mesozoic magnetic anomalies, western North Atlantic, Map MF 915, U.S. Geol. Surv., Reston, VA., 1977.

Schouten, H. and K. Klitgord, The memory of the accreting plate boundary and the continuity of fracture zones, Earth and Plan. Sci. Lett., 59, 255-266, 1982.

Sheridan, R.E., C.L. Drake, J.E. Nafe and J. Hennion, Seismic refraction study of continental margin east of Florida, Bull. Am. Assoc. Petr. Geol., 50, 1927-1991, 1966.

Spudich, P.K.P. and D.V. Helmberger, Synthetic Seismograms from Model Ocean Bottoms, J. Geophys. Res., 84, 189-204, 1979.

Spudich P. and J. Orcutt, Petrology and porosity of an oceanic crustal site: results from wave form modelling of seismic refraction data, J. Geophys. Res., 85, 1409-1433, 1980a.

Stephen. R.A., K.E. Louden, and D.H. Matthews, The oblique seismic experiment on DSDP Leg 52, Geophys. J. Roy. Astr. Soc., 60, 289-300, 1980.

Stephen R.A., Travel-Time curves for a simple seafloor model, Mar. Geophys. Res., 5, 315-326, 1982.

Stoffa, P.L., P. Buhl, J.B. Diebold, and F. Wenzel, Direct mapping of seismic data to the domain of intercept time and ray parameter - a plane wave decomposition, Geophys., 46, 255-267, 1980.

Taner, M.T. and F. Koehler, Velocity Spectra - digital computer derivation and application of velocity functions, Geophys., 34, 859-881, 1969.

Tucholke, B.E., Geologic Significance of seismic reflectors in the deep western North Atlantic Ocean basin, SEPM Special Publication No. 32, 23-37, 1981.

Tucholke, B.E., Relation between acoustic stratigraphy and lithostratigraphy in the western North Atlantic Basin, in Tucholke, B.E., Vogt, P.R., et al., 1979, Initial Reports of the Deep Sea Drilling Project, v.43: Washington (U.S. Govt. Printing Office), p.827-846.

White, R.S., Oceanic upper crustal structure from variable angle seismic reflection-refraction profiles, Geophys. J. Roy. Astr. Soc., v.20, p.683-726, 1979.

CHAPTER 2

Hyperbolic Stacking of Wide-angle Reflections from Deep-Sea Sediments

K. Rohr

W.H.O.I.-M.I.T. Joint Program

W.H.O.I.

Woods Hole, Ma. 02543

Submitted to J. Geophys. Res. W.H.O.I. Contribution No. 5230

2.1 ABSTRACT

Wide-angle reflections from deep sea sediments were analysed by stacking along hyperbolae; the details in the sediment structure that are achieved here are greater than any that have previously been made with wide-angle reflections on the Bermuda Rise. A 40 in^3 airgun source was used in the western North Atlantic; the reflections were recorded with six ocean bottom hydrophones. The arrivals are stacked and semblance calculated along hyperbolic trajectories in T-X space and these two functions are multiplied together. This analysis allows an objective comparison of a large data set and an interpretation of the sediments' velocity structure. Events in the semblance x stack function can be correlated with normal incidence reflection data and are identified with the well known reflectors A^C, A*, β and acoustic basement. A low velocity event is observed after the basement arrival and is identified as shear reflections from acoustic basement. Compressional to shear conversion occurs at β implying a Poisson's ratio of 0.40 for sediments beneath β. The stacking velocity and two-way travel time values are easily picked from the semblance x stack functions and can be interpreted for a velocity-depth function by an iterative modelling scheme or inversion. The results for the four layers agree closely. The upper sediments are 1.72 km/s and 0.27 km thick, sediments below A^C are 2.00 km/s and 0.2 km thick, below A*, 2.52 km/s and 0.25 km thick and below β, 3.1 km/s and 0.13 km thick. These velocities agree with the velocimeter measurements

made nearby at DSDP Site 387 and interpretations of interval velocity taken on thicker sections of these units on older crust.

2.2 INTRODUCTION

An effort was made in April, 1980 to measure the degree of homogeneity of oceanic crust by deploying eight ocean-bottom hydrophones in a 10 x 15 km square in the North Atlantic Ocean (Fig. 1) and performing a variety of seismic experiments. This paper discusses the hyperbolic stacking of wide-angle reflections from the sediments and acoustic basement by a 40 in^3 airgun source (Fig. 6). This method of analysis is frequently applied to multi-channel data, but its ability to measure velocity as a function of depth has seldom been used in the study of deep-sea sediments.

The sediments' physical properties are of interest in their own right, and for their role in the propagation of seismic energy into the basaltic crust. The sediments affect not only the travel times of seismic signals from the crust, but can also prevent energy of different phase velocities from ever reaching the upper crust. This latter effect is particularly important in the conversion of compressional to shear energy (Spudich and Helmberger, 1979, White and Stephen, 1980). In the western North Atlantic consolidated limestones overlie the basaltic basement; the properties of these sediments could significantly affect the propagation of seismic energy into the crust.

Sediments in this area of the western North Atlantic Ocean, the

southern Bermuda Rise, generally are too thin to give reflections which can be easily analysed with a surface receiver and a long source pulse. The arrivals tend to occur at similar times and interfere with each other, and typically only a single value of compressional velocity for the entire sediment column (Houtz, 1980) is measured. In another study, fourteen sonobuoys (Naini and Ewing, unpublished) were deployed in a 30 by 30 km area 20 km east of our study area and measured average sediment velocities of 1.9- 2.3 km/s. A 40 in^3 airgun was used as in this study, but only two profiles were of sufficient quality to distinguish Horizon A*. The velocities measured below A* were 2.5 and 2.9 km/s. In our study use of a source with a short outgoing pulse, a bottom instrument and a sensitive analytic technique allow the discrimination of four subbottom arrivals and an interpretation of the velocity structure of the four layers.

2.3 EXPERIMENT AND DATA

The location of the study was carefully chosen on the basis of a Navy aeromagnetic contour chart to ensure that the crust had been formed predominantly by simple sea-floor spreading processes. Mesozoic magnetic anomalies M16 and M17 are linear and parallel on the crust studied (Fig. 1 and 2), implying formation ~140 mybp during an episode of constant direction of sea-floor spreading; the work of Schouten and Klitgord (in press) shows that in this area the spreading rate between anomalies M11 and M21 was approximately

constant at 0.9 cm/yr. A fracture zone exists 20 km north of the experiment area, and no structural complications such as ridge jumps or seamounts are evident in the magnetic or topographic data (Fig. 2 and 4).

The deep towed hydrophone provides a high resolution seismic reflection profile of the reflectors within the study area (Fig. 3), (Purdy and Gove, 1982). Three continuous reflectors are observed at 0.20, 0.30, and 0.50 s two-way travel time below the sea floor. Below
these reflectors an intermittent fourth reflector and acoustic basement can be observed. Arrivals from the fourth deepest sedimentary reflector are observed only where basement is deeper than 0.7 s.

These reflectors can be correlated with the seismic stratigraphy of the western North Atlantic as outlined by Tucholke (1979): reflector A^t, the top of mid-Eocene siliceous turbidites, occurs at 0.20 s below the sea-floor; A^c, the top of upper lower Eocene to lower middle Eocene cherty mudstones, occurs at 0.30 s; A* ,the top of Maestrichtian chalk overlying mid-Cretaceous green and black claystones, is at 0.50 s, and β, the top of Neocomian limestones, is at 0.70 s.

The dense coverage of normal incidence seismic reflection profiles allows a sediment thickness map to be constructed (Fig. 3). The lines shown in Fig. 4 were run with 40 in^3, 300 in^3, and 1000 in^3 airguns; all line crossings were checked for at least

0.1 s agreement. The depth to sea floor was approximately constant ($\pm$0.03 s) at 6.9 s two-way travel time or 5.1 km so that a map of two-way travel time to basement minus two-way travel time to sea floor is equivalent to a basement topography map. The fracture zone in the north (~31°25'N, 68°20'W) is poorly defined, but evident in the large (greater than 1.0 s) variations in basement depth. South of the fracture zone the basement gradually deepens from 0.4 s to 0.8 s two-way travel time below the sea-floor and two ridges ~30 km long (~31°27'N, 68°25'W and 31°20'N, 68°17'W) lie parallel to the magnetic lineations. Both ridges have the typical slow-spreading oceanic crust morphology of steep inward (eastward) facing scarps. Considerable 'random' variations on the order of 0.1 s are superimposed on this main topographic pattern.

Eight ocean-bottom hydrophones (OBH's) (Koelsch and Purdy,1979) were deployed in a cross pattern (Fig. 5) in a sediment pond east of the eastern ridge, and the 40 in^3 airgun was fired along lines of different azimuths. Extensive use of Loran C provided accurate navigation within the study area. Firing the airgun every 20 seconds provided a shot spacing on the order of 30-40 meters.

Fig. 6 shows a typical record section from OBH 4, which was in the center of the cross, shot while steaming eastward from the instrument. (For simplicity in discussion, parallel to the magnetic lineations will be called north-south and perpendicular east-west.) The first arrival is the direct water wave; it is followed by reflections from the sediments and acoustic basement.

The data were digitized using a standard procedure (Purdy et al., 1982). An amplitude filter was applied to the high frequency data to pick the arrival time of the direct water wave. The high signal to noise ratio, usually greater than 10, and consistent character of the arrival made the amplitude filter as reliable as picking arrivals by eye. The water wave arrival times were smoothed and then used to compute horizontal range with an average water speed of 1.515 km/s.

2.4 TECHNIQUE OF ANALYSIS

The large volume of the data collected prompted the use of an analytic technique which would be fast, allow an objective comparison of the data and ultimately, provide an interpretation of the data for a velocity-depth function. Computations of semblance and stack along hyperbolic trajectories in T-X space meet these criteria. Hyperbolic paths were used because the reflectors' true travel-time curves can be approximated as hyperbolae with less than $1^{o}/o$ error for the structures usually encountered on the southern Bermuda Rise (Stoffa, Diebold, and Buhl, 1982). Each line of data is mapped into stacking velocity two-way travel time ($\underline{V}$-T_o) space (Fig. 7). For laterally homogeneous isovelocity layers, the ($\underline{V}$-T_o) plot should consist of several peaks concentrated on the true stacking velocity of each reflector (Taner and Koehler, 1969). These $\underline{V}$-T_o maps are generally simpler than the original data and, therefore, more easily compared. Velocity interpretation involves

picking four or five pairs of $\underline{V}$ and T_o values instead of several hundred pairs of time-distance data.

Stoffa et al. (1980) devised a method which combines the semblance and stack functions. This method was applied to semblance and stack computed along linear paths in T-X space, but can be applied equally well to these functions computed along hyperbolic paths. The semblance is a measure of how similar the amplitudes are in a given sweep across the array and the stack is the sum of the amplitudes of all arrivals in the sweep (Taner and Koehler, 1969). Stack and semblance are computed separately and then multiplied together (Fig. 7); before multiplication, however, the semblance is filtered from 0-10 Hz and then a threshold level is set. That is, all values of semblance greater than a constant value are considered significant and set equal to one while all values below that value are considered insignificant and are set equal to zero (Fig. 7b). The resultant binary semblance function is multiplied by the stack leaving only those stacked values which have significant semblances (Fig. 7c). The power of the semblance x stack function is then taken and contoured (Fig. 7d).

The advantage of using the semblance x stack function instead of just the semblance or stack is that it preserves the amplitude information in the stack and tends to eliminate the effects of spatial aliasing and arrivals which occur only over short ranges. The amplitude information in the stack function is preserved since the stack is multiplied by one. Spatial aliasing is the result of

finite and or insufficient sampling of the data in horizontal range; spatially aliased results tend to have low values of semblance and thus are eliminated by setting a threshold for the semblance. Other signals, such as sound from passing ships, may be in the data set, but only signals with high values of semblance (i.e., coherent over many shots), remain in the semblance x stack function.

2.5 EFFECT OF LATERAL HETEROGENEITY AND VELOCITY GRADIENTS ON THE TECHNIQUE

The assumption that the reflecting media may be considered as laterally homogeneous isovelocity layers over the length of each profile is open to question. Deep-sea sediments, as far as have been mapped in the deep ocean, are laterally homogeneous in their physical properties over areas of hundreds of square kilometers, but can vary vertically on scales of millimeters to hundreds of meters. The sediment-basement interface is rough on scales of centimeters to kilometers both vertically and horizontally, and is the most obvious lateral heterogeneity in the oceanic crust. Basement itself is laterally heterogeneous on the scale of meters or less, and may or may not be heterogeneous on scales detectable with a 10 Hz seismic source e.g. 0.3-0.5 km (Purdy, 1982a). Refraction studies indicate the presence of velocity gradients on the order of 1.0 to 4.0 /s in the upper crust (Helmberger and Morris, 1969, 1970, Kennett, 1977, Whitmarsh, 1978, Stephen et al., 1980, Spudich and Orcutt, 1980, Ewing and Purdy, 1982). How these factors affect the measurement of

stacking velocity ($\underline{V}$) is discussed below.

Al-Chalabi (1974) has shown that the stacking velocity, $\underline{V}$, of a reflector at the base of thin isovelocity layers is affected by the root mean square velocity (V_{rms}) of those layers' velocities, not by the details of the layers' velocity structure. Since a velocity gradient may be considered a stack of very thin isovelocity layers in which velocity increases with depth, we may therefore conclude that for a given V_{rms} the $\underline{V}$ measurement is not affected by the exact shape or magnitude of the gradient. This also implies that knowledge of $\underline{V}$ does not contain information about the precise velocity structure or gradient between two reflectors; it is simply an average.

Normal incidence seismic reflection profiles from a deep towed hydrophone can resolve the topography of the sediment-basement interface (Purdy et al., 1981) (Fig. 3); this topography's effects on a hyperbolic analysis of the wide-angle reflections from this interface can, therefore, be predicted. Basement reflections measured on shots out to 5 km range have reflected from basement at less than 1 km range. A variety of topographic features exist over distances of 1 km: scarps, dips of less than 10° and variations in depth of a few hundredths of a second from shot to shot.

Analysing data from a fault scarp would result in at least two peaks of energy each at different two-way travel times. Since these reflections would probably be observed over short ranges, the definition of the $\underline{V}$ would be poor for arrivals from either side of

the fault. Scarps, by definition, involve changes in basement depth; the T_o of each set of arrivals should be different.

Data from a dipping reflector would be measured at different stacking velocities, but at approximately the same two-way travel times. Travel times of energy reflected from a dipping basement were calculated and straight lines fit to them in T^2-X^2 space in order to measure $\underline{V}$ and T_o. The sediment structure as discussed below (Table 2) was used in the computations. With no dip the reflector's stacking velocity and normal incidence travel time are 1.70 km/s and 4.25 s. Shooting downdip results in higher stacking velocities 1.75 km/s to 1.84 km/s for dips of 5-10°, and the normal incidence travel time decreases by .01 s. Shooting updip causes the stacking velocity to decrease to 1.42 to 1.58 km/s, for 5°-15° dip, and the normal incidence time to decrease by less than .03 s.

Topographic variations in depth on the order of 0.01s from shot to shot, increase the standard deviation of the $\underline{V}$, but do not affect the mean $\underline{V}$ measured (Al-Chalabi, 1974). Stacking velocities measured for the basement reflection should therefore have a greater spread of energy in the semblance x stack function than the upper sedimentary reflectors.

The effect of energy refracted from a velocity gradient in the uppermost crust on the semblance x stack plots was tested by calculating theoretical time-distance curves out to 5.0 km for basement with initial velocities of 4.2 and 5.2 km/s and gradients of 1.0, 2.0 and 4.0 /s (Fig. 8). Refracted energy from basement

with low initial velocity, e.g., 3.5 km/s, was observed only at ranges greater than 4.7 km; arrivals over such a short distance would have low values of semblance and be eliminated by setting a threshold level for the semblance. Models with low initial velocities therefore, were not considered. The sediment structure used is the same as was used above (Table 2), and the stacking velocities of the reflected and refracted diving energy were computed in T^2-X^2 space.

As range increases the arrivals from the basement velocity gradient are more likely to arrive earlier than the basement reflection (Fig. 8). Since semblance and stack are computed across the whole set of seismograms, it seems likely that an hyperbola would sweep the basement reflection and the arrivals from the velocity gradient. Basement with an initial velocity of 4.2 km/s and gradients of 1.0, to 4.0 /s resulted in stacking velocities of 1.71-1.77 km/s . Basement with an initial velocity of 5.2 km/s and gradients of 1.0, 2.0 and 4.0 /s gave stacking velocities of 1.74-1.81 km/s . In both cases the computed T_o was within 0.03 s of the T_o of the basement reflection, 4.25 s.

If the gradient arrivals are within a signal length (~0.10 s) of the reflected arrivals, then hyperbolae of many different stacking velocities fit through both sets of arrivals and result in energy spread in the V direction on the semblance x stack plot. Arrivals from basement with the initial velocity 4.2 km/s occurred within 0.10 s of the reflected arrivals from 3.5 to 5.0 km for all

gradients studied; arrivals from the higher velocity basement tend to occur earlier and be separated by more than 0.15 s from 4.5 to 5.0 km range.

If basement is flat lying, but laterally heterogeneous in its velocity structure, only the amplitudes of the reflections are affected. If there is a gradient in the upper crust, then any lateral heterogeneity in the gradient could show up in the semblance x stack functions as smearing of the basement reflection or an additional peak of energy at high velocities.

2.6 APPLICATION OF TECHNIQUE TO DATA

Lines with data recorded between one and five kilometers horizontal range were analysed as described; twenty eight lines met this range criterion. Only lines which begin within one km range of the instrument were analysed; this decreases spatial aliasing caused by not having recorded data exactly at 0.0 km. Also, data within the first kilometer are important in defining the two-way normal incidence travel time (T_0). Beyond 5 km range, reflected energy from the direct water wave, and subbottom reflectors tend to arrive within a few tenths of a second of each other; artefacts could easily be produced by trying to analyse this superposition of wave trains. Only arrivals at less than 5 km range were analysed; this preserves the ability to visually test the results of the analysis, since the arrivals in this range are more or less distinct from each other (Fig. 4 and 11). Instruments 4 and 3 received data

from a wide variety of azimuths (Fig. 5); instruments 1, 5, 6, and 8 received only one or two lines each.

The threshold level used on the semblance used was .07, an order of magnitude greater than the semblance value expected for noise. For these data one hundred to one hundred and thirty shots typically comprise one line; if the data were all uncorrelated noise, the expected value of the semblance would be .007-.010.

One can observe the progressive increase in time and velocity of the events as expected from a laterally homogeneous stack of isovelocity layers in which velocity increases with depth (Fig. 7d). The power of the semblance x stack function was averaged over one signal length, a .1 s time window, and then contoured.

2.7 RESULTS

The twenty eight lines which were analysed showed similar patterns of sedimentary reflectors (Fig. 9 and 16) and can be correlated with the seismic stratigraphy. Most differences between lines can be attributed to variable basement topography and its affects on the overlying sediments.

Two methods of comparison are used to evaluate the data. The first is a sum of the semblance x stack functions from each line and the second is a plot of each event's $\underline{V}$ and T_o vs. azimuth of the shooting line relative to spreading direction. The sums allow a quick evaluation of features seen in all or most of the data, and the azimuthal plots allow an evaluation of line to line

variability. The results from OBH 4 are discussed in some detail since they display most of the features of interest.

2.7.1 RESULTS: OBH 4

The sum of the semblance x stack analyses (Fig. 9) performed on ten lines (~1200 shots) received by OBH 4 shows that the first three events are quite consistent and that energy deeper than 4.2 s is more complicated and variable. The spread in $\underline{V}$ of the direct water wave at 3.4 s is spatial aliasing caused by the fact that the closest shots on the ten lines are at 0.35-0.8 km range, not at 0.0 km. Events at 3.75, 3.95, and 4.15 s two-way travel time (T_o) can be correlated with the reflectors A^c, A* and β; their stacking velocities are typically 1.52, 1.54, and 1.60 km/s, respectively (Table 1). Values of the basement's $\underline{V}$ and T_o vary more from line to line, and typically in each plot energy is observed over wide ranges of $\underline{V}$ and T_o. In some of the semblance x stack functions peaks of energy occur later and at higher velocities than the basement arrival (Fig. 12). An anomalous event occurs on more than half of the semblance x stack plots; it is at 4.4 s and 1.5 km/s, roughly 0.15 s after the basement reflection, and with the same stacking velocity as the direct water wave.

Stacking velocity and two-way travel time pairs were picked for each line and averages were computed for the different events (Table 1). Data from OBH 4 show very small variations, typically 0.01 km/s and .01 s for the sedimentary events, with variability increasing to 0.05 km/s and 0.04 s for the basement arrival.

A plot of stacking velocity and two-way travel time as functions of azimuth (Fig. 11) shows that A^C and A* are consistent on all lines and that the variation of the deeper arrivals breaks into two main groups: the data east of the instrument: 000°-180° (lines 4S, 4SSE 4ESE, 4E, 4NE, and 4N) and those west of the instrument: 225°-325° (lines 4SW, 4W, 4WNW and 4NNW).

The semblance x stack plots north, south and east of OBH 4 show several features, elongated or smeared basement arrivals, and energy arriving later than basement (Fig. 10); these features could be caused by either basement topography or a velocity gradient in the upper basement. Basement is typically at 1.70 km/s, 4.25 s, but at 000° and 135° (line 4N, Fig. 27) for example, energy is smeared from 1.70-1.76 km/s and high velocity energy at 1.80-1.85 km/s can be observed. The data show generally coherent basement reflections with evidence of small variations in basement topography, and interference of the reflections over a few hundred meters (4E)(Fig. 4). The smearing of the basement arrivals typically seen east of OBH 4 could be caused either by small scale vertical topography or a velocity gradient in the upper crust. The high velocity post basement event could be caused either by a dipping fault block, or a velocity gradient. Since a scarp is not evident in the wide-angle data, a velocity gradient is probably the cause.

The lines to the west of OBH 4 have semblance x stack plots with numerous small peaks (Fig. 10), which are caused by a fault scarp. Some peaks are not on the expected continuous $\underline{V}$-T_0 curve

from laterally homogeneous media in which velocity increases with depth. The basement reflection is discontinuous or highly interfered with at ranges greater than 2.0 km (Fig. 13). This corresponds to a reflection from the basement at distances of 0.35-.40 km horizontally from the instrument. Each of the hyperbolae fits short segments of the actual reflectors. On line 4W (Fig.13) the basement reflection actually appears to arrive 0.20 sec earlier at ranges greater than 2.5 km; it seems likely that complicated basement topography such as a fault scarp parallel to the magnetic lineations exists approximately 350 m west of OBH 4.

The event at 4.4 s and 1.5 km/s is interpreted as a shear reflection from basement, with conversion occurring at reflector β. It can be clearly seen on many of the records (4ESE) (Fig. 14), and typically has high amplitudes at greater than 2.0 km range. Arriving only one second after the direct water wave, it can not be a multiple within the 3.42 s one-way travel time deep water. Nor can it be a multiple within the sediments since their P-wave velocities in the sediments generally have velocities greater than 1.5 km/s. Shear waves within the sediments have low velocities and could reflect from the acoustic basement. A ratio of the travel time of the shear energy (T_s) from the converting reflector to basement to the travel time of the compressional wave energy (T_p) in the same layer gives the P- to S-wave velocity ratio:

$$V_p/V_s=(z/T_p)/(z/T_s)=T_s/T_p. \qquad (2.1)$$

where z is the vertical distance traveled. This ratio can then

be used to calculate a Poisson's ratio for the interval in question. Between reflector β and basement the average V_p/V_s is 2.5, which corresponds to a Poisson's ratio of 0.4. Between reflectors A^c and A* the computed Poisson's ratios are less than or approximately equal to zero, which is physically impossible. Furthermore neither β nor the low velocity arrival are strong or consistently observed on lines west of OBH 4 where the basement rises abruptly. The actual velocities of this layer are discussed below.

2.7.2 RESULTS: OBH'S 3, 1, 5, 6, 8

A detailed look at the results from OBH 3 shows that they are dominated by topographic variation around the instrument. The sum of the semblance x stack functions (Fig. 15) for eight lines of varying azimuths shows reflectors A^c and A* as discrete peaks followed by energy smeared from 4.1 to 4.4 s and 1.58 to 1.85 km/s; this spread in T_o indicates that the reflectors are varying in depth around the instrument.

In the azimuthal plot (Fig. 16) reflector A^c and basement are the only consistent events on all of the lines. The average values for $\underline{V}$ and T_o (Table 1) are comparable to those for OBH 4; the standard deviations, however, are higher. The data are highly variable; line 3N (Fig. 17) contains many arrivals whereas 3W has virtually none. A* can only be clearly seen on three lines K3N, K3SW, K3NE and K3S. Basement varies in depth from 4.15 to 4.24 s, and in stacking velocity from 1.62 to 1.72 km/s; it is shallowest in

the south and deepens to the north. The basement arrivals show discontinuities and or interference (Fig. 17).

Data received by instruments 1, 5, 6, and 8 (Table 1) showed many of the same features as the data from OBHs 3 and 4. Reflectors A^C, A*, β and basement can be seen in most of the lines received by OBHs 1, 5, and 6. On lines 5SWB, 6E and 6NB2 the basement reflector is variable in travel time and shows interference; their semblance x stack plots have numerous discontinuous peaks. OBH 8 is situated on the flank of a ridge and only basement shows up in the semblance x stack functions. It lies 0.9 s below the seafloor northeast of the instrument and 0.6 s southwest of the instrument.

2.8 VELOCITY INTERPRETATION

Modelling and inversion methods were used to interpret interval velocities and thicknesses from the wide-angle reflection data. To take advantage of the V-To information, and bypass the problems of hand-picking arrival times, T-X data were calculated using the equation of an hyperbola and the V-To values for each reflector. The hyperbolic equation fits the T-X data, and is accurate when used to calculate the slope, i.e., the ray parameter (Fig. 18). It was, therefore, possible to use both a modelling interpretation method requiring accurate T-X values and an inversion method requiring accurate p-values. The high velocities in the lower layers precluded use of the standard approximation of Dix (1955) (Fig. 18

and 19).

From the modelling solution (Table 2) T-X data were calculated by ray tracing through homogeneous isovelocity layers and the hyperbolic approximation was tested. A straight line was fit to the data for each reflector in T^2-X^2 space to determine the coefficients of the best-fitting hyperbola. Each hyperbola fit the T-X data to within several msec (Fig. 18); errors were the largest (3 msec, 0.15 $^{o}/o$) for the deeper layers. The p-value calculated by differentiating the hyperbola (Fig. 18) also differs most in the deeper layers from the p-value used to calculate each T-X pair, on the order of 4-6$^{o}/o$, and more typically is less than 2$^{o}/o$.

Generating T-X data from the $\underline{V}$-T_o information was considered preferable to picking travel times by hand which is highly subjective and time consuming. Arrivals were picked by hand for lines 4E and 4W and were interpreted by iterative modelling (Fig.19). Only two subbottom reflectors were sufficiently clear to pick their travel times; other arrivals are present in the data set, but could not be picked. The velocities interpreted for these two layers agree in general with the more detailed structure discussed below. In large data sets the amount of time spent trying to pick each arrival time is an additional undesirable feature of this approach. For inversion there are difficulties not only in picking arrival times, but also in measuring p from noisy data. Slant stacking provides a measure of p in the data, but mapping into tau-p space eliminates the T-X data necessary for the ray parameter

inversion. Furthermore, spatial aliasing, which is particularly severe when trying to fit straight lines to curves, does not allow the discrimination of all three sedimentary reflectors (Rohr, 1982)

The iterative modelling technique ray traces through a variety of velocity-depth models until the calculated travel times fit the observed travel times. It was first developed at the University of Cambridge (Limond and Patriat, 1977) and used by White (1979). In this method T-X data from each interface are used successively to solve for the overlying layer's velocity and thickness. Theoretical T-X values are calculated for the first layer by ray tracing through an initial model and the variance of the observed minus the calculated travel times is computed. The velocity of that layer is changed and theoretical T-X values recalculated. This procedure is repeated many times; the solution velocity is considered to be that velocity which minimizes the variance of the observed minus the calculated travel times. Data from the next layer is then computed, using the solution values of velocity and thickness of the first layer and an estimate of the second layer's velocity. White (1979) calculated the theoretical travel times for various reflectors in media with linear velocity gradients and solved for their isovelocity layer velocities and thicknesses. The solution velocity for each layer was equal to the velocity at mid-depth in the initial model.

The solution to the T-X data generated by the average $\underline{V}$-T_o values for OBH 4 is shown in Fig. 21 and listed in Table 2. There

are approximately 900 m of sediment. The upper 500 m have typical sedimentary velocities of 1.7-2.0 km/s and the lower 400 m have higher velocities of 2.5-3.1 km/s.

The ray parameter method of Dix (1955) was also applied to the data. This is a more rigorous approach to the data than the approximation published in the same paper, but it has been little used except in thin layers (Bryan, 1974). This method measures the slope (the ray parameter, p) locally on the T-X curve for each reflector and finds T-X points on each reflector with the same p value. The difference between the travel times and the ranges of these points give interval velocities and thicknesses. For any two reflectors this computation can be repeated for any number of points with matching p values. This method works well for layers greater than 0.02 of the thickness of the overlying layers (Bryan, 1974); the layers under consideration are between 0.04 and 0.03 the thickness of the overlying layers. As in the approximate equations no information concerning the details of a specific velocity gradient are contained in the travel times alone.

Computing T-X values out to 5 km, and matching p values to within 0.001 s/km gave 40-50 velocity-thickness calculations for each layer; the results were simply averaged for each layer (Fig. 22). As in the modelled solution, the upper layers have typical velocities of 1.7-2.0 km/s and the lower layers are higher than usual at 2.5-3.1 km/s.

As a test of the accuracy of this application of the ray

parameter method, the ray parameter solution was used to generate T-X data and their $\underline{V}$ and T_o values calculated in T^2-X^2 space. These values were then interpreted as described above (Fig. 22); the results are within 0.1 km/s and 0.01 km of the initial model in all layers.

2.9 REGIONAL CORRELATION

Corroboration of the sediments' velocities interpreted in this way can be obtained both from DSDP drilling results and from other seismic studies in the area.

The Glomar Challenger drilled the sedimentary sequence down to basement at Site 387 approximately 60 n.mi. north of the area studied here; reflectors A^c, A*, and β were penetrated. Compressional velocities and bulk density were measured on hand samples (Demars et al., 1979) and acoustic impedance was calculated as a function of depth (Tucholke et al., 1979). Contrasts in acoustic impedance were correlated with the reflectors seen in the seismic section, and the two-way travel time between the reflectors was measured. From this information and the thickness of the drilled units, interval velocities were calculated (Tucholke et al., 1979).

The DSDP interval velocities agree with the velocities interpreted here down to reflector A* (Fig. 20 and 21), but below this reflector the results computed from wide angle reflections are higher in velocity. The normal incidence seismic profile (Tucholke,

et. al., 1979) from which each reflector's two-way travel times were picked shows diffuse hyperbolae where β and basement have been identified. Using the interval velocities calculated above from wide-angle reflections and the drilled unit thicknesses to compute the two-way travel times of β and basement would place β and basement .06 and .11 s earlier than the published picks. The seismic data do not preclude such a possibility; the picks were made on legs of diffraction hyperbolae.

Correlation of the velocimeter measurements of the sediments recovered at Site 387 (Demars et al., 1979) is readily accomplished. From the seafloor to A^C the velocimeter measured compressional velocities of 1.54 -1.62 km/s and from A^C to A*, 1.7-2.2 km/s; interpretation of wide-angle reflections gave interval velocities of 1.72 km/s for the seafloor to A^C and 2.00 km/s for A^C to A*. The A* to β interval ranged in velocimeter measurements from 1.8-2.2 km/s whereas wide angle reflections measured an interval velocity of 2.5 +/- 0.1 km/s. Demars et al. (1979) believe that sample disturbance of the clays has resulted in lower velocity and density measurements as much as 30^o/o less than are actually found in situ. The β to basement interval had velocimeter measurements from 2.8-4.4 km/s, which agree with an interval velocity of 3.1 km/s. Drilling disturbance may not have affected them very much especially since carbonates do not react as strongly to pressure changes as do clays.

Houtz, Lepichon, and Ewing (1967) in a detailed study of the

sediments' velocity structure in the western North Atlantic found three layers to be characterisitic of the region. The unconsolidated sediments with velocities of 1.6 to 2.2 km/s, semi-consolidated sediments (Layer A) with velocities of 1.7-2.9 km/s, and consolidated sediments (layer β) with velocities of 2.7-3.7. The top two layers' measured here correspond to their unconsolidated sediments, while the velocities of the lower two layers are in good agreement with the interval velocities for layers A and β. Horizon A was later found to be a complex of reflectors (Tucholke, 1979). Most of the measurements of layers A and β were on thicker accumulations of sediments than those studied here.

Measurements of the physical properties of semi-consolidated limestone are few, but support the inference drawn earlier that below reflector β the sediments have a Poisson's ratio of 0.4. For a P-wave velocity of 3.1 km/s (as interpreted above) this implies a S-wave velocity of 1.24 km/s. No shear velocity measurements were made on these sediments at Site 387. Ludwig, Nafe and Drake (1963) published a compilation of compressional and shear wave velocities, and computed Poisson's ratio as a function of density for marine sediments; densities of 2.2-2.6 gm/cc, as measured below, typically correspond with Poisson's ratio of .42-.39. In one study (Laughton, 1957) a globigerina ooze with a bulk density of 1.62 gm/cc was taken from less than 200 m subbottom and was compressed uniaxially to pressures of 512 to 1024 kg/cm^2; the P-wave velocity increased from 1.6 to 2.68 and 3.06 km/s. Shear waves were detected and had

velocities of 1.2 and 1.57 km/s, corresponding to a Poisson's ratio of 0.37 and 0.32. Clays treated in the same manner did not transmit shear waves.

Sediments with a Poisson's ratio of 0.4 overlying basement should affect the shear waves refracted within the basaltic crust. A sedimentary layer with Poisson's ratio of 0.4 should reduce the amount of compressional energy converted to shear at the sediment-basement interface for any given P-wave velocity or Poisson's ratio in the basement (Spudich and Helmberger, 1979, White and Stephen, 1981). Observations here indicate that β exists to the east of the instrument but not to the west, and one would expect little refracted shear energy to be observed east of the OBH 4. Purdy (1982b), however, notes that shear refractions from the moho were observed in the explosive lines shot east of OBH 4, but not in the data shot to the west of the instrument. For any shear conversion to take place underneath β, the Vs in the basement must be on the order of V_p in the sediments, ≈3.0 km/s; for a Poisson's ratio of 0.25 to 0.3 this would indicate a basement V_p of 5.25 to 5.6 km/s in the upper basement. For no shear conversion to take place west of the instrument, either the topography is rough on the scale of one seismic wavelength, 200-500 m, as is observed, or the basement V_s is less than the sediment V_p (2.5 km/s). Both conditions are likely to be present.

2.10 CONCLUSIONS

This study of wide-angle reflections from deep sea sediments on the Bermuda Rise shows that:

1) a combination of semblance and stack which have been calculated along hyperbolic trajectories in T-X space gives a detailed picture of the sedimentary layering end velocity structure in upper oceanic crust;

2) reflectors A^C, A*, β and acoustic basement are identified in normal incidence records and the semblance x stack functions;

3) compressional to shear conversion occurs at the top of β; the shear phase reflects from basement giving a Poisson's ratio of 0.40;

4) basement topography is the main lateral heterogeneity clearly seen in the wide-angle reflection data;

5) the stacking velocity two-way travel time information can be easily interpreted for a velocity-depth function either by iterative modelling or inversion by the ray parameter method. The results from both methods agree to wthin .1 km/s and .01 km;

6) between the sea-floor and reflector A^C the sediments are .27 km thick and 1.72 km/s; between A^C and reflector A*, 0.2 km thick and 2.00 km/s, between A* and reflector β, .25 km thick and 2.52 km/s, between β and basement .13 km thick and 3.1 km/s;

7) interval velocity measurements *in situ* agree within a few tenths of a km/s with the velocimeter results at DSDP Site 387 (Demars et al.) and are within the range of velocities reported for these layers reported in a suite of measurements made largely on older crust (Houtz, et al., 1968).

TABLE 2.1 Two-way travel-time- stacking velocity values averaged for OBH's 4; 3; and 1,5,6,8.

	Two-Way Travel Time (s)		Stacking Velocity (km/s)	
	OBH 4			
W	3.43 +/-	0.01	1.50 +/-	0.01
A^C	3.75	0.01	1.52	0.01
A*	3.95	0.01	1.55	0.01
β	4.15	0.01	1.62	0.02
B	4.24	0.05	1.68	0.04
B'	4.31	0.10	1.81	0.05
	OBH 3			
W	3.43	0.01	1.50 +/-	0.01
A^C	3.71	0.03	1.51 +/-	0.01
A*	3.94	0.05	1.55 +/-	0.01
β	4.10	0.04	1.60	0.01
B	4.21	0.05	1.68	0.05

TABLE 2.1 (cont.)

	Two-Way Travel Time (s)		Stacking Velocity (km/s)	
	OBH 1,5,6,8			
W	3.43	+/- 0.01	1.50	+/- 0.-1
A^C	3.76	0.04	1.52	0.01
A*	3.93	0.05	1.54	0.01
ß	4.09	0.05	1.63	0.01
B	4.24	0.09	1.70	0.08

TABLE 2.2 Interval velocities and thickness solutions obtained from modelling and inversion.

	Modelling				Inversion			
	Interval Velocity (km/s)		Interval Thickness (km)		Interval Velocity (km/s)		Interval Thickness (km)	
				OBH 4				
W	1.5		5.145		1.5		5.145	
A^C	1.70	+/- 0.095	0.269	+/- 0.018	1.72	+/- 0.03	0.27	+/- 0.01
A*	2.00	0.01	0.197	0.003	1.99	0.01	0.198	0.001
β	2.49	0.11	0.247	0.010	2.52	0.11	0.245	0.010
B	3.12	0.32	0.126	0.051	3.29	0.69	0.129	0.050

Figure 1. Western North Atlantic Ocean (after Schouten and Klitgord, 1978) showing area of study (black box) south-west of Bermuda. Mesozoic magnetic anomalies M-0, M-16 and M-25 shown in heavy black lines. Crust studied is south of a fracture zone and was formed during a period of constant velocity spreading.

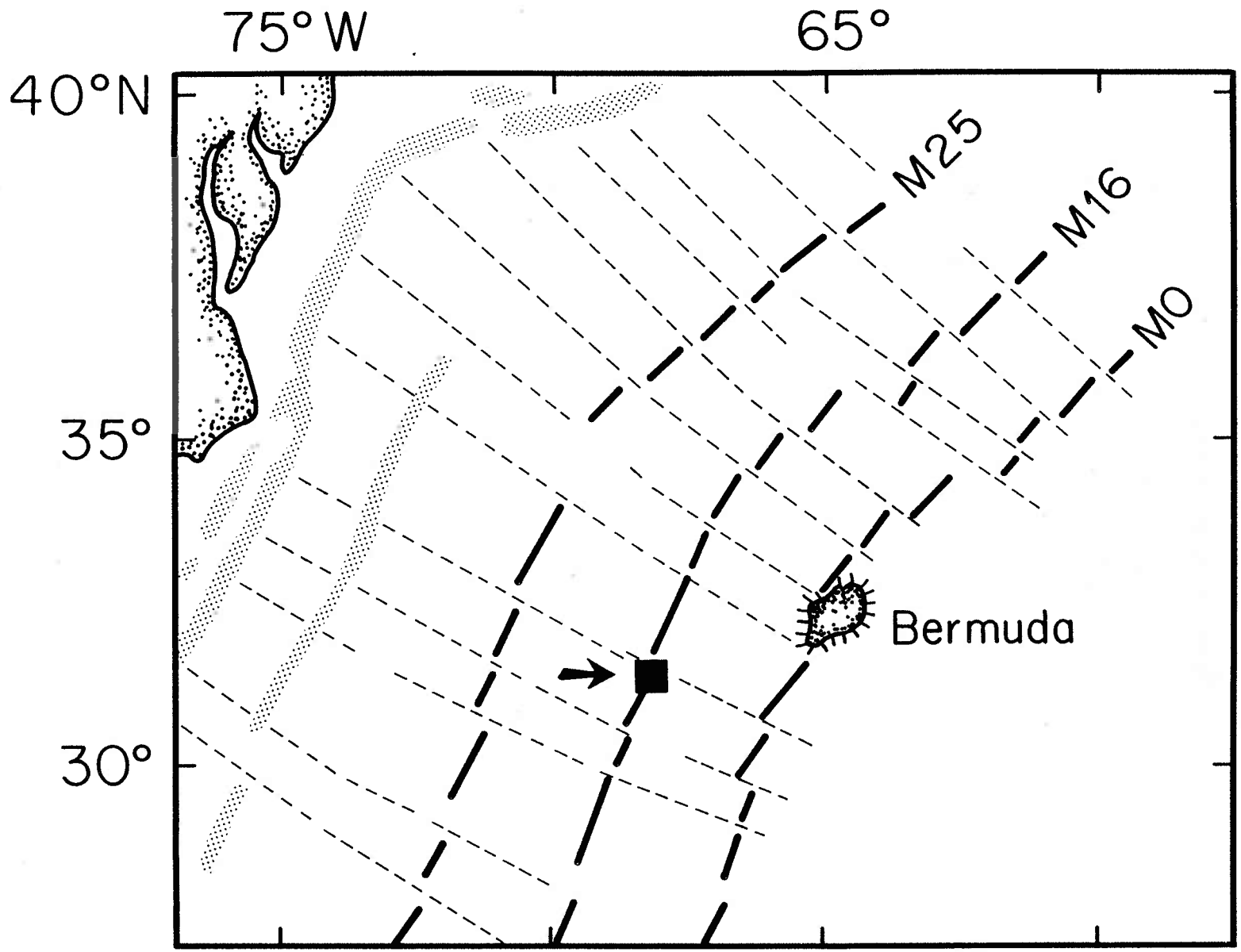
75° W
65°
40°N
35°
30°
M25
M16
M0
Bermuda

Figure 2. Magnetic anomalies in area of study, detail of Navy aeromagnetic contour chart. Fracture zone can be seen cross cutting the north-east corner of the chart. The parallel, linear pattern of the magnetic anomalies indicates that sea-floor spreading did not change direction and that there are no ridge jumps in the area. Box indicates area of Figure 5.

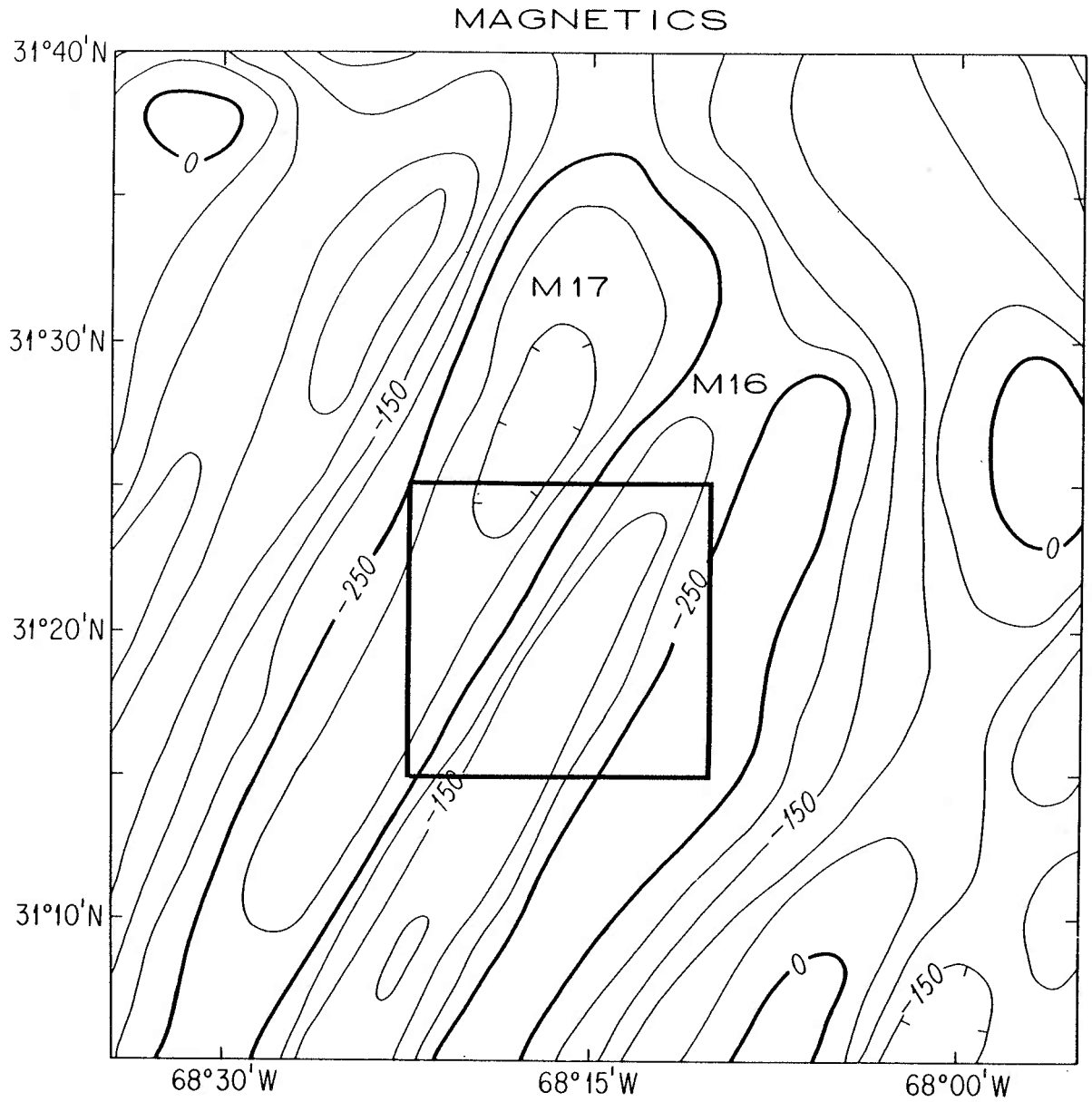
MAGNETICS
31°40'N
31°30'N
31°20'N
31°10'N
68°30'W
68°15'W
68°00'W
M17
M16
0
-150
-250
-250
-150
-150
0
-150
0

Figure 3. Deep towed hydrophone record (Purdy and Gove, 1982) in area of study shot while steaming parallel to a flow-line. A flow-line is here used to mean a line parallel to the local spreading direction when the crust was formed. The data have been filtered 80-155 Hz, stacked five-fold and deconvolved. The arrival skirting the very top of the figure is the direct water wave received by the deep towed hydrophone; the signal's variability in arrival time is due to the hydrophone's variable height above the sea floor.

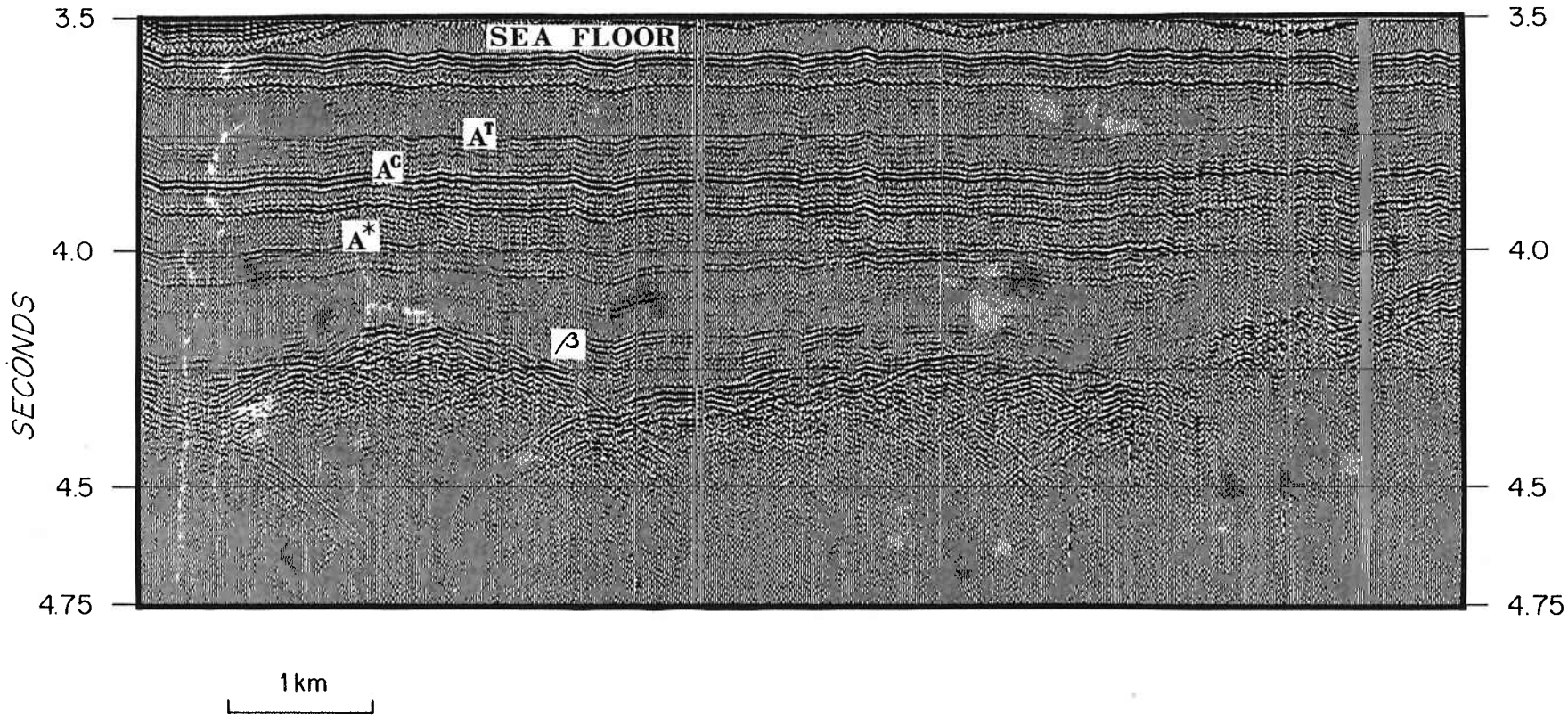
SEA FLOOR
A^T
A^C
A*
B
3.5
4.0
4.5
4.75
SECONDS
1 km

Figure 4. Contour chart of sediment thickness as picked from 40 in^3, 300 in^3, and 1000 in^3 airgun normal incidence seismic reflection records. Stippled area denotes sediments less than 0.50 sec thick. Contour interval is 0.1 sec. The fracture zone can be clearly seen in the peaks and troughs in the northeast corner of the chart. The two ridges parallel to magnetic lineations can be seen in the shading. The experiment was carried out east of the easternmost ridge. Arrow indicates direction of magnetic lineations.

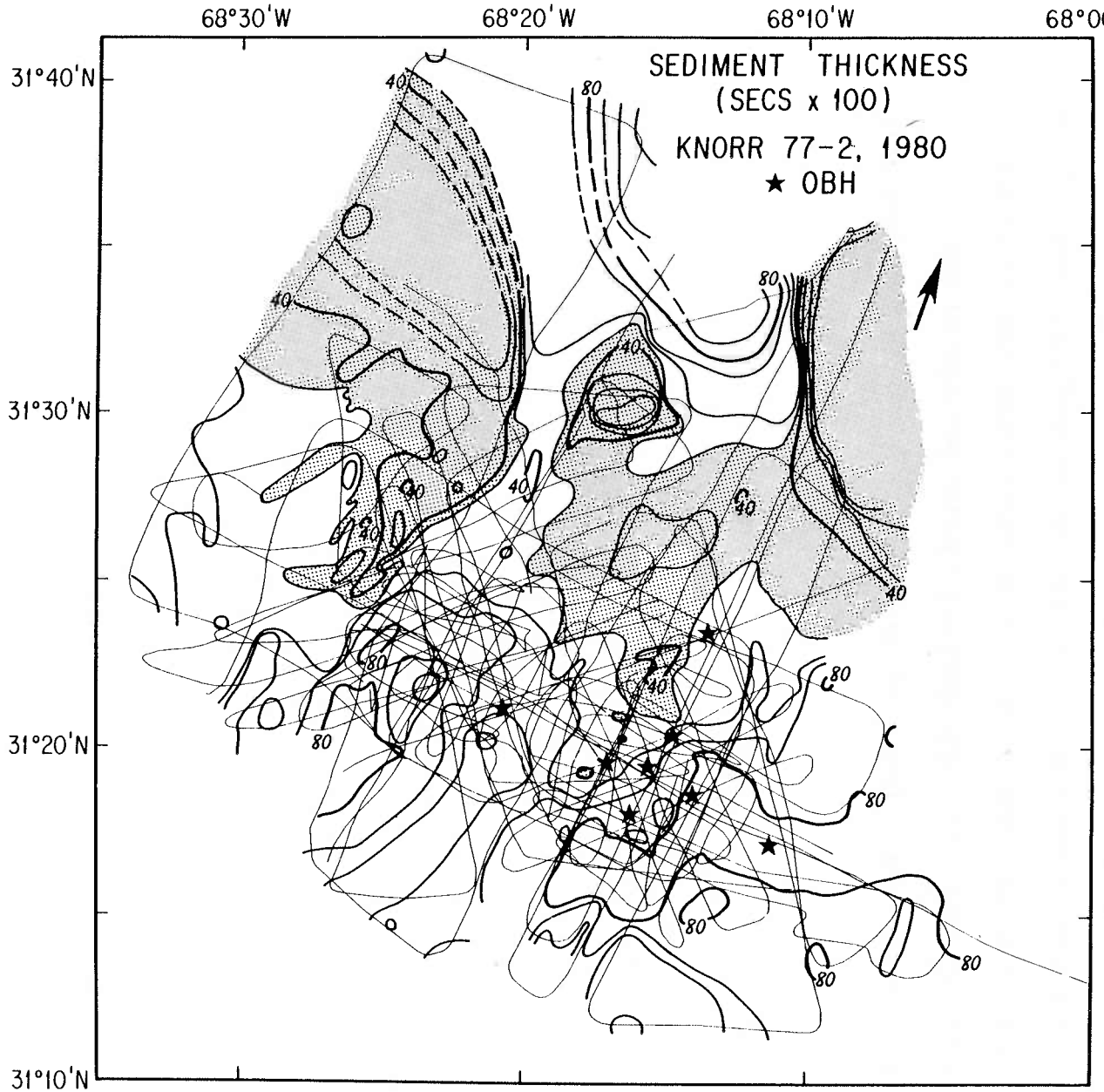
68°30'W
68°20'W
68°10'W
68°00'W
31°40'N
31°30'N
31°20'N
31°10'N
SEDIMENT THICKNESS
(SECS x 100)
KNORR 77-2, 1980
★ OBH
40
80

4.

Figure 5. Ocean-bottom hydrophone (OBH) positions and 40 in^3 airgun track lines. Heavy lines indicate track lines analyzed by hyperbolic stacking. Only lines which came within one kilometer of the instrument at their closest approach were analyzed in order to minimize spatial aliasing. Arrivals out to 5 km were used since beyond this range arrivals from the different reflectors are not clearly separated in time.

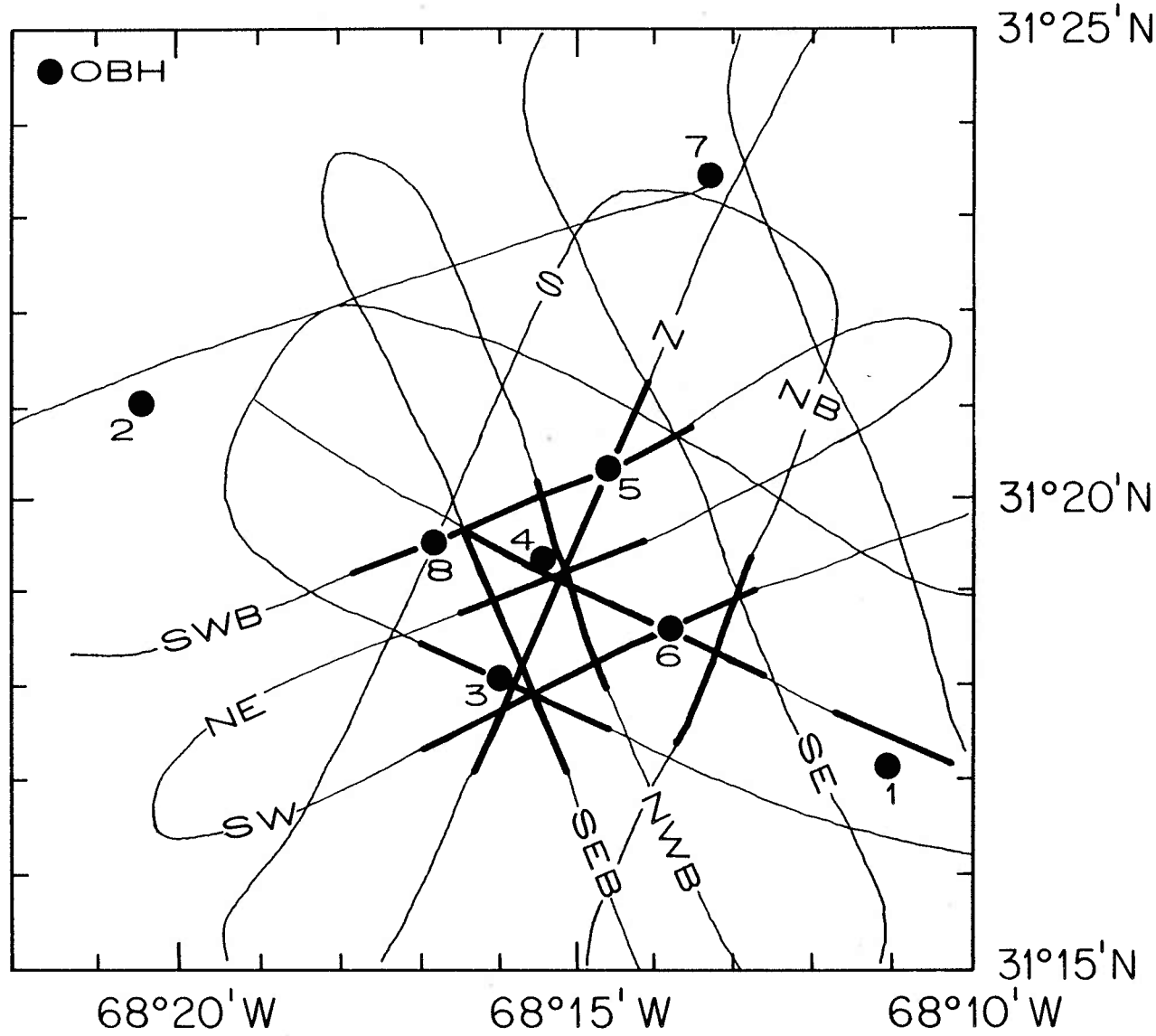
OBH
1
2
3
4
5
6
7
8
S
N
NB
SWB
NE
SW
SE
SEB
NWB
31°25'N
31°20'N
31°15'N
68°20'W
68°15'W
68°10'W

Figure 6. Line 4E: ocean-bottom hydrophone (OBH) record section recorded by OBH 4 while shooting east, along a flow-line towards younger crust. Heavy lines indicate the compressional basement reflection and between 3.4 and 5.7 km the shear basement reflection; conversion occurs at the top of layer β.

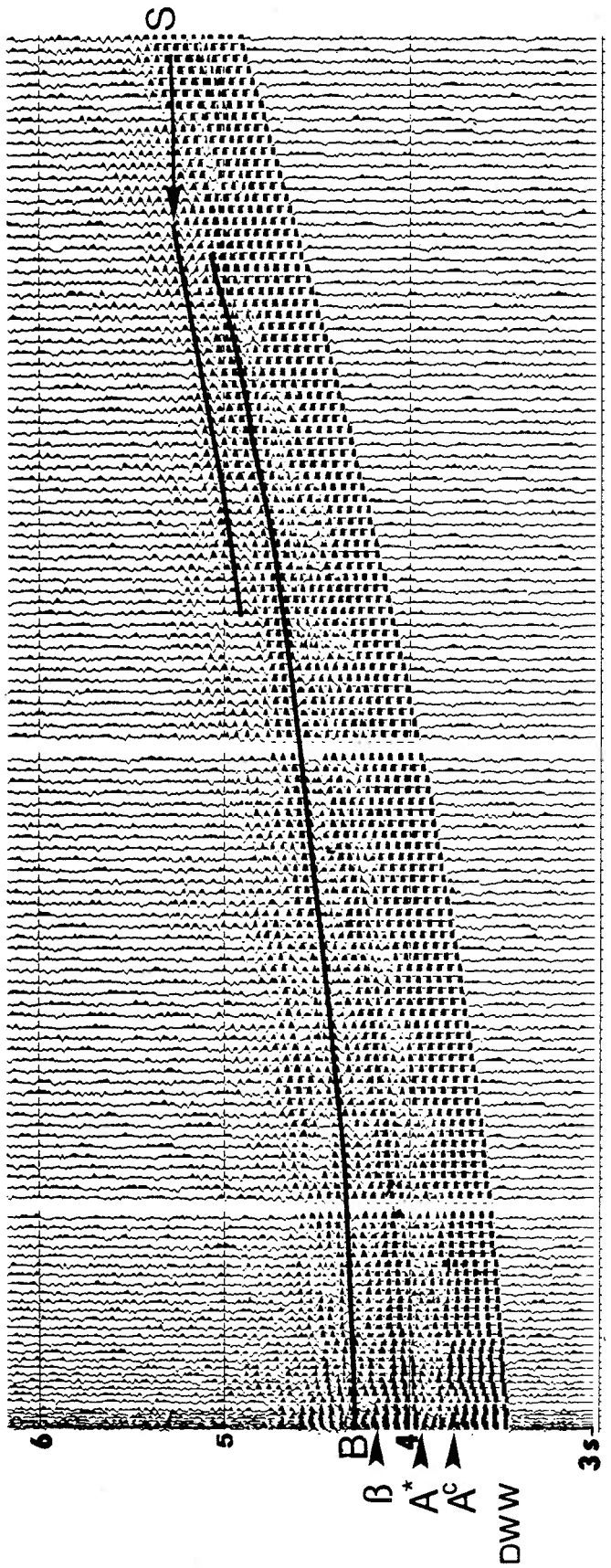

6.

Figure 7. Semblance x stack analysis of Line 4E; semblance and stack have been calculated along hyperbolic paths in T-X space between stacking velocities of 1.4 and 2.1 km/s and two-way normal incidence travel times of 3.3 and 4.8 s. A)pure stack, B)semblance filtered 0-10 Hz and a threshold level of 0.07, C) stack multiplied by the semblance function, D) power of stack x semblance function averaged over 0.1 sec window and contoured 0-54 db at 6 db interval.

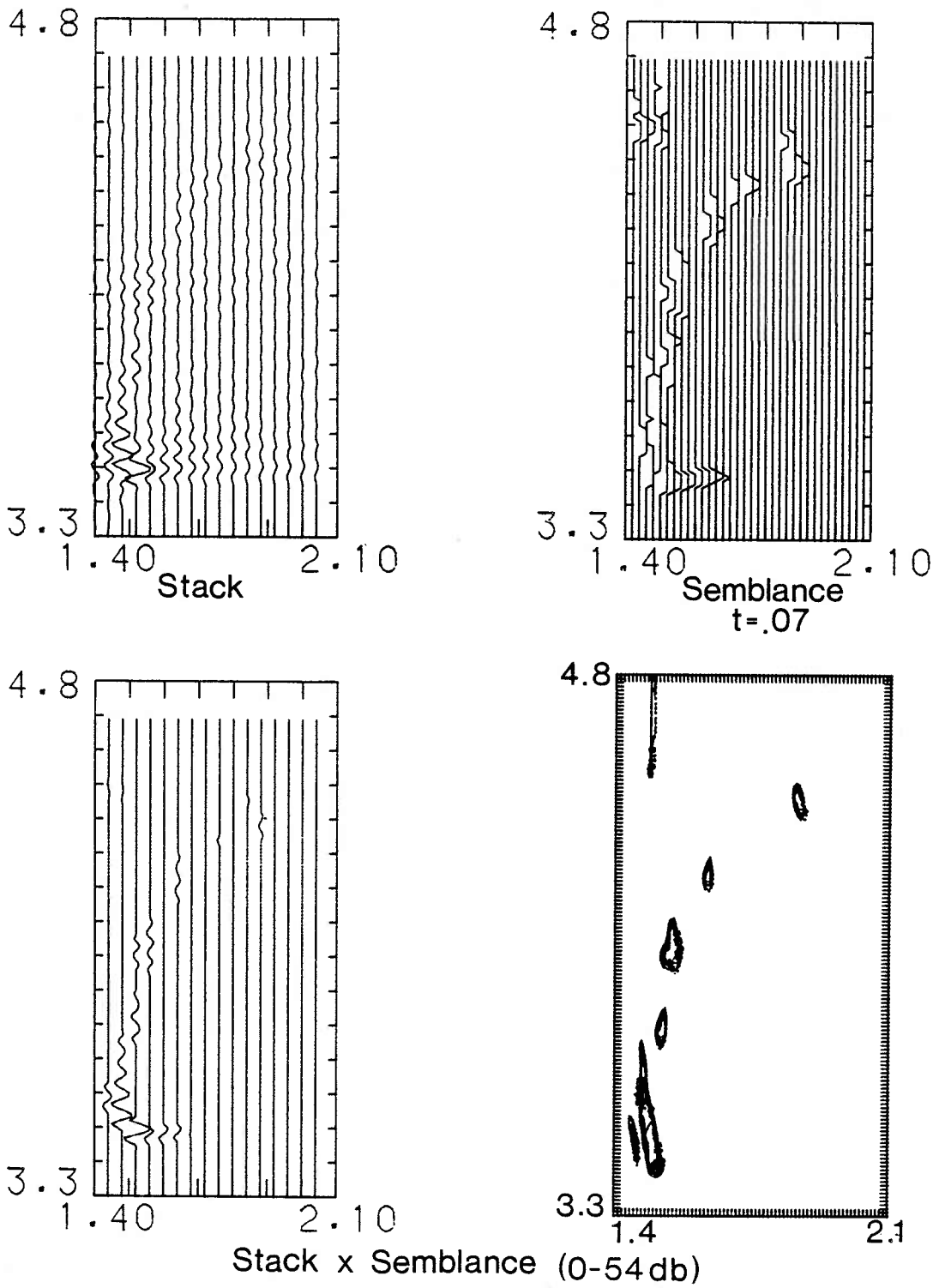
4.8
3.3
1.40
2.10
Stack
4.8
3.3
1.40
2.10
Semblance
t=.07
4.8
3.3
1.40
2.10
4.8
3.3
1.4
2.1
Stack x Semblance (0-54db)

7.

Figure 8. Time-distance curves for reflections and diving reflections from basement with a velocity gradient. The overlying layer has a velocity of 3.2 km/s. A)basement velocity at top of interface (Vo) is 5.2 km/s and velocity gradient (G) is 2.0 /s B) Vo is 4.2 km/s and G=2.0 /s

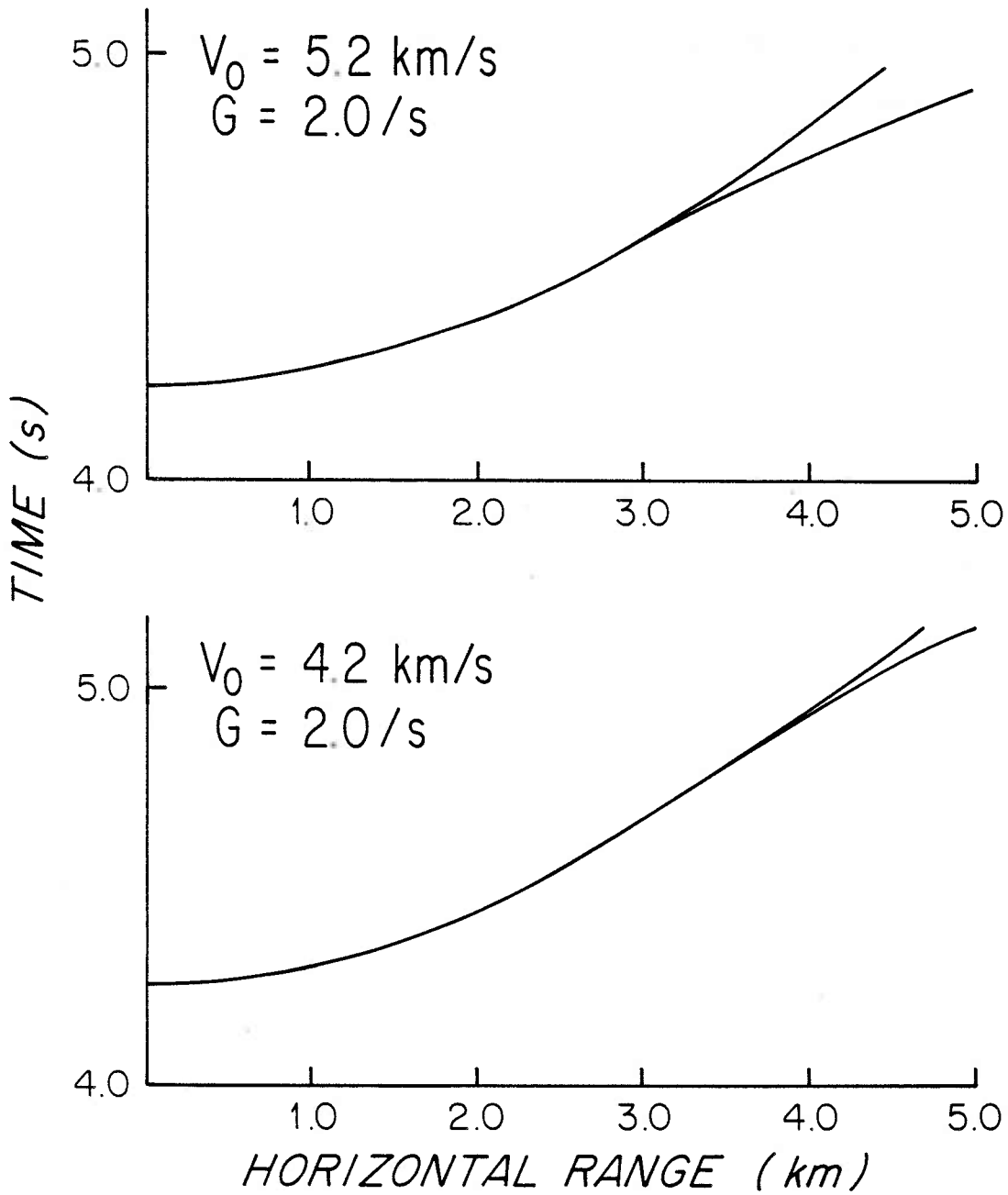
5.0
V_0 = 5.2 km/s
G = 2.0/s
4.0
1.0
2.0
3.0
4.0
5.0
TIME (s)
5.0
V_0 = 4.2 km/s
G = 2.0/s
4.0
1.0
2.0
3.0
4.0
5.0
HORIZONTAL RANGE (km)

Figure 9. Power of semblance x stack function, sum of the results from ten lines received by OBH 4. Star in the lower right corner indicates azimuthal coverage of lines. Spread of energy in the stacking velocity direction of the direct water wave is spatial aliasing caused by not having data at 0.0 km horizontal range. A^C and A* are tightly grouped; β is slightly spread in stacking velocity and basement is quite spread in stacking velocity and two-way travel time. This is caused by topographic variability within one line and from line to line and by energy refracted within a velocity gradient at the top of the crust. Energy at 1.5 km/s and 4.3 s is caused by a scarp west of the instrument and energy at 1.5 km/s and 4.4 s is a shear reflection from the basement.

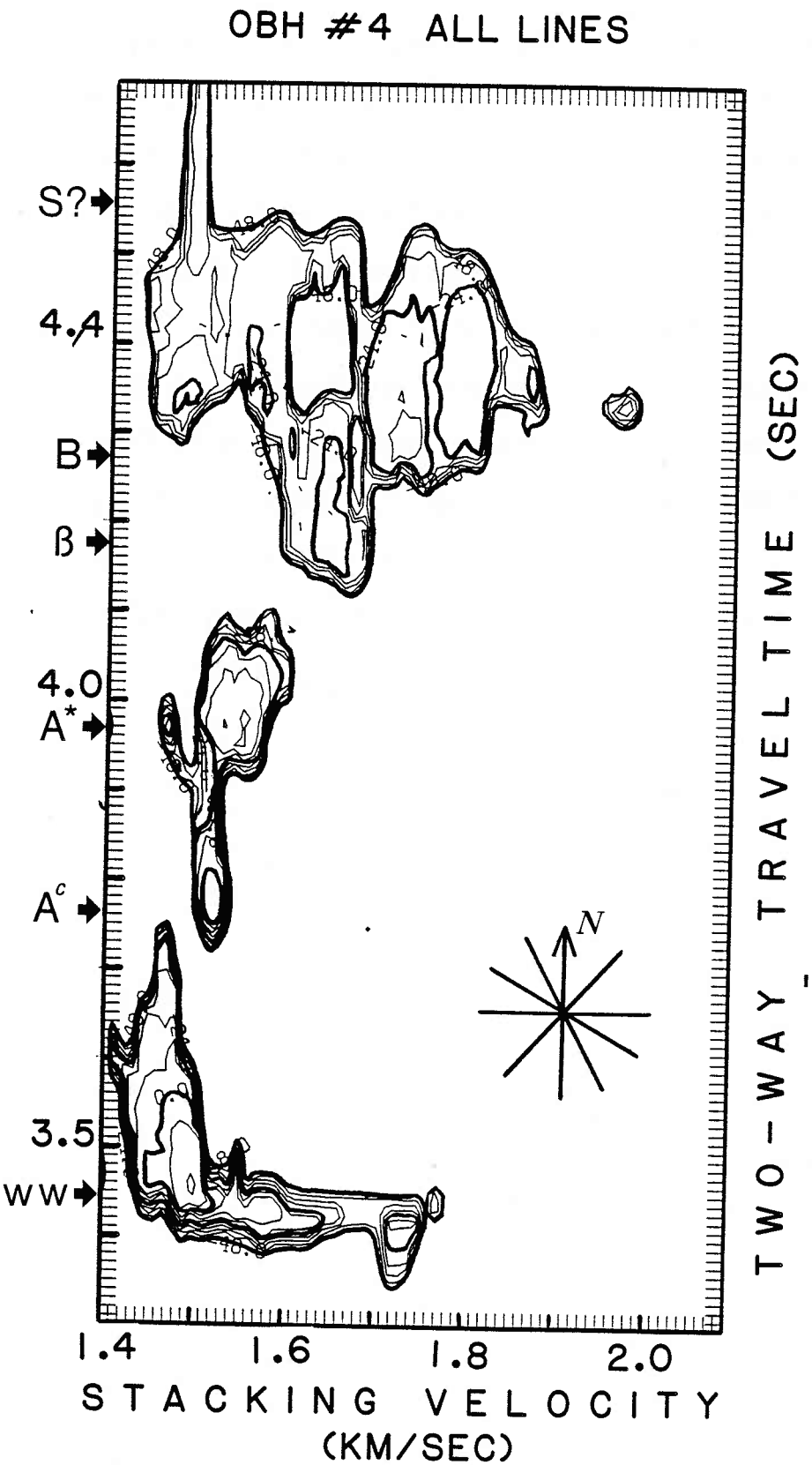
OBH #4 ALL LINES
S?
4.4
B
ß
4.0
A*
A^c
3.5
WW
N
1.4
1.6
1.8
2.0
STACKING VELOCITY
(KM/SEC)
TWO-WAY TRAVEL TIME (SEC)

Figure 10. Plots of semblance x stack plots of lines 4N, 4E, 4S and 4W. Contoured from 0-54 db at 6 db intervals. Note spread in basement events on lines 4N and 4S, the post-basement event on line 4N and the two events at 4.2 s on line 4E.

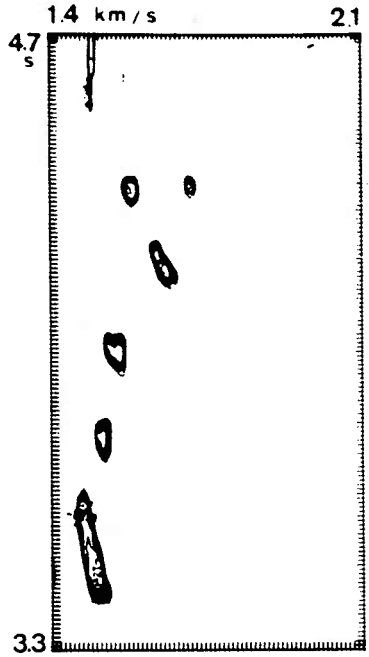

4W

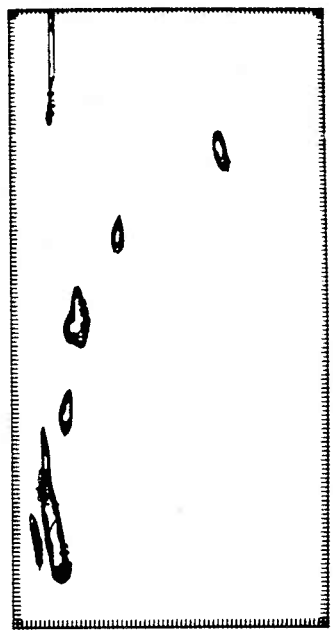

4E

SEMBLANCE x STACK (0-54db)

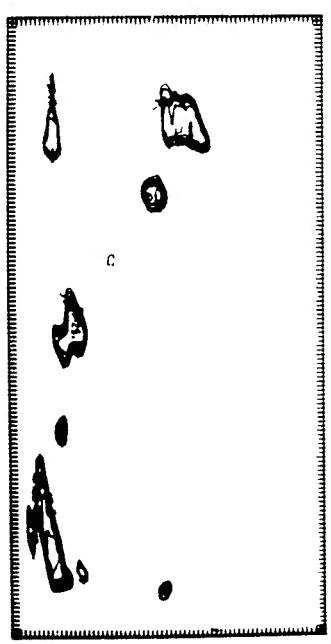

4S

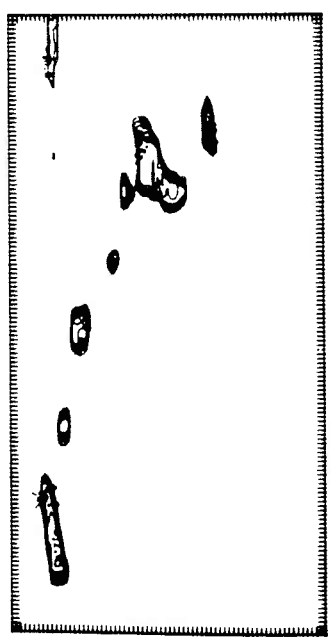

4N

Figure 11. Plot of stacking velocity (V) and two-way travel time (To) picks from semblance x stack plots of each line analyzed from OBH 4. A) Two-way travel time vs azimuth, B) Stacking velocity vs azimuth. Line drawn indicates the range of values that the energy was over 18 db; symbol denotes the actual picked value. A^c occurs consistently at 0.3 s after the direct water wave and at 1.52 km/s; A* occurs at 0.52 s and 1.55 km/s. β is not observed on all lines; it occurs at 0.7 s and velocities between 1.6 and 1.65 km/s. Basement occurs at 0.7 to 0.9 s after the direct water wave and at velocities of 1.65 to 1.72 km/s. Arrivals after basement occur on lines between 000 and 180° azimuth at 0.9 to 1.0 s and have velocities of 1.79 to 1.95 km/s. Arrivals off the increasing velocity two-way travel time curve are observed on lines between 240 and 330° azimuth and are caused by the scarp west of the instrument.

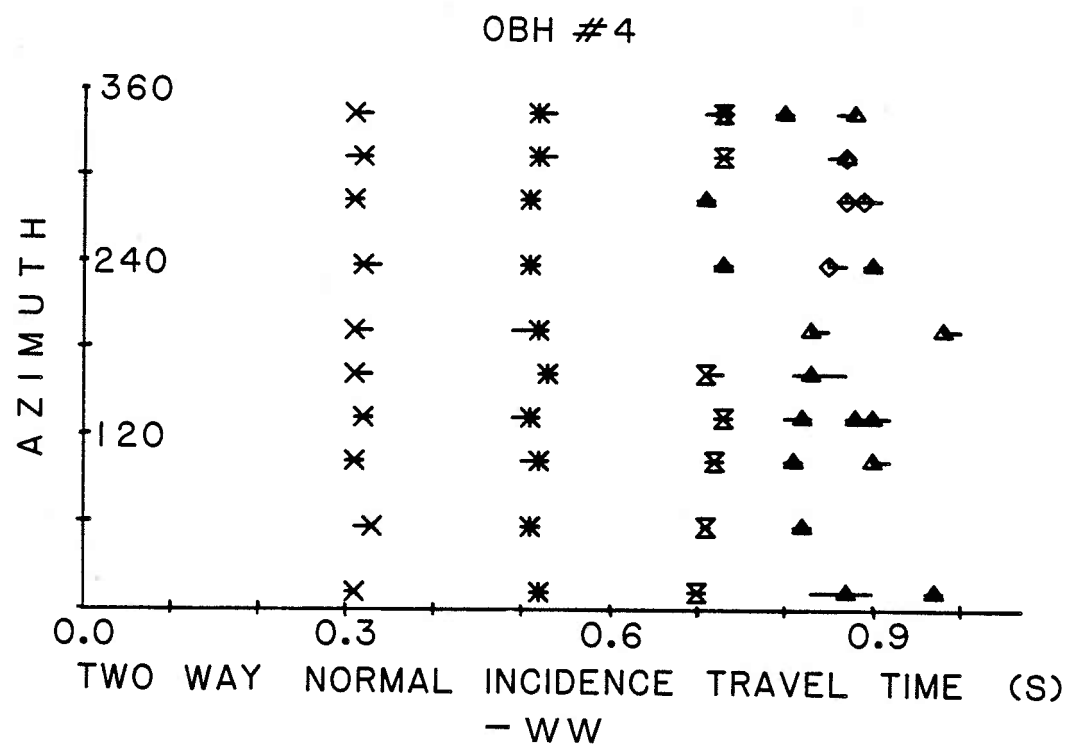
OBH #4
360
240
120
AZIMUTH
0.0
0.3
0.6
0.9
TWO WAY NORMAL INCIDENCE TRAVEL TIME (S)
– WW

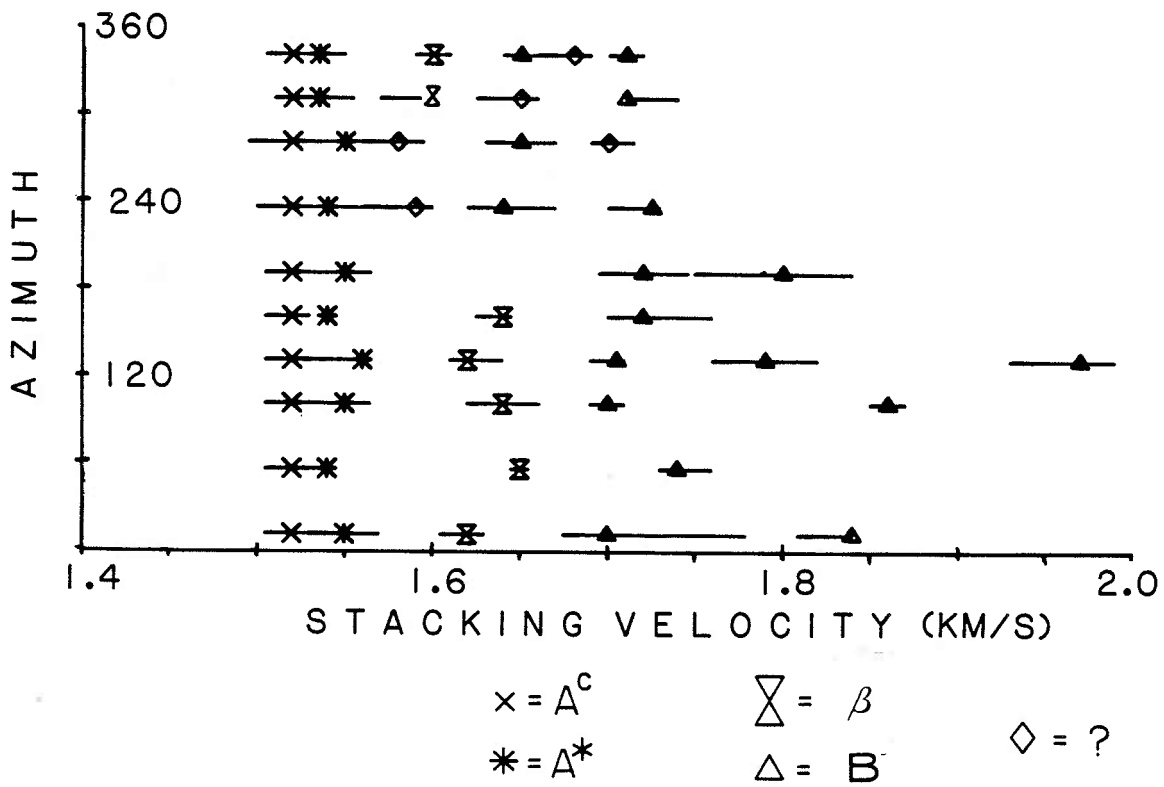
360
240
120
AZIMUTH
1.4
1.6
1.8
2.0
STACKING VELOCITY (KM/S)
× = A^c
⧖ = β
◇ = ?
✳ = A*
△ = B

Figure 12. 40 in^3 airgun data Line 4N, received by OBH 4 shot while steaming north. Note large increase in amplitude of the basement reflection at critical point, ~3.5 km horizontal range. Heavy line indicates compressional basement reflection.

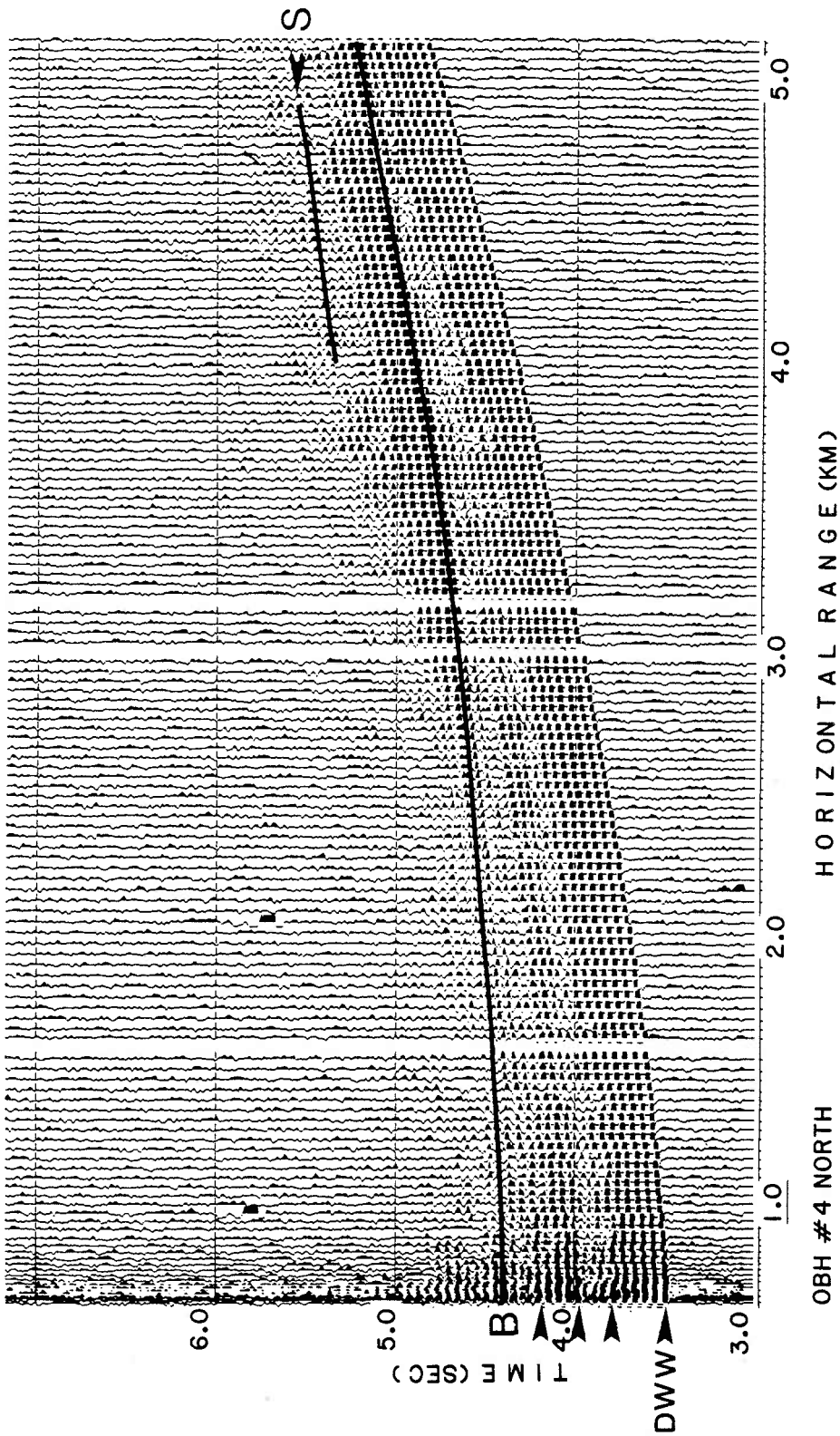
S
B
DWW
6.0
5.0
4.0
3.0
TIME (SEC)
1.0
2.0
3.0
4.0
5.0
HORIZONTAL RANGE (KM)
OBH #4 NORTH

Figure 13. 40 in^3 airgun data Line 4W. Data have been filtered 0-10 Hz. Note break in basement reflector at 2 km horizontal range with basement reappearing earlier at 2.5 km horizontal range. Heavy lines indicate compressional basement reflections. No shear reflections were observed at ranges greater than 3.0 km because basement has risen above the level of β exists.

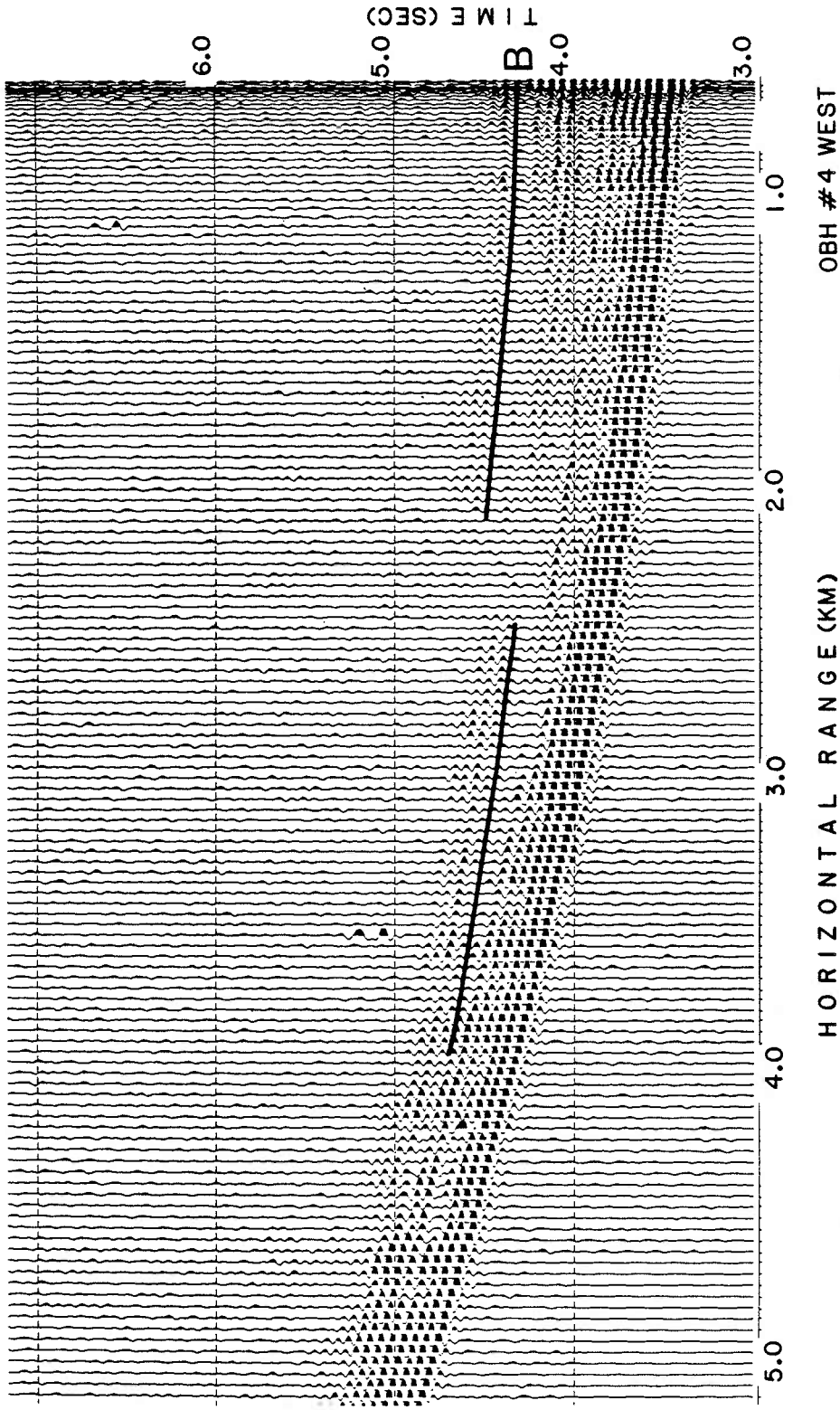
TIME (SEC)
6.0
5.0
B
4.0
3.0
1.0
2.0
3.0
4.0
5.0
HORIZONTAL RANGE (KM)
OBH #4 WEST

Figure 14. Detail of 40 in^3 airgun data Line 4SSE showing arrivals from low stacking velocity event from 3.5 km, 5.0 s to 3.9 km, 5.1 s. Also note post-critical decrease in basement reflection amplitude greater than 3.3 km. This is expected when energy is converted to transmitted shear at the sediment-basement interface.

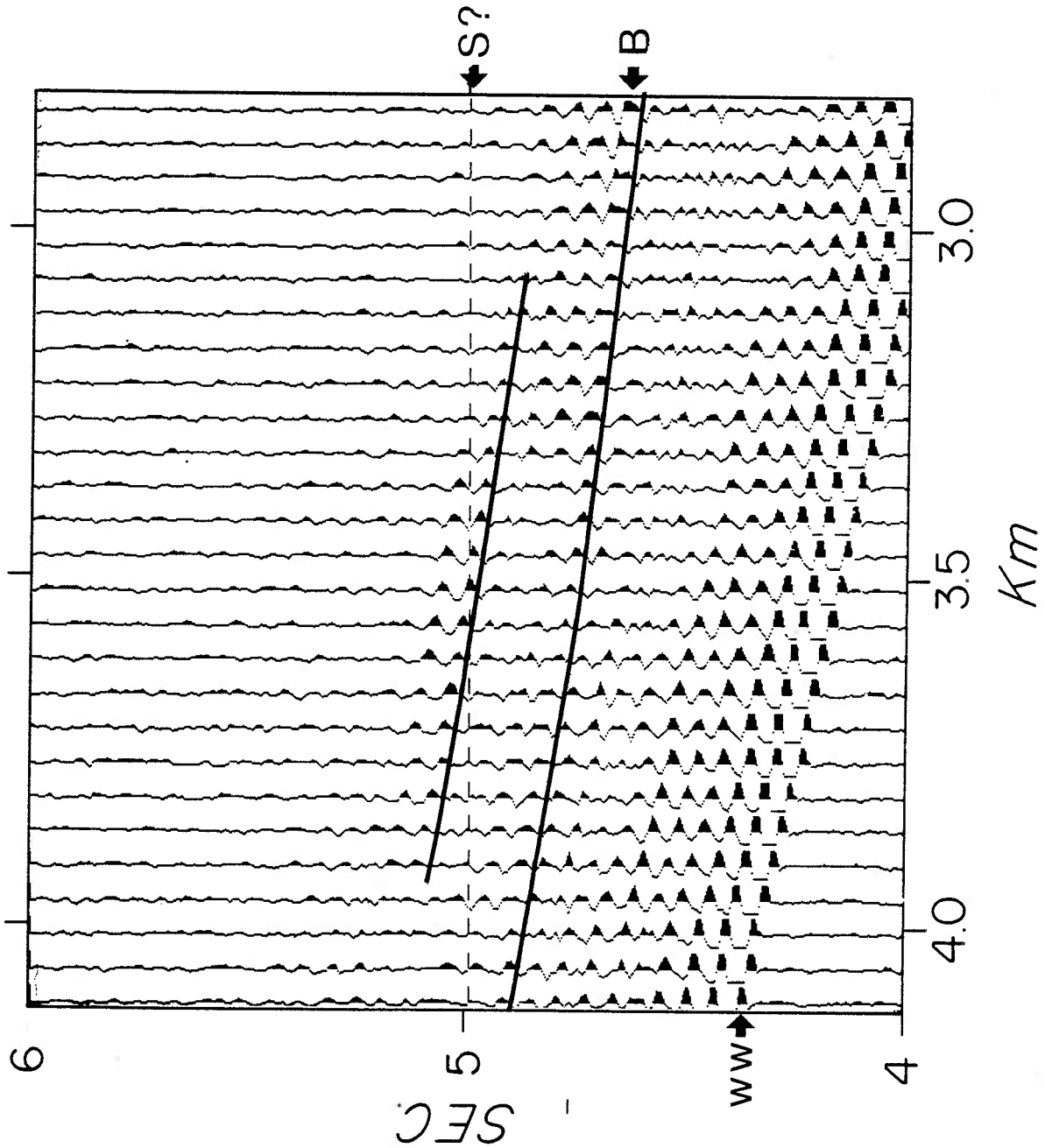
S?
B
WW
6
5
4
SEC
3.0
3.5
4.0
Km

Figure 15. Power of semblance x stack function, sum of the results from ten lines received by OBH 3 contoured from 0 to 54 db at a 6 db interval. Heavy lines drawn at 54, 24 and 0 db. Continuous spread of energy from 4.0 to 4.4 s is caused by variability in two-way travel time of the reflectors on the different lines. As on OBH 4, energy at 1.5 km/s and 4.2 s is caused by topographic varibility within one line and energy at 1.5 km/s and 4.4 s is caused by shear reflections from basement with compressional to shear conversion occurring at the top of β. Star in the lower right corner indicates azimuthal coverage of lines.

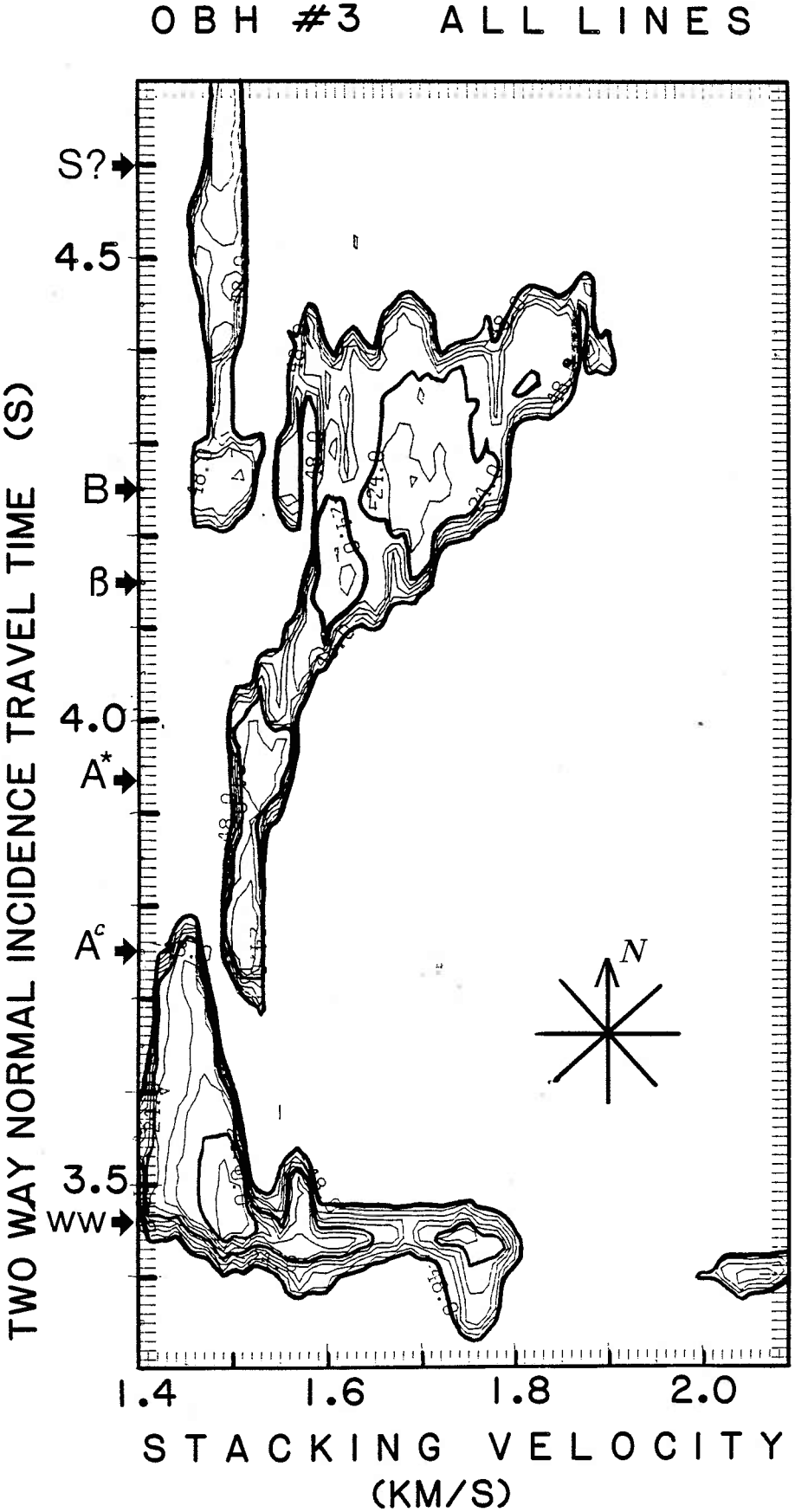
OBH #3 ALL LINES
S?
4.5
B
β
4.0
A*
A^c
3.5
WW
TWO WAY NORMAL INCIDENCE TRAVEL TIME (S)
N
1.4
1.6
1.8
2.0
STACKING VELOCITY
(KM/S)

Figure 16. Plot of stacking velocity (V) and two-way travel time picksfrom semblance x stack plots of each line analyzed from OBH 3 A) Two-way normal incidence travel time vs Azimuth, B)Stacking velocity vs. Azimuth. Compare to Fig. 10 and note greater variability in both two-way travel times and stacking velocities for all reflectors.

OBH #3

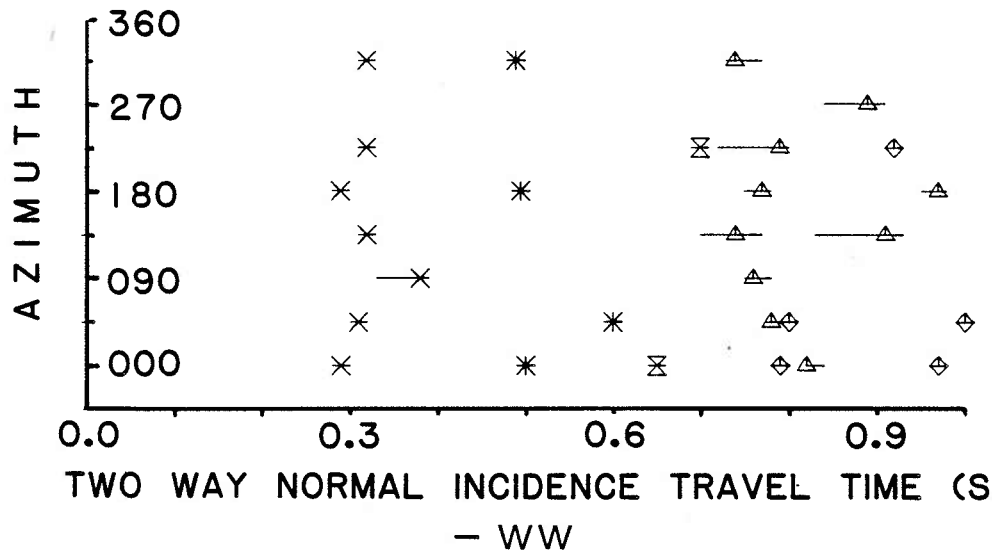
AZIMUTH
360
270
180
090
000
0.0
0.3
0.6
0.9
TWO WAY NORMAL INCIDENCE TRAVEL TIME (S)
– WW

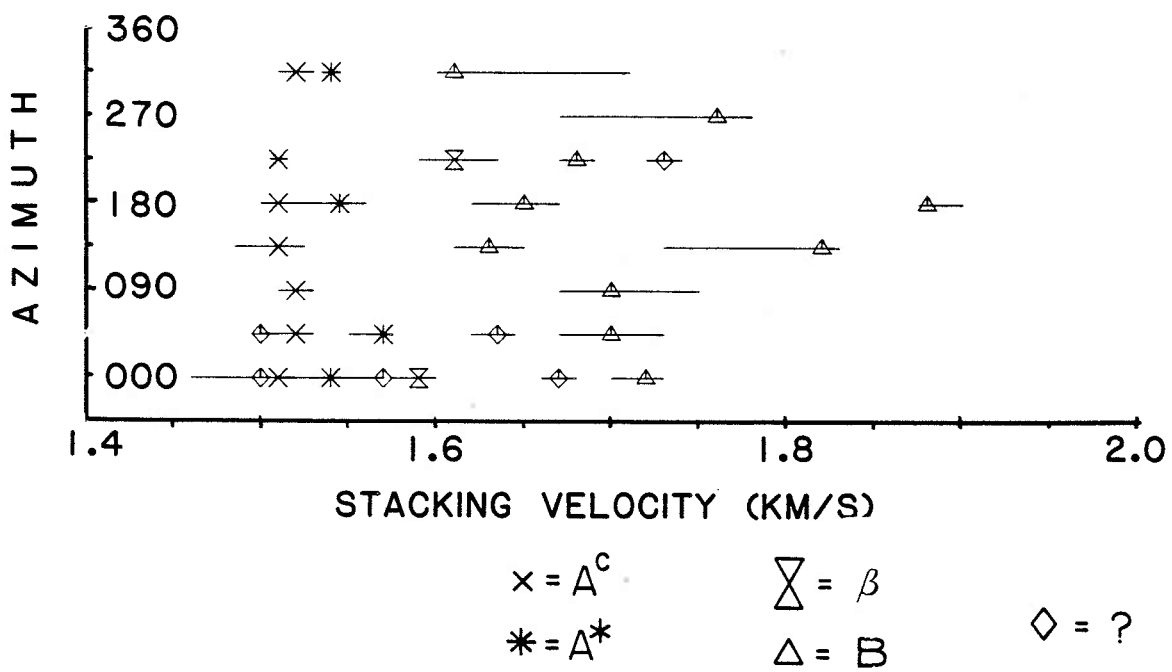
AZIMUTH
360
270
180
090
000
1.4
1.6
1.8
2.0
STACKING VELOCITY (KM/S)
× = A^c
✳ = A*
⧖ = β
△ = B
◇ = ?

Figure 17. 40 in^3 airgun data Line 3N, OBH 3 shot while steaming perpendicular to a flow-line. Note incoherence of basement reflection; this is caused by topographic variability along the line.

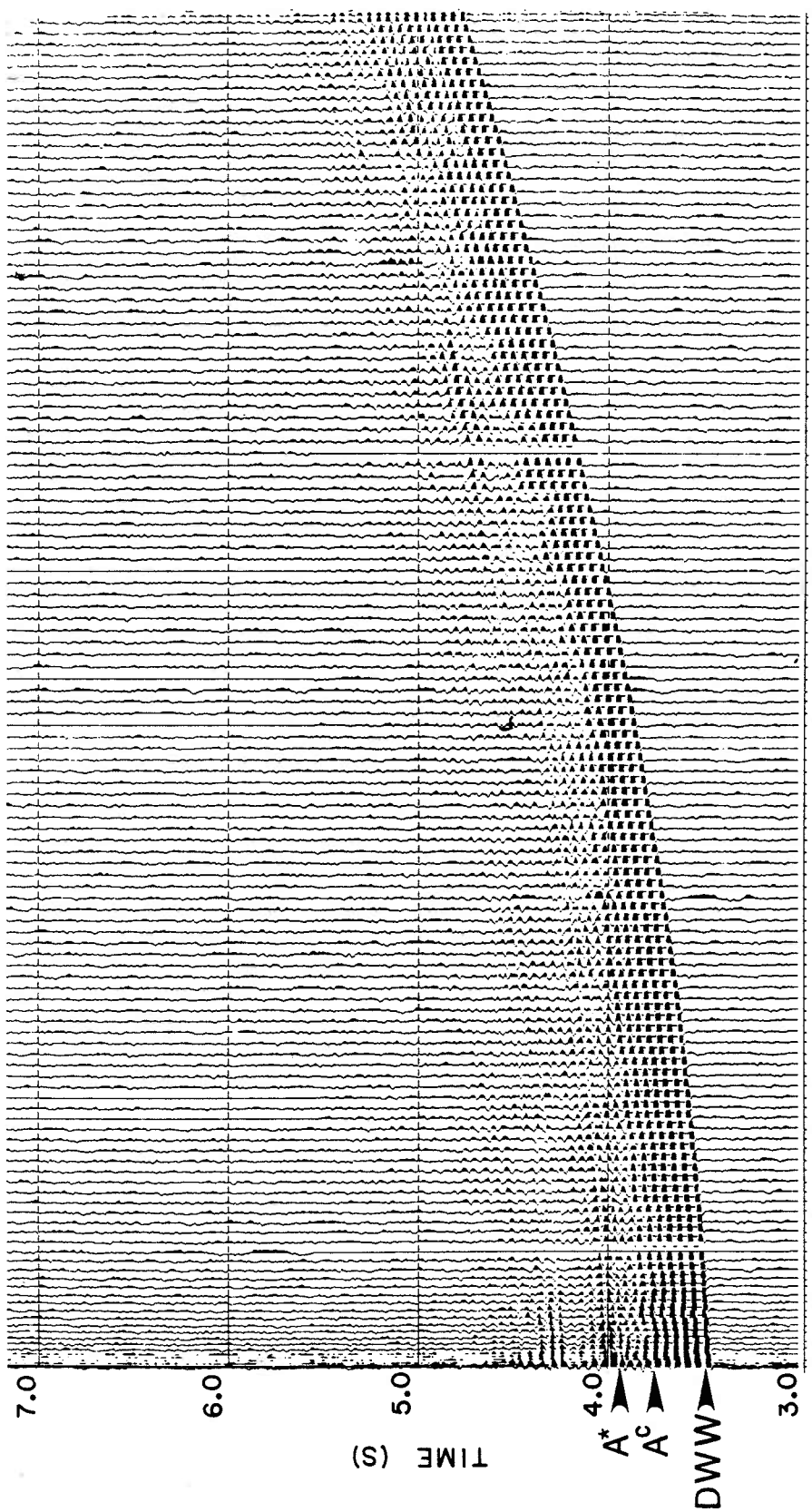
OBH #3 NORTH
1.0
2.0
3.0
4.0
HORIZONTAL RANGE (KM)
TIME (S)
7.0
6.0
5.0
4.0
3.0
A*
Ac
DWW

17.

Figure 18. Percent errors from using hyperbolic approximation. T-X data were calculated by ray tracing through the velocity-depth function in Table 2A and compared to values calculated from the equation of the best fitting hyperbola. A) Errors from calulating Time from the hyperbolic equation B) Errors from calulating the ray parameter by differentiating the hyperbola. Numbers 1-4 refer to reflectors calcuated from the four reflectors: A^C, A*, β and basement, respectively.

ERRORS FROM HYPERBOLIC APPROXIMATION

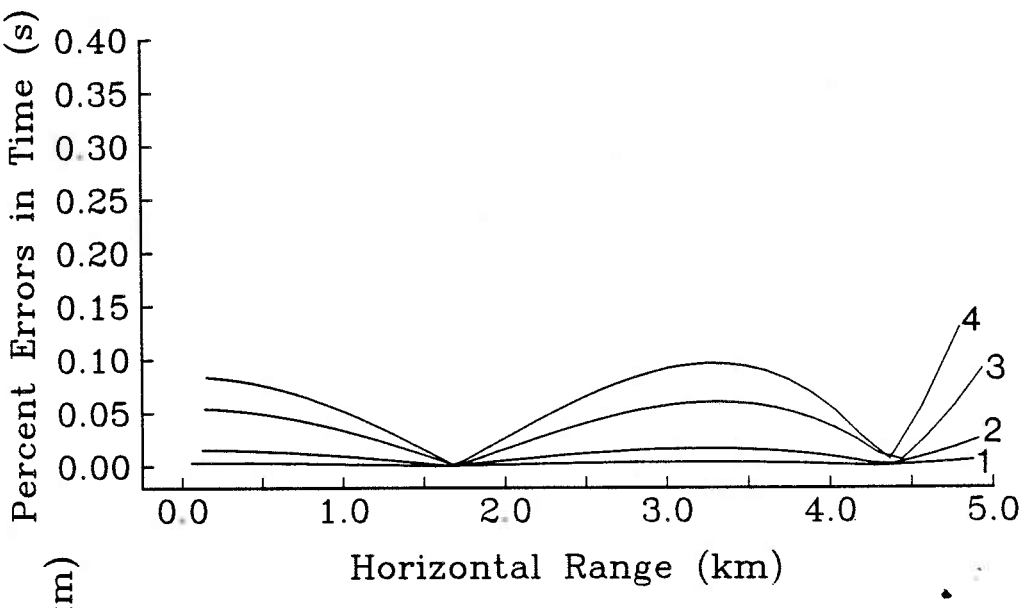

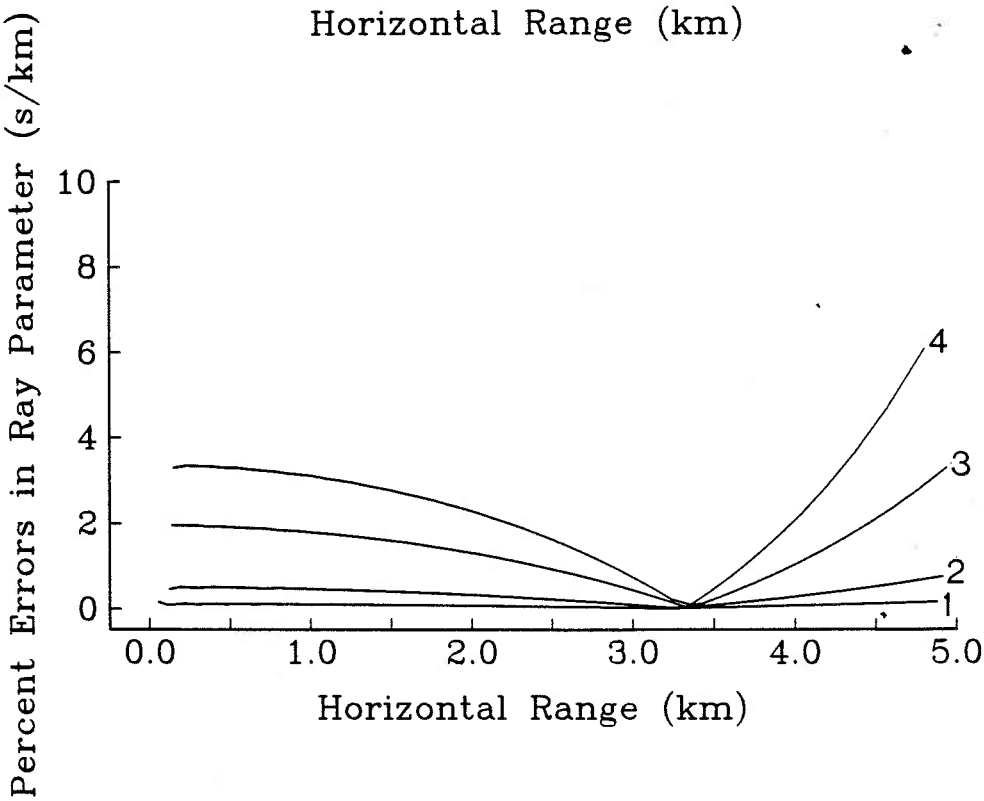

Figure 19. Velocity-depth solutions from average stacking velocity and two-way travel time picks from OBH 4 by Dix approximation. Errors were calculated from the standard deviations of the stacking velocities; the errors for layer β were too large to fit in the figure. Interval velocity from DSDP Site 387 (Tucholke et al., 1979) is also shown.

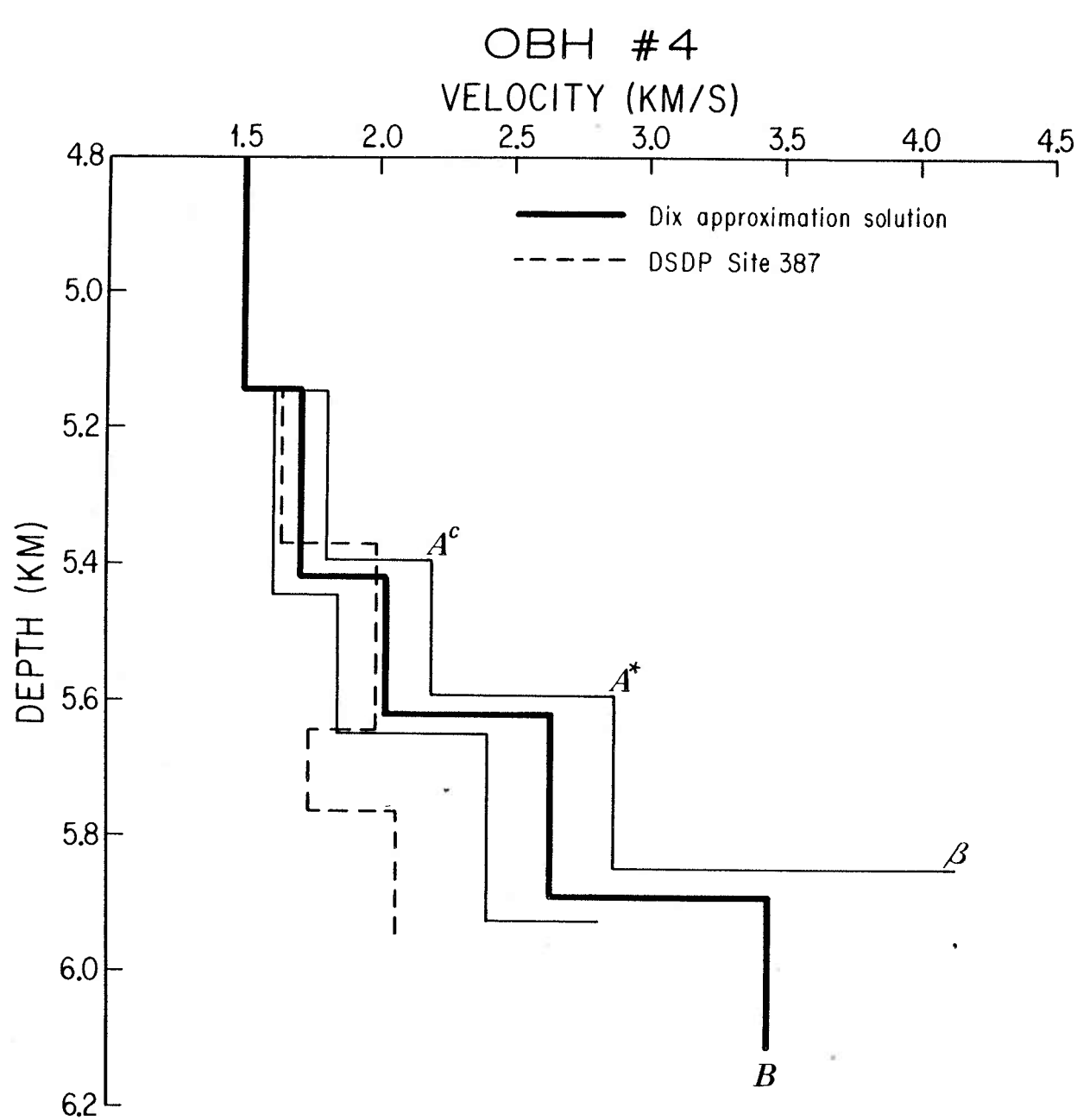
OBH #4
VELOCITY (KM/S)
1.5
2.0
2.5
3.0
3.5
4.0
4.5
Dix approximation solution
DSDP Site 387
DEPTH (KM)
4.8
5.0
5.2
5.4
5.6
5.8
6.0
6.2
A^c
A^*
β
B

Figure 20. Velocity-depth solutions from iterative modelling of travel time picks from Lines 4E and 4W. Fine lines have been drawn one standard deviation from the solution. On 4W the deepest reflector disappears at 2.0 km and a strong reflector appears 0.1 sec earlier (Fig.13). No one solution could accomodate both sets of travel times in a laterally homogeneous layer model; hence two solutions are shown for this line.

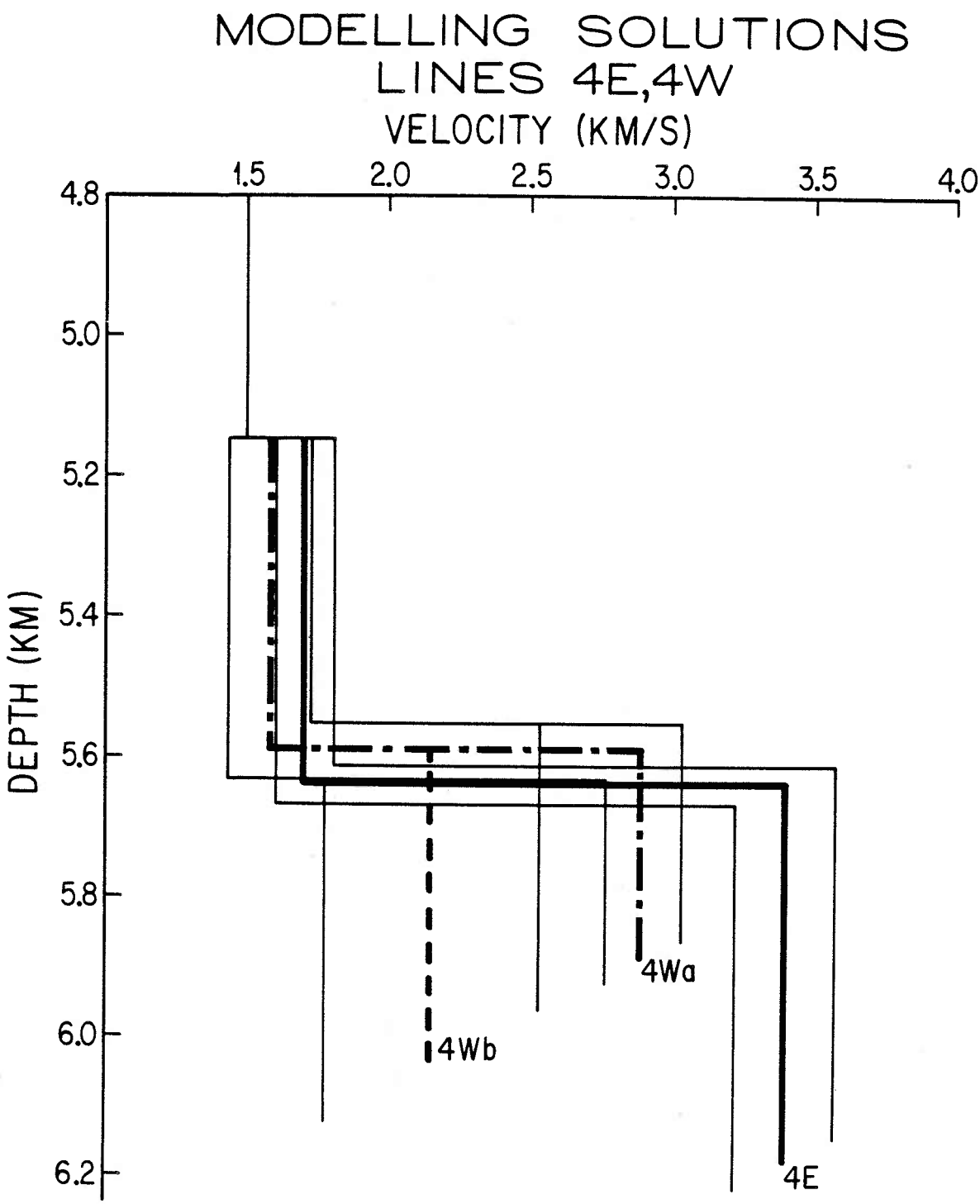
MODELLING SOLUTIONS
LINES 4E,4W
VELOCITY (KM/S)
1.5
2.0
2.5
3.0
3.5
4.0
4.8
5.0
5.2
5.4
5.6
5.8
6.0
6.2
DEPTH (KM)
4Wa
4Wb
4E

Figure 21. Iterative modelling solution (heavy line) of T-X values generated by average $\underline{V}$-T_o values from OBH 4. Iterations on an initial velocity-depth function were performed until the T-X values calculated for the model fit the input data in a least sqares sense. Errors (- - -) are calculated from standard deviations of $\underline{V}$-T_o values. Interval velocity (-- --) from DSDP Site 387 (Tucholke et al., 1979) is also shown.

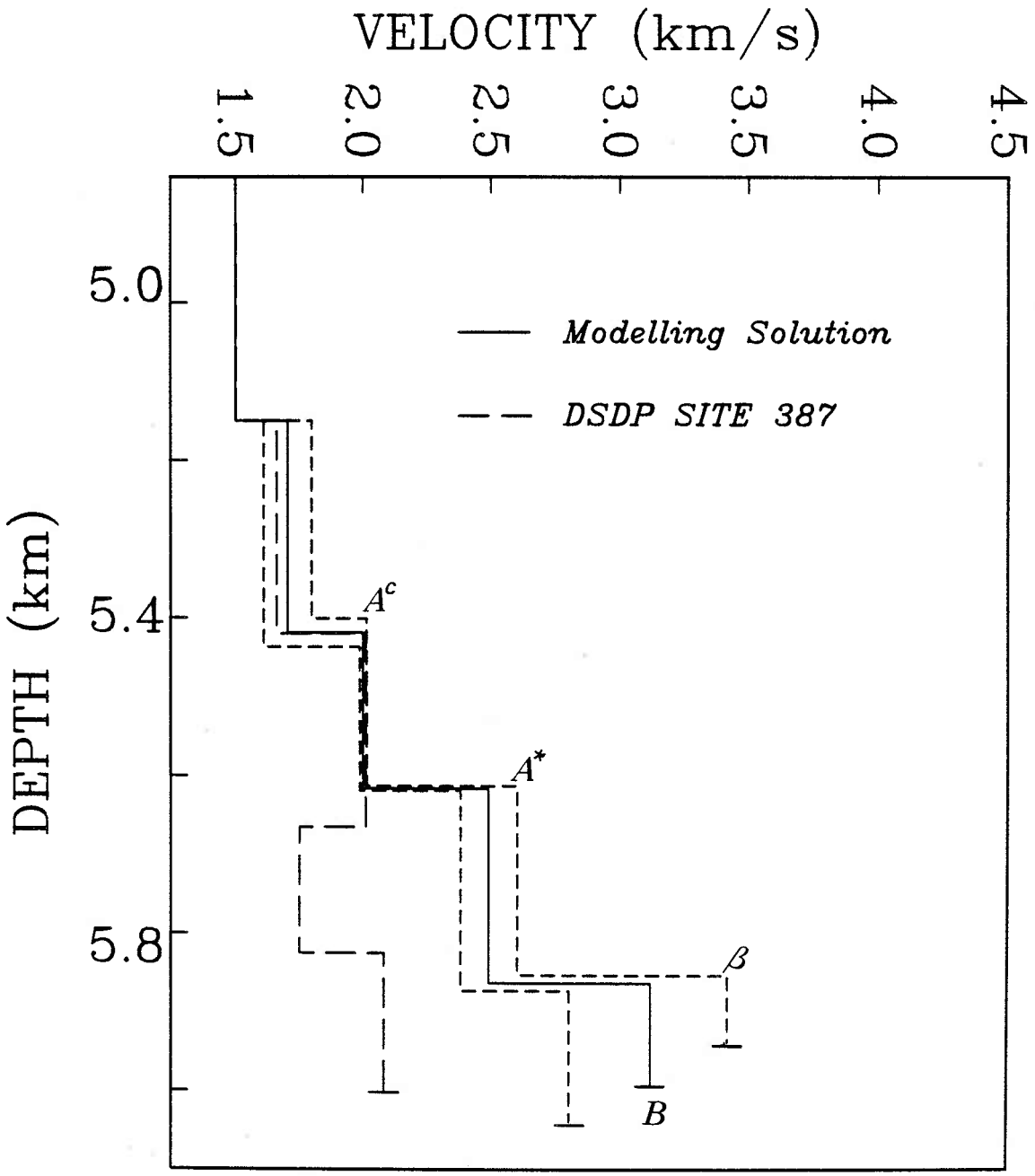
VELOCITY (km/s)
1.5
2.0
2.5
3.0
3.5
4.0
4.5
DEPTH (km)
5.0
5.4
5.8
Modelling Solution
DSDP SITE 387
A^c
A^*
β
B

Figure 22. Ray parameter inversion (heavy line) for T-X and ray parameter values generated by average $\underline{V}$-T_0 values from OBH 4. Ray paremeters on each reflector were matched to 0.001 s/km and each matching pair used to calculate the interval velocity and thickness. Forty or fifty such computations were made for each layer for values between 0. and 5. km range and then averaged. Errors (- - -) are calculated from standard deviations of $\underline{V}$-T_0 values. Interval velocity (-- --) from DSDP Site 387 (Tucholke et al., 1979) is also shown.

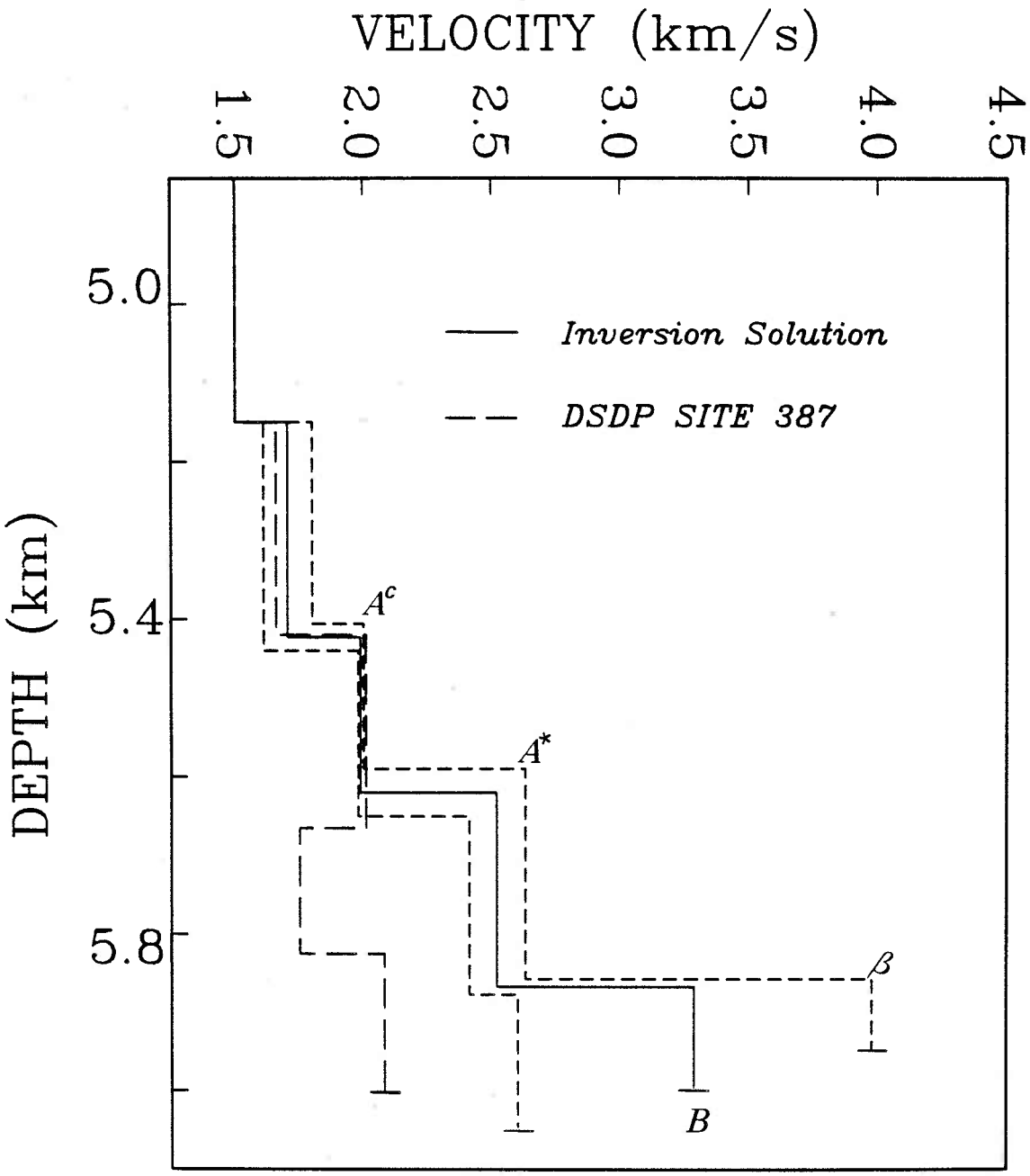
VELOCITY (km/s)
1.5
2.0
2.5
3.0
3.5
4.0
4.5
DEPTH (km)
5.0
5.4
5.8
Inversion Solution
DSDP SITE 387
A^c
A^*
β
B

Figure 23. Model used to generate time-distance data (---) which were then interpreted with the ray parameter method (-·-). The ray parameter method is close to the initial velocity-depth model.

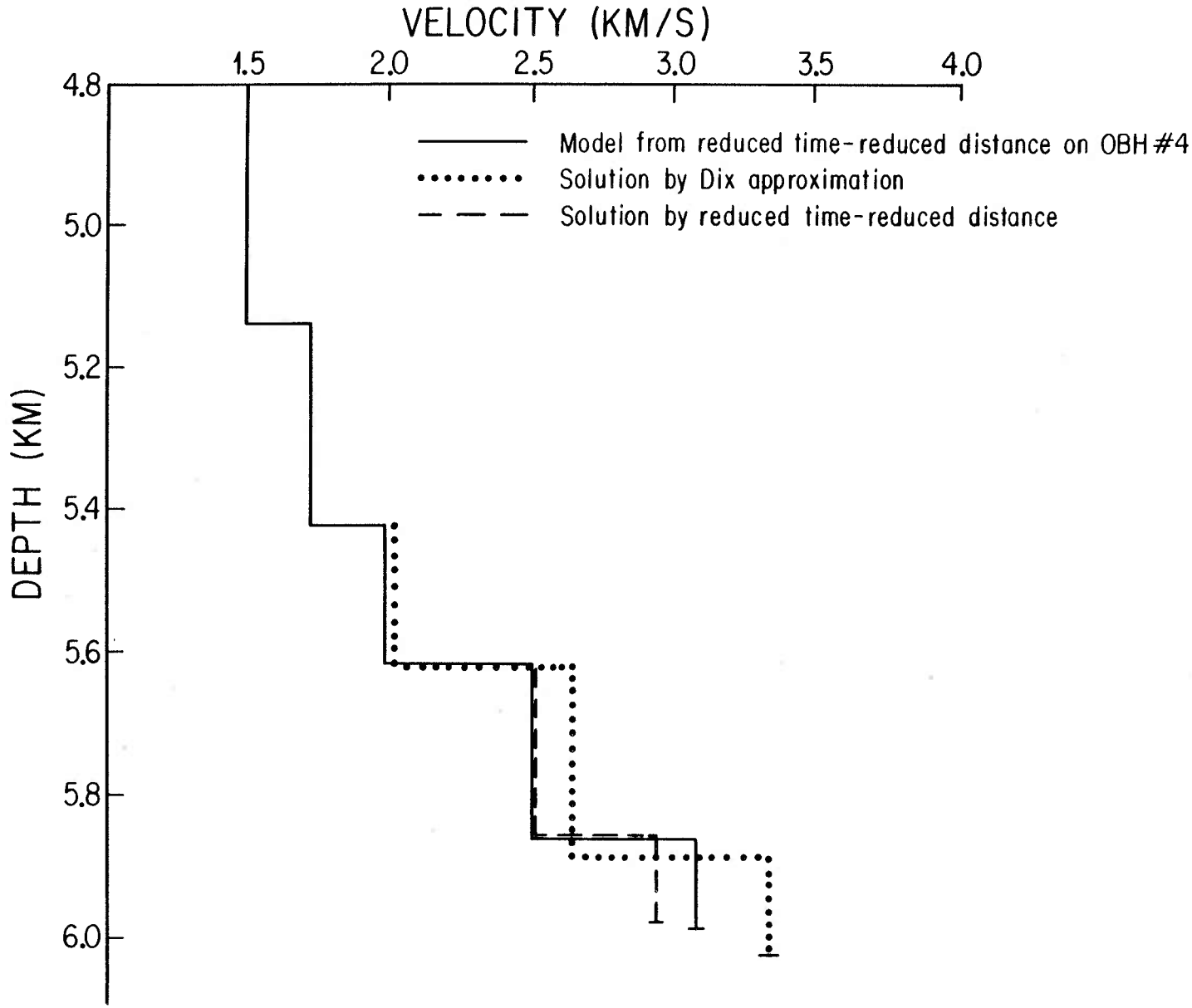
VELOCITY (KM/S)
1.5
2.0
2.5
3.0
3.5
4.0
4.8
5.0
5.2
5.4
5.6
5.8
6.0
DEPTH (KM)
Model from reduced time-reduced distance on OBH#4
Solution by Dix approximation
Solution by reduced time-reduced distance

REFERENCES

Al-Chalabi, M., An analysis of stacking velocity, rms, average and interval velocities over a horizontally layered ground, Geophys. Prosp., 22, 458-475, 1974.

Bryan, G., Sonobuoy measurements in thin layers, in Hampton, L.(ed.), Physics of Sound in Marine Sediments, Plenum Press, N.Y., 1974, p. 118-143.

Christenson, N.I. and M.H. Salisbury, Structure and constitution of the lower oceanic crust, Rev. Geophys. Space Phys., 13, 57-86, 1975.

Demars K.R., V.A. Nacci, and W.E. Kelly, Engineering and other physical property data, leg 43, in Tucholke, B.E., Vogt, P.R., et al., 1979, Initial Reports of the Deep Sea Drilling Project, 43: Washington (U.S. Govt. Printing Office), p.757-768.

Diebold, J.B. and P.L. Stoffa, The traveltime equation, tau-p mapping, and inversion of common mid-point data, Geophys., 46, 238-254, 1980.

Dix, C.H., Seismic velocities from surface measurements, Geophys., 20, 67-86, 1955.

Ewing, M. and J. Ewing, Seismic refraction measurements in the Atlantic Ocean basins, in the Mediterranean Sea, on the Mid-Atlantic Ridge, and in the Norwegian Sea, Geol. Soc. Amer. Bull., 70, 291-318, 1959.

Ewing, J. and G.M. Purdy, Upper crustal velocity structure in the ROSE area of the East Pacific Rise, J. Geophys. Res., in press.

Helmberger, D.V. and G.B. Morris, A travel time and amplitude interpretaition of a marine refraction profile: transformed shear waves,
Bull. Seism. Soc. Amer., 68, 593-600, 1970.

Houtz, R. E., Comparison of velocity characteristics in western North Atlantic and Norwegian Sea sediments, J. Acoust. Soc. Amer., 68, 1409-1414, 1980.

Houtz, R. E., J. Ewing, and X. LePichon, Velocity of Deep Sea Sediments from Sonobuoy Data, J. Geophys. Res., 73, 2615-2641, 1968.

Houtz, R. E. and J. Ewing, Detailed sedimentary velocities of the western North Atlantic Margin, J. Geophys. Res., 68, 5235-5258, 1963.

Katz, S. and M. Ewing, Seismic refraction measurements in the Atlantic Ocean, 7, Bull. Seism. Soc. Amer., 67, 475-510, 1956.

Kauffman, H., Velocity functions in seismic prospecting, Geophys., 18, 289-297, 1953.

Kennett, B.L.N., Towards a more detailed seismic picture of the oceanic crust and mantle, Mar. Geophys. Res., 3, 7-42, 1977.

Koelsch, D.E. and G.M. Purdy, An ocean bottom hydrophone instrument for seismic refraction experiments on the deep ocean, Mar. Geophys. Res., 4, 115-125, 1979.

Limond, W. Q., and P. Patriat, The accuracy of Determination of seismic interval velocities from variable angle reflection (disposable sonobuoy) records, Geophys. J. Roy. Astr. Soc., 43, 905-938, 1973.

Laughton, A.S., Sound Propagation in compacted ocean sediments, Geophys., 22, 233-260, 1957.

Ludwig, W.J., J.E. Nafe, and C.L. Drake, 1970, in A.E. Maxwell (ed.), The Sea v.4, Interscience, 1970, p.53-84

Purdy, G.M., The variability in seismic structure of Layer 2 near the East Pacific Rise at 12^{o} N, J. Geophys. Res., 86, 1982a.

Purdy, G.M., The seismic structure of 140 my old crust in the western central North Atlantic Ocean, Geophys. J. Roy. Astr. Soc., in press, 1982b.

Purdy, G. M. and L.A. Gove, Reflection profiling in the deep ocean using a near bottom hydrophone, Mar. Geophys. Res., 5, 301-314, 1982.

Purdy, G.M., J.I. Ewing, and G.M. Bryan, A deep-towed hydrophone seismic reflection survey around IPOD Sites 417 and 418, Mar. Geol., 35, 1-19, 1980.

Purdy, G.M., L.A. Gove, D. E. Koelsch, G. Power, and M.D. Allison, The Woods Hole Oceanographic Institution System for Reduction and Handling of Marine Seismic Refraction Data, Unpub. WHOI Tech. Rep., 1982.

Rohr, K., The application of tau-p mapping to low signal to noise ratio wide-angle reflection data, subm. to Geophysics, 1982.

Schouten, H. and K. Klitgord, The memory of the accreting plate boundary and the continuity of fracture zones, Earth and Plan. Sci. Lett., (in press).

Spudich, P.K.P. and D.V. Helmberger, Synthetic Seismograms from

Model Ocean Bottoms, J. Geophys. Res., 84, 189-204, 1979.

Stephen. R.A., K.E. Louden, and D.H. Matthews, The oblique seismic experiment on DSDP Leg 52, Geophys. J. Roy. Astr. Soc., 60, 289-300, 1980.

Stoffa, P.L., P. Buhl, J.B. Diebold, and F. Wenzel, Direct mapping of seismic data to the domain of intercept time and ray parameter - a plane wave decomposition, Geophys., 46, 255-267, 1980.

Stoffa, P.L., J.B. Diebold, and P. Buhl, Velocity analysis for wide aperture seismic data, Geophys. Prosp., 30, 25-57, 1982.

Taner, M.T. and F. Koehler, Velocity Spectra - digital computer derivation and application of velocity functions, Geophys., 34, 859-881, 1969.

Tucholke, B.E., Relation between acoustic stratigraphy and lithostratigraphy in the western North Atlantic Basin, in Tucholke, B.E., Vogt, P.R., et al., 1979, Initial Reports of the Deep Sea Drilling Project, v.43: Washington (U.S. Govt. Printing Office), p.827-846.

Tucholke, B.E., P.R. Vogt, et al., 1979, Site 387: Cretaceous to Recent Sedimentary Evolution of the western Bermuda Rise, in Tucholke, B.E., Vogt, P.R., et al., 1979, Initial Reports of the Deep Sea Drilling Project, v.43: Washington (U.S. Govt. Printing Office), p.323-392.

White, R.S., Oceanic upper crustal structure from variable angle seismic reflection-refraction profiles, Geophys. J. Roy. Astr. Soc., v.20, p.683-726, 1979.

White, R.S. and R.A. Stephen, Compressional to shear conversion in oceanic crust, Geophys. J. Roy. Astr. Soc., 63, 547-565, 1980.

CHAPTER 3

The Application of Tau-P Mapping to Low Signal-to-Noise Ratio Wide-Angle Reflection Data

K. Rohr

W.H.O.I.-M.I.T. Joint Program

W.H.O.I.

Woods Hole, Ma. 02543

Submitted to Geophysics WH.O.I. Contribution No. 5290

3.1 ABSTRACT

A tau-p analysis (Stoffa, et al., 1980) was performed on wide-angle reflection data from upper oceanic crust in order to measure the initial velocity and velocity gradient in the upper basaltic layer (Layer 2). In spite of an exceedingly careful mapping procedure, the large uncertainties in tau caused by a low signal-to-noise ratio and the topography of the basement reflector combined with the properties of the tau-sum inversion to result in a poorly constrained velocity-depth curve. Stacking the same data along hyperbolae gives a more detailed picture of the sedimentary velocity structure.

3.2 INTRODUCTION

The slant stacking technique was developed to analyse refracted and reflected seismic arrivals in the same data set (Stoffa et al., 1980). This method avoids deviations from the hyperbolic approximation for wide-angle reflections at large distances. Refractions from the boundary between two isovelocity layers should map to a single point in tau-p space, and precritical and postcritical reflections within the data set map to quarter-ellipses. The tau-sum inversion (Diebold and Stoffa, 1980) allows the critical and postcritical energy in the tau-p map to be interpreted for a detailed velocity-depth function.

While refractions from oceanic layer 2 (here referred to as basement) indicate the presence of gradients as large as 3/s in the

top of this layer (Helmberger and Morris, 1969, 1970; Kennett, 1977; Whitmarsh, 1978; Stephen et al., 1980; Spudich and Orcutt, 1980; Ewing and Purdy, 1982), few reliable measurements exist. The direct water wave and sedimentary reflectors generally interfere with the arrivals from the top few hundred meters and therefore are difficult to interpret. Wide-angle reflections from the top of layer 2, however, are frequently observed and their amplitudes are very sensitive to the velocity structure of the interface. The tau-p map should have high amplitudes near each reflector's critical ray parameter value and thus be a direct indication of the initial velocity in the top of the reflecting medium. Also, since the tau-p values of diving wave energy can be inverted for the velocity gradient, this method was thought to be useful in addressing the problem of the upper oceanic basement structure.

The data discussed here (Fig. 1) were collected on the southern Bermuda Rise in water ~5 km deep and sediments ~1 km thick (Rohr, 1982). A 40 in^3 airgun was fired at a shot spacing of 30-40 m, and the reflections were recorded with an ocean-bottom hydrophone (Koelsch and Purdy, 1979). Six 5 km long lines shot along different azimuths relative to the instrument are discussed. Wide-angle reflections from shots at ranges of less than five km are analysed because at these ranges the direct water wave, sedimentary and basement reflections are distinct from each other; beyond this they interfere with each other.

3.3 ANALYSIS

The tau-p mapping performed here follows the general approach of Stoffa et al. (1980) with a few modifications. The stack and semblance functions are calculated separately between ray parameter values of 0.01 and 0.47 s/km and tau values of 3.0 and 5.5 s, and then multiplied together. To preserve the amplitudes of the stack, the semblance is filtered 0-10 Hz and a threshold level of 0.25 is set. Above this level the semblance values are set to one and below it the semblance values are set to zero. The modifications implemented here consist first, in determining computationally the length of the subarray to be used, rather than by trial and error, and second, in recombining the subarray information on the basis of the power of the semblance, rather than by summing all subarrays.

Straight lines are good approximations to curves only over short distances, so slant stacking and semblance computations are generally performed on subsets of the entire data set. Since the coefficients of the hyperbolae best fitting the reflectors in the data set are known from hyperbolic stacking (Rohr, 1982), the lengths of the 'best fitting' subarrays can be determined computationally. Travel times for each reflector were calculated every 30 m, similar to the shot spacing in the data, and a straight line was fit to a subset of the travel times. The differences in time between the straight line and the computed travel times were recorded at different ranges and for different subarray lengths. If more than 90% of the data points were within 0.01 s of the

straight line, the fit was considered good. For hyperbolae of stacking velocities from 1.5 to 1.8 km/s a subarray 1.0 km long met this criterion. The curvature did not change sufficiently between 0. and 5. km to require a change in subarray length as range increases. For a complete representation of the entire seismic line in tau-p space, the subarray was moved 0.25 km for each computation, resulting in fifteen to sixteen subarrays to cover 5 km of data.

In order to evaluate the amplitudes in the final tau-p map for the presence of critically reflected energy, one must have confidence that the high amplitudes observed in the tau-p map are the result of high amplitude events in the T-X data and are not the sum of numerous moderate to small amplitude events. Since the results of each subarray computation overlap slightly in tau-p space, the recombination of this information must be done carefully. One must ensure that each event in tau-p space comes from one and only one subarray. An 'event' in tau-p space is here defined as a set of points for which the semblance x stack function has energy i.e., where the filtered semblance function exceeds the threshold level. The event begins where the threshold level is first exceeded in tau-p space and continues with increasing tau until the semblance drops below the threshold for a constant p-value. A set of reflections in T-X space from one reflector maps into a set of events in tau-p space. For each event, (where the semblance exceeds the threshold level) in each subarray, the power of the semblance is computed. The subarrays' power for each event is compared and the

subarray with the highest power for each event is found. The subarrays with the highest power are compiled into the final tau-p map.

For inversion specific tau-p values are picked from the semblance x stack function of each subarray. This results in many more values to define the curve than if only the compiled tau-p map were used. Diebold et al. (1981) chose to pick the maximum of the events as the locus of the tau-p point. An onset of an arrival, however, does not necessarily correspond to its maximum amplitude. For this reason we chose the 'onset' of events (where the semblance first exceeds the threshold value) as the locus of the tau-p point. The exact value of the semblance chosen is somewhat arbitrary; changing the value of the threshold by a few percent would change the tau-p pick by a few hundredths of a second. Since the difference between the tau values of successive points is inverted, this makes little difference to the final solution.

3.4 RESULTS

The results of the tau-p mapping of two lines are shown in Fig. 2. Correlation of the normal incidence tau values (p=0.0) to the normal incidence reflection profiles allows the events to be identified as the direct water wave, sedimentary reflectors A^c, A* (Tucholke, 1979), basement and shear basement reflections (Rohr, 1982). On line 4 North the basement follows the quarter-ellipse pattern closely and the apparent critical p-value can be identified as 0.23

$\pm$0.02s/km, corresponding to 4.35 $\pm$ 0.35 km/s. Interference between the reflected and refracted energy moves the critical point to greater horizontal ranges and therefore greater p values making this velocity estimate, in fact, a lower limit. The postcritical reflections are also of high amplitude, as expected when there is little energy converted to shear at the interface. Line 4 East, however, shows a more irregular pattern in the basement reflections.

A compilation of the tau-p points from all subarrays of six lines (Fig. 3) shows events from the direct water wave and four reflectors in an overlapping quarter-ellipse pattern. Reflectors A^C and β (Tucholke, 1979) are poorly resolved, whereas A^* and basement are observed on all lines over a wide range of p values. The scatter in tau (~ 0.03s on the basement) is caused by the topography of these reflectors. The shear events are rather variable in their occurrence in tau-p space from line to line, but are evident as one reflector in the compilation.

3.5 INVERSION

Only the basement events were interpreted since this is the reflector of interest and it is the only one with a sufficient number of postcritical events to use the tau-sum inversion method (Diebold and Stoffa, 1980). Tau-p values were picked for the basement reflector in each subarray and were inverted for the velocity structure below A*, the deepest sedimentary reflector visible on the tau-p map. A polynomial was fit to the values and

the smooth function was evaluated every 0.01 s/km.

Interpretations of lines 4 South, 4 East and a compilation of basement tau-p values (Fig. 4) show roughly the same thickness of sediments (~600 m), and only line 4 East shows a velocity gradient in basement. It is ~ 1.0/s and has an uppermost velocity of 6.2 km/s. Refraction data shot to the same instrument (Purdy, 1982) indicate upper crustal velocities of ~5.2 km/s; variations in the tau-p values from deepening topography have probably caused the apparent high velocity. Lines 4 East and the compilation show first order discontinuities at ~ 300m below A*, whereas line 4 South shows a smooth velocity gradient throughout the sediments. These differences are due to the details of smoothing and weighting the data.

These data have been previously interpreted by computing stack and semblance along hyperbolae in T-X space (Rohr, 1982). The velocity-depth function (Fig. 4) obtained was used to calculate theoretical tau-p values (Fig. 2). These fit the observed tau-p values quite well and show that the hyperbolic approximation is good for these data. Furthermore, reflectors A^C and β are better defined by this method. By comparison, the sediments' velocities interpreted from the tau-p map are too fast and the layers, therefore, are too thick. One could iterate between tau-p and velocity-depth profiles (Diebold et al., 1981) until a 'good' fit was obtained, but the large scatter in tau did not seem to justify such a painstaking procedure.

The ambiguities in interpreting the tau-p picks arise not only from the scatter in the data and but also from the character of the inverse equation. This is true whether interpreting just one line or a compilation of six lines. One inverts the difference between successive tau values which is typically on the order of 0.02 s. When the error for each tau value is equal to or larger than this difference, the error in the layer becomes larger than the layer itself:

$$Z + \delta Z = (T_2 \pm \delta T - T_1 \pm \delta T)/p = (T_2 - T_1 \pm 2\delta T)/p \quad (3.1)$$

$$\text{e.g.} \qquad = (0.02 \pm 0.04) \,/\, 0.3 = 0.07 \pm 0.14 \quad (3.1a)$$

Also, a very small change in tau, such as 0.01, results in a large change in the thickness since 1/p is always greater than 1.

3.6 SUMMARY

The data discussed here are not well constrained in tau, because of low signal-to-noise ratio and natural variability in topography of the reflectors. The properties of the inversion combined with the large errrors in tau result in a poorly constrained velocity-depth profile. Analysis of the same data along hyperbolae allows an interpretation of the sediments' velocity structure which is consistent with, but more detailed than the tau-p map. Thus, for low signal to noise ratio data consisting predominantly of precritical arrivals stacking along hyperbolae is more sensitive to the reflectors and is more easily interpreted for a velocity-depth function.

FIGURE CAPTIONS

Figure 1. Line 4 East: record section recorded by ocean-bottom hydrophone (OBH) 4 while shooting east. Heavy lines indicate the compressional basement reflection and between 3.4 and 5.7 km the shear basement reflection; conversion occurs at the top of layer β (Rohr, 1982).

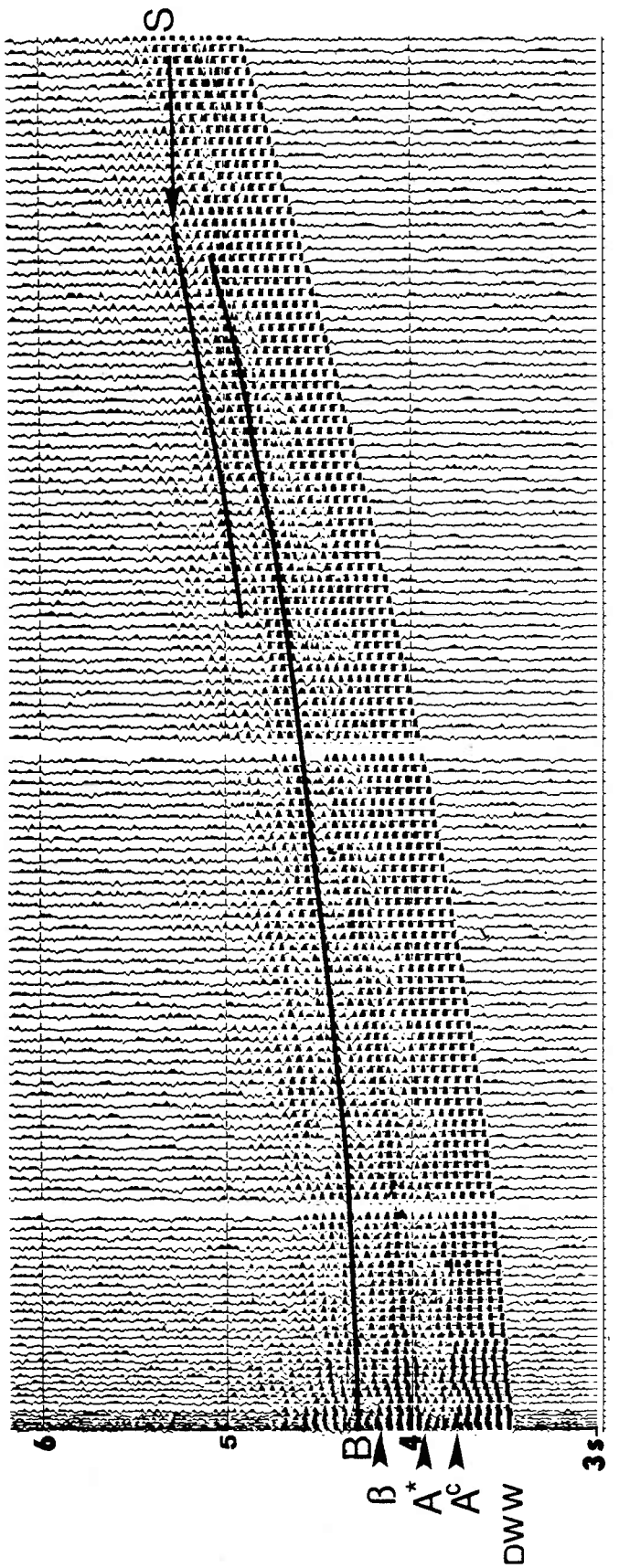

Figure 1.

Figure 2. Tau-p maps of lines 4 East and 4 North. The power of the semblance and stack function has been averaged over one signal length (0.10 s) and contoured 0 to 60 db every 6 db. A)Line 4 North: the water wave is the lowest quarter ellipse pattern, A* is the next and basement is the deepest. The basement critical p value is 0.23 $\pm$ 0.02s/km and high amplitude postcritical events are also observed at increasing p values. B) Line 4 East has a complicated basement pattern.

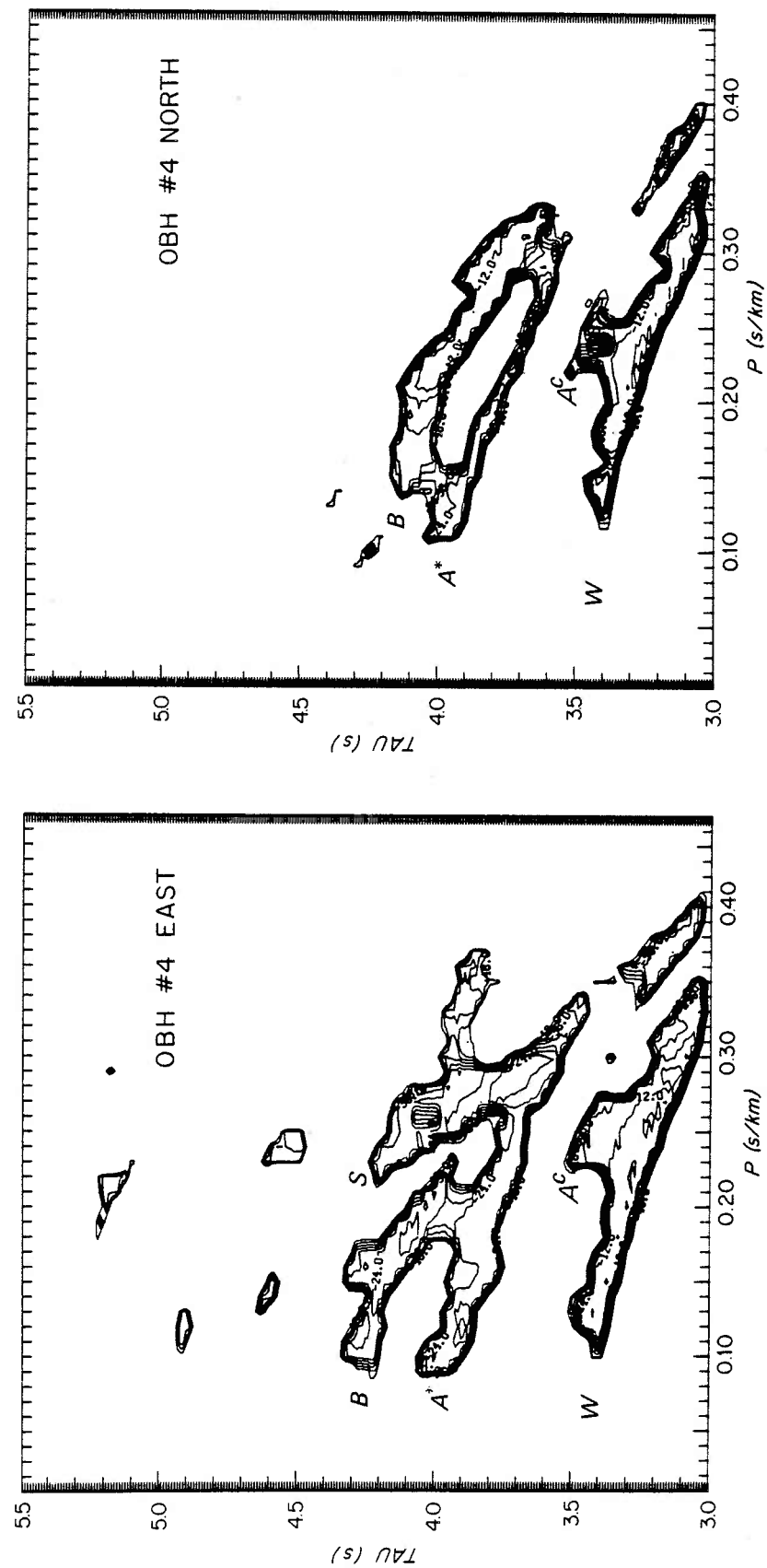
OBH #4 NORTH
OBH #4 EAST
TAU (s)
P (s/km)
5.5
5.0
4.5
4.0
3.5
3.0
0.10
0.20
0.30
0.40
A*
B
S
W
A^C

Figure 2.

Figure 3. Compilation of tau-p picks from each subarray on six lines received by OBH 4. The picks were chosen as the onset of each event in semblance, i.e. where semblance exceeds the threshold level. The fine lines are theoretical tau-p values calculated from a hyperbolic analysis of the same data (Rohr, 1982.). The water wave (W), reflector A*, and basement (B) were observed on all lines. Reflector A^C and β are poorly resolved. The shear reflections (S) are from basement; conversion from compressional to shear energy occurs at β. Given only the tau-p map their origin would not be interpretable. A different symbol is used for each line analysed.

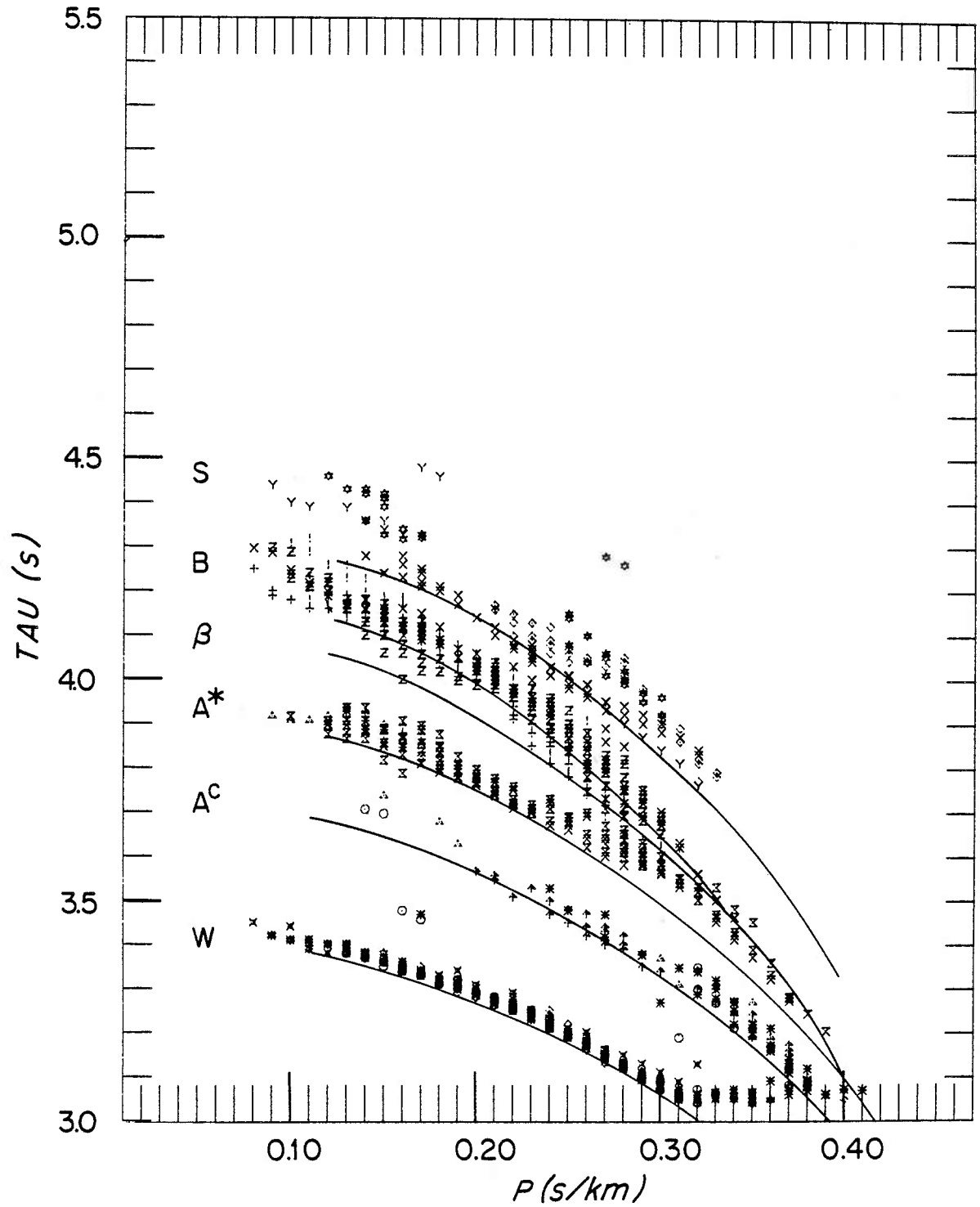

Figure 3.

Figure 4. Velocity-depth interpretations of basement tau-p values by the tau-sum method. Only basement was interpreted giving the velocity structure below reflector A*. Polynomials were fit to the tau-p values and evaluated every 0.01 s/km. Errors were computed from the standard deviation of the polynomial fit. A) line 4 South, B) line 4 East, C) line 4 North, D) from a compilation of the basement tau-p values from six lines, E) velocity- depth interpretation from hyperbolic analysis (Rohr, 1982.). The differences between the tau-sum inversions are caused by differences in the topography of each reflector and the details of smoothing the data. They are faster and thicker than the inversion from the hyperbolic analysis.

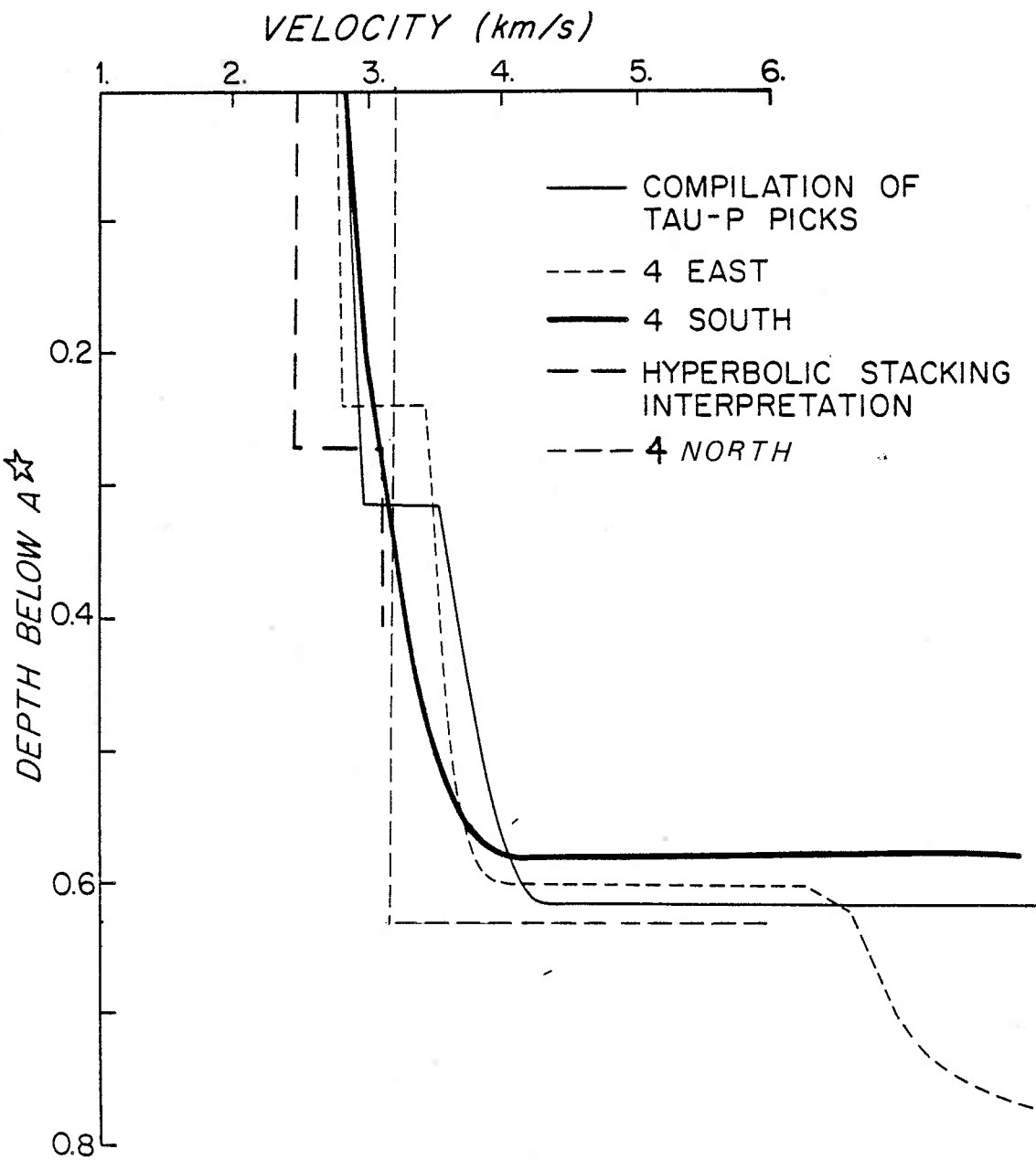
VELOCITY (km/s)
1.
2.
3.
4.
5.
6.
DEPTH BELOW A ☆
0.2
0.4
0.6
0.8
COMPILATION OF TAU-P PICKS
4 EAST
4 SOUTH
HYPERBOLIC STACKING INTERPRETATION
4 NORTH

Figure 4.

REFERENCES

Diebold, J.B. and P.L. Stoffa, 1980, The traveltime equation, tau-p mapping, and inversion of common mid-point data: Geophys., v.46, p.238-254.

Diebold, J.B., P.L. Stoffa, P. Buhl, and M. Truchan, 1981, Venezuela Basin crustal structure: J. Geophys. Res., v.99, p.7901-7923.

Ewing, J. and G.M. Purdy, Upper crustal velocity structure in the ROSE area of the East Pacific Rise: J. Geophys. Res., v.87. p.8397-8402.

Helmberger, D.V. and G.B. Morris, 1970, A travel time and amplitude interpretaition of a marine refraction profile: transformed shear waves: Bull. Seism. Soc. Amer., v.68, p.593-600.

Kennett, B.L.N., 1977, Towards a more detailed seismic picture of the oceanic crust and mantle: Mar. Geophys. Res., v.3, p.7-42.

Koelsch, D.E. and G.M. Purdy, 1979, An ocean bottom hydrophone instrument for seismic refraction experiments on the deep ocean: Mar. Geophys. Res., v.4, p.115-125.

Purdy, G.M., 1982, The seismic structure of 140 my old crust in the western central North Atlantic Ocean: Geophys. J. Roy. Astr. Soc., in press.

Rohr, K., 1982, Hyperbolic Stacking of Wide-angle Reflections from Deep-Sea Sediments, subm. to J. Geophys. Res.

Stephen. R.A., K.E. Louden, and D.H. Matthews, 1980, The oblique seismic experiment on DSDP Leg 52: Geophys. J. Roy. Astr. Soc.,

v.60, p.289-300.

Stoffa, P.L., P. Buhl, J.B. Diebold, and F. Wenzel, 1980, Direct mapping of seismic data to the domain of intercept time and ray parameter - a plane wave decomposition: Geophys., v.46, p.255-267.

Tucholke, B.E., Relation between acoustic stratigraphy and lithostratigraphy in the western North Atlantic Basin, in Tucholke, B.E., Vogt, P.R., et al., 1979, Initial Reports of the Deep Sea Drilling Project, v.43: Washington (U.S. Govt. Printing Office), p.827-846.

Chapter 4

Variations of the Amplitudes of Reflections from Oceanic Basement

K. Rohr

W.H.O.I.-M.I.T. Joint Program

W.H.O.I.

Woods Hole, Ma. 02543

4.1 ABSTRACT

A study of the amplitudes of wide-angle reflections from the sediment-basement interface shows that the uppermost portion of Layer 2 is homogeneous on the 0.15-1.00 km scale, but not on the 3.0-8.0 km scale. The amplitude vs range patterns of the basement reflections recorded on 30 seismic lines were examined; most patterns are affected by the rough topography of the sediment-basement interface. Three lines have smooth travel-time curves and appear to be unaffected by topography. The amplitude patterns of these lines are different from each other; they can be modelled by synthetic seismograms computed from velocity structures which have different thicknesses of a transition zone between the limestone sediments and the basaltic crust.

4.2 INTRODUCTION

The amplitudes of wide-angle reflections have been infrequently used in the study of the seismic structure of upper oceanic crust, yet they contain much information about the physical state of the upper crust. The amplitudes of the wide-angle reflections are sensitive to the compressional (P) and shear (S) wave velocity contrast at the sediment-basement interface (Spudich and Helmberger, 1979, White and Stephen, 1979). If these values are known in the upper medium (the sediments) one can then interpret the P and S wave velocities in the lower medium, the basaltic layer 2. White (1979) has discussed the factors affecting the amplitudes of wide-angle reflections in oceanic crustal studies and has interpreted the amplitudes of two sets of basement reflections.

Studies of seismic refractions give a general picture of the structure of the upper portion of the crust, but they are only rarely capable of directly measuring it. Analyses of the amplitudes of seismic refractions have shown that the velocity structure of the crust consists of velocity gradients of different values, not isovelocity layers (Helmberger and Morris, 1969, 1970, Kennett, 1977, Whitmarsh, 1978, Stephen et al., 1980, Spudich and Orcutt, 1980, Ewing and Purdy, 1982) and the structure in the uppermost 0.5 to 1.0 km of the crust has been inferred from refractions deeper in the crust (Ewing and Purdy, 1982). Refractions from the first few hundred meters of Layer 2 are rarely observed by instruments placed above this layer (Stephen, 1982), because of interference effects

from the basement reflection as well as earlier arrivals. Borehole seismometers placed within or below the top of Layer 2 do not suffer the same interference effects, but have been infrequently deployed.

This paper discusses the amplitudes of wide-angle reflections as observed on 30 airgun lines received by six ocean-bottom hydrophones (OBH's) (Koelsch and Purdy, 1979) located within 15 km of each other. We attempt to interpret the changes of amplitude of the basement reflection with range according to the structure of the oceanic crust. This is possible on three lines only; the interpretation is frustrated by variations in topography of the sediment-basement interface on many of the lines studied.

4.3 EXPERIMENT

Wide-angle reflections from upper oceanic crust in the western North Atlantic were recorded during cruise 92 of the R/V KNORR (Fig. 1). The oceanic basement is ~140 my old and was formed by sea-floor spreading at a rate of ~1cm/yr. The water is 5.1 km deep and the sediments are typically 0.7 s thick (Rohr, 1982) (Fig. 2). Eight ocean-bottom hydrophones were deployed in a cross-shaped pattern ~10 km long and 15 km wide (Fig. 3). A 0.66L (40 in^3) airgun which produced a dominantly 20 Hz signal 0.2 s long was fired along lines of varying azimuths to the instruments (Fig. 2); shot separation is approximately 30-40 m. For simplicity in discussion, parallel to the magnetic lineations will be called north-south and perpendicular east-west. A standard processing method was used to

digitise the data (Purdy, et al 1982) at 0.01 s intervals and to compute the horizontal ranges (Rohr, 1982). The data (Fig. 4) show arrivals from the direct water-wave, and reflections from the three sedimentary reflectors (A^c, A*, β) (Tucholke, et al., 1979) and acoustic basement. Of particular relevance to this study is the existence of β above the basement; this reflector is usually associated with the top of Neocomian limestones (Tucholke, et al., 1979).

4.4 PREDICTED AMPLITUDE VARIATIONS

The changes in amplitude which occur for critical and postcritical reflections from the sediment-basement interface are the most useful in the interpretation of the velocity structure at the sediment-basement interface. While slight changes in the precritical reflection amplitudes can be interpreted for the velocity structure (Ostrander, 1982), the data described here are too noisy to allow the interpretation of minute variations in amplitude. The change in amplitude of the reflections from precritical to postcritical angles of incidence, however, is predicted to be large (Fig. 5). The reflection coefficient vs ray phase velocity diagram shown here was calculated from the Zoeppritz equations for semi-consolidated limestones of P wave velocity of 3.1 km/s (Table 1) (Rohr, 1982) and a Poisson's ratio 0.4 overlying basement with P wave velocities from 3.5-5.0 km/s and Poisson's ratio of 0.3. The precritical reflection coefficients vary from

0.1-0.3 whereas the critical reflection coefficients vary from 0.8-1.0 and postcritical from 0.4-0.8. The magnitude of the increase in reflection coefficients at the critical point depends on the P and S wave velocity contrast at the interface. The location of the P-wave critical point (usually referred to as 'the' critical point) depends only on the P wave structure at the interface. The magnitude of the P-wave postcritical reflections depends both on the P and S wave structure, since shear wave transmission typically increases between the P and S wave critical points.

In actuality, waves not rays, are being reflected from the sediment-basement interface, and interference with the energy refracted from the basement diminishes the amplitude of the critical reflections at the ray theoretical critical point (Cerveny, 1967; White, 1980); this effect is frequency dependent. The first large amplitude reflections observed are in fact postcritical reflections. Since this effect will almost always be present in field observations, we will simply call the increase in amplitude the critical point. The difference in range between the critical point and the first observed increase in amplitude can be as much as 1 km for an ocean bottom instrument, a 20 Hz source, the sediment structure described in Table 1, and basement with a velocity of 5.2 km/s.

4.5 OBSERVED AMPLITUDE VARIATIONS

To reliably interpret the variations in amplitude of the

basement reflections in terms of the velocity structure one must be sure that other sources of amplitude variation are not present. Ideally one would interpret wide-angle reflections from a flat interface between laterally homogeneous media. To date, this is the only structure which can be modelled rapidly and easily. Lateral variations in the velocity structure across the interface will affect the reflection amplitudes as will any deviations of the shape of the interface from a planar surface.

The oceanic basement is a notably rough interface; it is commonly identified by numerous diffraction hyperbolae. On nearly half the lines collected the basement reflections are so disrupted as to preclude modelling the amplitude variations. West of OBH 4 a fault scarp (Rohr, 1982) (Fig. 6) is evident in the basement reflections and on a line shot northeast of OBH 3 (Fig. 7) little coherent energy is returned from the sediment-basement interface.

In the remainder of the data the travel-times of the basement reflections vary by 0.1 s or less. The variations in amplitude observed within seven lines received by OBH 4 are quantified and discussed below.

4.6 ENERGY VS RANGE

To quantify the changes observed in amplitudes of the basement reflections, the energy of each reflection was calculated for each shot. The amplitudes recorded within a 0.1 s time window were squared and summed. The position of the time window was calculated

from the equation of the hyperbola best fitting the basement reflections. Since the data have been stacked along hyperbolae in an analysis of the sediment velocities (Rohr, 1982), the coefficients of the hyperbolae are easily obtained.

The compilation of profiles of the basement reflection's energy as a function of horizontal range is shown for seven lines of shots received by OBH 4 in (Fig. 8). The western halves of the seismic lines are all disrupted by a fault (viz. Fig. 6) (Rohr, 1982) and, therefore, are not included in this analysis. The actual values of energy have had a ten-point (~0.35 km) running average applied to them in order to eliminate the very short scale variations in amplitude caused by changes in airgun firing pressure, airgun depth, sea state, etc.

The compilation (Fig. 8) of the seven lines analysed from OBH 4 shows a scatter of values at all ranges with a marked increase in both the average value and the scatter at 3.0 km. The large amplitude reflections observed at ranges greater than 3 km are postcritical reflections. Tracing rays from a surface shot to an instrument on the sea-floor shows that critical point for basement with a velocity of 5.0 km/s is at 2.5 km range. The sediment structure (Table 1) used in the ray tracing was computed from the same data set discussed here (Rohr, 1982). Similarly, critical point for basement of 3.5 km/s is at 4.0 km.

Examining the lines individually (Fig. 9) shows that only the lines shot perpendicular to the spreading direction (north-south)

have distinct critical points. Lines 4N, 4NNE and 4S show a marked increase in energy at ~3.5 km; the amplitude increase on line 4N is substantially larger than on 4S and 4NNE.

The four remaining lines show variations in the energy of the basement reflections not predicted by the Zoeppritz equations. Variations of the precritical reflections (at less than 2.5 km range) occur over distances of less than one kilometer. This could be caused either by lateral heterogeneities in the velocity structure or topographic effects of the interface. Ray tracing shows that rays which start at the sea surface at 1 and 2 km range from the OBH actually reflect from the basement 0.15 and 0.35 km from the instrument. Close examination of the records shows that the changes in amplitude of the basement reflections are associated with interference effects, changes in travel time of ~0.1 s, or both. These observations combined with the short distances involved (200 m) favor the interpretation that the amplitude variation is caused by topographic variations. If velocity heterogeneity is the cause of such variations, it must be approximately on the scale of the wavelength of the seismic energy; such effects are extremely difficult to model.

Ray tracing reflections from an inward-facing fault scarp shows that focussing and defocussing of the basement reflection can occur (Fig.10). Rays were shot from the receiver position on the sea-floor to the sea surface; their ray parameter (p) values varied from 0.1-0.3s/km and were incremented every 0.005s/km. The basement

bathymetry profile was taken from a normal incidence seismic reflection profile recorded by a deep-towed hydrophone east of OBH 4 (Purdy and Gove, 1982). The depth to basement was digitized in time, converted to depth using the sedimentary velocity profile in Table 1 and fit with a cubic spline. The ray, once past the deepest sedimentary reflector, β, is stepped down at increasingly fine distances until the point of intersection with the basement was found within 0.0001km. The angle of reflection was then computed from the incidence angle and the local gradient of the spline and the ray was traced back up through the sediments. Wave fronts, of course, behave in a more complex manner than rays, but here we use the simplistic correlation of ray density and amplitude. Fig. 10A shows the defocussing of rays at ranges greater than 3.0 km from the instrument and 10B shows the focussing of rays reflecting from the scarp face. The only parameter which is different in the two cases is the receiver's position with respect to the fault scarp.

Examining the data set closely shows that only three lines have basement reflections with little deviation in their travel-times from a smooth hyperbola. These are lines 4 North (Fig. 4), 3 Southeast (Fig. 11) and 2 West (Fig. 12). Inferring then that there is little topographic disturbance on these lines, their amplitude variations with range are interpreted in terms of the velocity structure at the sediment-basement interface.

4.7 SYNTHETIC SEISMOGRAM MODELLING

Synthetic seismograms computed from a velocity structure consisting of a transition zone of varying thicknesses between the sediments and basement produces record sections very similar to the three seismic lines which are free of topographic disruption. The Fuchs-Muller reflectivity algorithm (Fuchs and Muller, 1971) was used; the source was a 0.1s long and contained two cycles of a 20 Hz sine wave. This source was chosen because the basement reflections were generally 0.1 s long, and a fast-Fourier transform of data recorded on six lines by OBH 4 showed that the seismic energy was predominantly 20 Hz. Since the measurement of velocity gradients is frequency dependent, the consistent character of the airgun source is an important factor in the interpretation of the different lines. In all velocity-depth profiles the sediment structure (Table 1) remained the same as did the higher velocity basement. The latter had an initial velocity of 5.2 km/s, a gradient of 2/s and a Poisson's ratio of 0.3. The sediments immediately overlying the basement are semi-consolidated limestones and have a Poisson's ratio of 0.4 (Rohr, 1982). In each case the energy of the basement reflection was calculated as above within a 0.1s time window and plotted vs range (Fig. 14).

Line 4N (Fig. 4 and 13) is best modelled (Fig. 14) by a transition zone 150 m thick. This thickness is approximately equal to one wavelength of the incident compressional seismic energy. The largest energy of the basement reflections occurs at 3.5 km and the

energy then decays rapidly to a smaller amplitude.

Line 3SE (Fig. 11 and 15) is best modelled by a velocity profile with a transition zone 300m thick, equal to two wavelengths of the incident compressional energy. The postcritical increase in amplitude occurs at 4.0m km after a predicted zone of interference between the basement reflection and refraction.

Line 2W (Fig. 12 and 16) is best modelled by a velocity profile with no transition zone i.e. much less than a wavelength in thickness. There is a general increase in the amplitudes of the wide-angle reflections at 3.0 km; the amplitudes do not change significantly with range.

The amplitudes of the synthetic seismograms computed from a transition zone 150m thick was not sensitive to varying the Poisson's ratio of the transition zone and basement. In each case modelled, the compressional wave structure remained constant, only the shear wave structure was modified so that the Poisson's ratios were 0.25, 0.30, and 0.35. White (1979) modelled the changes in reflection coefficient at a sediment-basement interface for sediments with a Poisson's ratio of 0.5 overlying basement of different Poisson's ratio and found considerable variation in the amplitudes od the postcritical reflections. Here, however, the sediments immediately overlying the basement have a Poisson's ratio of 0.4 and the change in contrast is not measurable in the amplitudes of the postcritical wide-angle reflections.

4.8 DISCUSSION

The differences in the amplitude patterns of the basement reflections recorded on three seismic lines studied here indicate that the velocity structure of the uppermost Layer 2 is significantly different from line to line. Each line was received by a different instrument; these three instruments were located within 3 and 8 km of each other. Modelling the basement reflections' amplitudes by synthetic seismograms, albeit a non-unique method, does give an indication of the kind of structural variations capable of causing the amplitude variations observed. While many sets of velocity models could produce similar amplitude patterns, the family of models using a transition zone of thicknesses varying from 0-300m is simple.

The transition zone between the sediments and the basaltic crust is by definition, characterized by seismic velocities intermediate between the sediments and basalt; it most likely consists of a mixture of fractured altered basaltic material, sediments and alteration minerals. Fracturing is considered to be the main factor which lowers the velocity of the basaltic basement measured in the field to as low as 3.5 km/s relative to the hand specimens of basalt which have velocities of 6.0 km/s (Houtz and Ewing, 1976; Hyndman and Drury, 1976; Kirkpatrick, 1979). Fractures can occur either in a relatively regular pattern perpendicular to the spreading direction in basalt flows, or randomly as in a breccia. On old, sediment-covered oceanic crust fractures are likely to be filled

with both sediments and low temperature alteration products (Elthon, 1982). The actual assemblage of the minerals and their specific composition depends on both the temperature history of the rock and how much water has flowed through it. Alteration can lower the velocity of basalt from 6.0 km/s to 5.0 km/s (Christenson and Salisbury, 1973). Basalts of a similar age and which had been altered to different degrees were drilled at the nearby DSDP Sites 417A, 417D and 418A (Donnelly et al., 1981a); the basalt samples' compressional wave velocities ranged from 4.5-6.0 km/s with an average value of 5.5 km/s +/- 0.5 km/s (Hamano, 1979; Christensen et al., 1979). In the crust studied here the sediments immediately overlying basement are limestone with a compressional velocity of 3.1 km/s and the alteration minerals could be saponites, celadonite, or zeolites (Donnelly et al., 1979b; Honnorez, 1982) which tend to have velocities of 3.0 to 5.5 km/s.

An alternative explanation of the transition zone is that volcanic flows are intercalated with sedimentary layers. Seismic waves travelling through many layers tens of meters thick can not distinguish the layers individually, but travel at a velocity intermediate to that of the basalt and the limestone. DSDP has drilled such a volcanic complex in the south Pacific at Sites 462 and 462A (Larson, et al., 1981).

The location of the instruments supports the interpretation of the transition zone as a zone of highly fractured basalt. Transition zones 150-300m thick were measured by instruments located

near the base of a faulted block (Fig. 17), whereas no transition zone could be detected by the instrument which lay on relatively flat topography west of the same faulted block. A normal incidence seismic reflection profile recorded by a deep-towed hydrophone (Purdy and Gove, 1982) shot over instruments 2 and 4 shows the basement topography in detail (Fig. 17). OBH 3 was 3 km south of OBH 4 (along strike of the fault block) and although no deep-towed hydrophone profile was shot near the instrument, it must also be in a region of rough topography. Thus, fracturing and alteration is found to affect the basalt to greater depths in heavily faulted zones of high relief rather than comparatively flat-lying basalt.

A similar correlation of velocity and local topography can be found near DSDP Site 417. A deep towed hydrophone profile (Purdy et al., 1980) over 417 shows that 417A is on the top of an abyssal hill and that 417D is near the base of the hill to the west. At 417D the basalts were relatively fresh and an oblique seismic experiment (Stephen, 1979) found a sharp sediment-basement interface with the basement initial velocity of 4.8 km/s and a velocity gradient of 1.2/s. Thus, both the position and velocity profiles of line 2W and 417D are similar. At 417A the basalts were highly altered; no seismic experiment, however, was carried out to measure in situ velocities.

The thickness of the transition zone varies near each of the three instruments studied; this gives an indication of the scale of lateral heterogeneity in the uppermost Layer 2. In this experiment

the dominant frequency was 20 Hz so the wavelength of the seismic energy propagating through the limestones and the basement was 150-250m. Ray tracing shows that the basement reflections have reflected from the sediment-basement interface within 1 km of the instrument. On the three lines studied the basement reflections appear to be from a homogeneous interface, but each line is significantly different from the others. This implies that homogeneity may exist on a 0.15 to 1.00 km scale in the uppermost Layer 2 but not on the scale of the instrument separation, 3.0 to 8.0 km.

The lateral heterogeneity of Layer 2 has been much discussed (Ewing and Houtz, 1979; Spudich and Orcutt, 1980b), but few measurements of the scale or degree of heterogeneity have been made. Measuring lateral heterogeneity seismically is difficult because resolution is limited to a seismic wavelength (typically 0.5-1.0 km), and the lack of interpretation methods which are capable of including lateral heterogeneity in their solution. A seismic refraction study on young oceanic crust in the Pacific has shown that Layer 2 is homogeneous on the scale of 2 km, but heterogeneous on the scale of ~100 km (Purdy, 1982a). Discovery of basalts which were altered to very different degrees in oceanic crust ~110 my old at DSDP Sites 417A and 417D and 418A suggested that the uppermost Layer 2 is heterogeneous on the scale of ~1 km.

The experimental configuration discussed here allows a resolution of the velocity structure at the sediment-basement

interface not usually acheived by seismic refraction experiments. A 20 Hz source produces strong basement reflections, but weak seismic refractions because of the attenuation of high frequencies in the basaltic crust. Thus, the reflections discussed here have twice the resolution of refractions which are usually measured from 10 Hz seismic energy. Another factor aiding spatial resolution is that energy reflects from an interface over a limited area, whereas refracted energy travels both horizontally and vertically through the crust before reaching the recording instrument.

Varying the thicknesses of the transition zone between the sediments and the basalt significantly affects the shear wave refracted arrivals from the deep crust. For normally incident P-wave energy the time spent in the 150 m and 300m thick transition zones is 0.04s, and 0.08s respectively, and for shear waves 0.07 and 0.15s. White and Stephen (1980) have shown that the conversion of compressional to shear energy is most efficient at a sharp interface across which there is a strong contrast in the Poisson's ratio of the media, and when the compressional velocity of the incident energy is approximately equal to the shear wave velocity of the converted energy. The more gradual the change in velocity (as in a transition zone) the less conversion occurs. Thus the thickest (300m) transition zone should be the least efficient in the conversion of compressional to shear energy and the sharp interface should be the most efficient. The amount of energy converted affects the amplitudes of the Layer 3 and moho shear refractions;

for a refraction line across this section of oceanic crust one should observe great variability in the refracted shear arrivals' amplitudes, and their travel times could vary by as much as 0.15 s. This is in fact observed on refraction lines shot to these OBH's in the same experiment and reported in Purdy (1982b). The variability of shear refracted amplitudes has been noted in many experiments (Ewing and Ewing, 1959, Spudich and Orcutt, 1980b) and is most likely caused, as in this case, by the variability in the character of the sediment-basement interface.

The fact that on the majority of the thirty lines studied here the basement reflections are disrupted by topography shows that the shape of the sediment-basement interface is an important factor affecting the basement reflections' amplitudes. Purdy (1982a) has shown the importance of this interface's topography in the interpretation of refracted arrivals, and White and Stephen (1980) have discussed the effect that the roughness of this interface can have on the conversion of compressional to shear energy at the sediment-basement interface. This study shows that reflected energy can be focussed as well as scattered by the sediment-basement interface.

4.9 SUMMARY

The amplitude patterns of wide-angle reflections from the sediment-basement interface differ on three seismic lines recorded by three different instruments located 3-8 km apart from each

other. Modelling by synthetic seismograms suggests that varying thicknesses of a transition zone between the limestone sediments and the basaltic crust exist beneath the instruments. Greater thicknesses of the transition zone have been interpreted to exist underneath the instruments located at the base of a fault block. The transition zone may be a mix of fractured altered basalt, sediments, and low temperature alteration minerals; different thicknesses of such a layer can be interpreted to indicate that weathering and hydrothermal alteration are spatially heterogeneous processes. Thus, the uppermost portion of Layer 2 is homogeneous on a scale of 0.15-1.0 km, but heterogeneous on a scale of 3 to 8km. On other lines studied the amplitudes of the basement reflections were affected by the rough topography of the sediment-basement interface, and they could not be interpreted by a laterally homogeneous model. Topography of the sediment-basement interface affects both the amplitudes of the compressional and shear refractions (Purdy, 1982a; White and Stephen, 1980); the presence of varying thicknesses of the transition zone will be most noticeable in the shear wave refractions.

TABLE 4.1 Two-way travel-time- stacking velocity values averaged for OBH's 4

	Two-Way Travel Time (s)		Stacking Velocity (km/s)	
	OBH 4			
W	3.43 +/-	0.01	1.50 +/-	0.01
A^C	3.75	0.01	1.52	0.01
A*	3.95	0.01	1.55	0.01
β	4.15	0.01	1.62	0.02
B	4.24	0.05	1.68	0.04
B'	4.31	0.10	1.81	0.05

Figure 1. Western North Atlantic Ocean (after Schouten and Klitgord, 1978) showing area of study (black box) south-west of Bermuda. Mesozoic magnetic anomalies M-0, M-16 and M-25 shown in heavy black lines. Crust studied is south of a well located fracture zone and was formed during a period of constant spreading velocity.

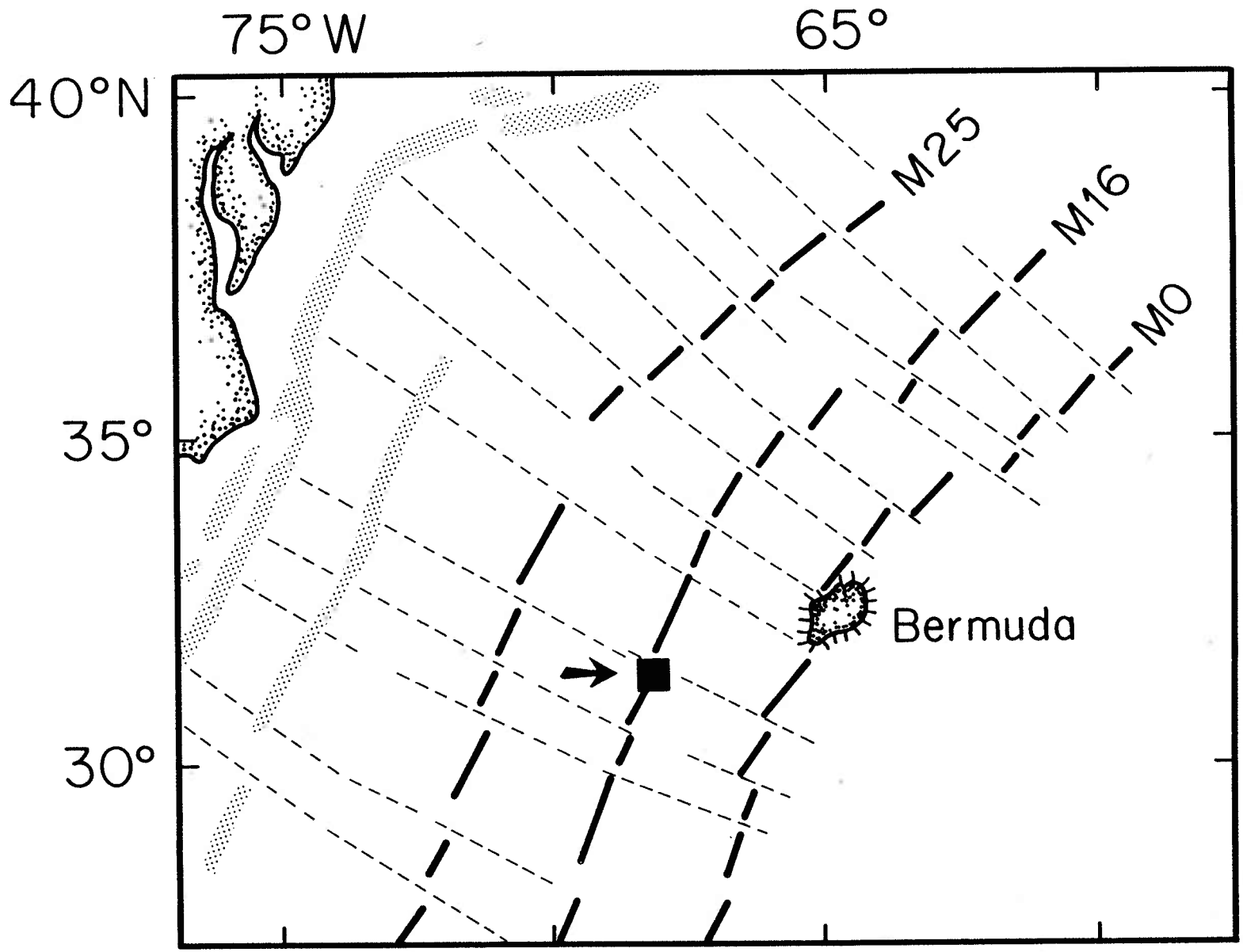

1.

Figure 2. Contour chart of sediment thickness as measured from 0.66L (40in^3), 4.95L (300 in^3), and 16.5L (1000 in^3) airgun normal incidence seismic reflection records. Stippled area shws sediments less than 0.50 s thick. Contour interval is 0.1 s. The fracture zone can be clearly seen in the peaks and troughs in the northeast corner of the chart. The two ridges parallel to magnetic lineations can be seen by the decrease in thickness of the sediments to less than 0.4 s. The experiment was carried out east of the easternmost ridge. Arrow indicates direction of magnetic lineations.

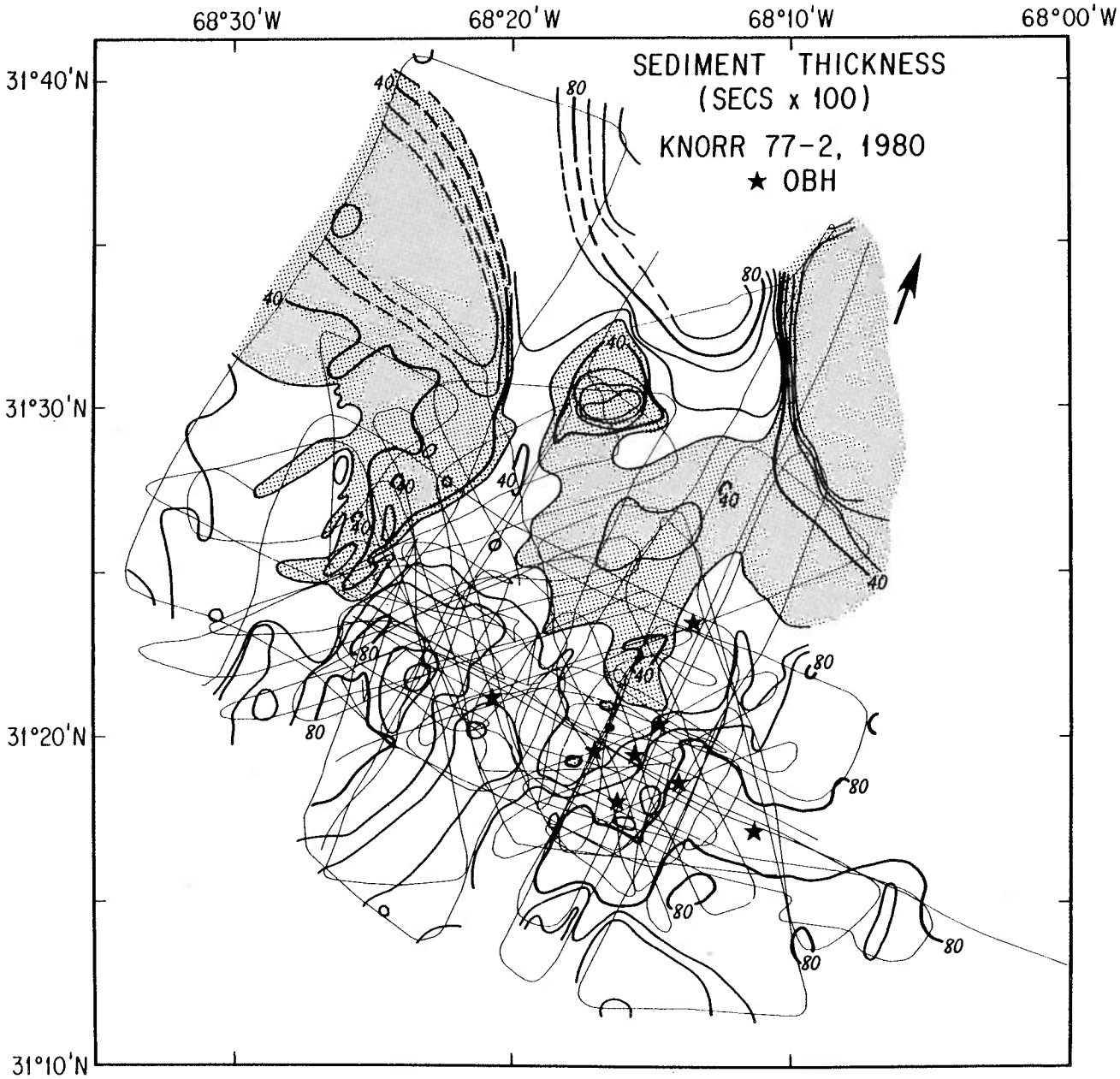
68°30'W
68°20'W
68°10'W
68°00'W
31°40'N
31°30'N
31°20'N
31°10'N
SEDIMENT THICKNESS
(SECS x 100)
KNORR 77-2, 1980
★ OBH
40
80

Figure 3. Ocean-bottom hydrophone (OBH) positions and 0.66L ($40in^3$) airgun track lines. Heavy lines indicate track lines analyzed by hyperbolic stacking. Only lines which came within one kilometer of the instrument at their closest approach were analyzed; arrivals out to 5 km were used since beyond this range arrivals from the different reflectors are not clearly separated in time. For simplicity in discussion, parallel to the magnetic lineations will be called north-south and perpendicular east-west.

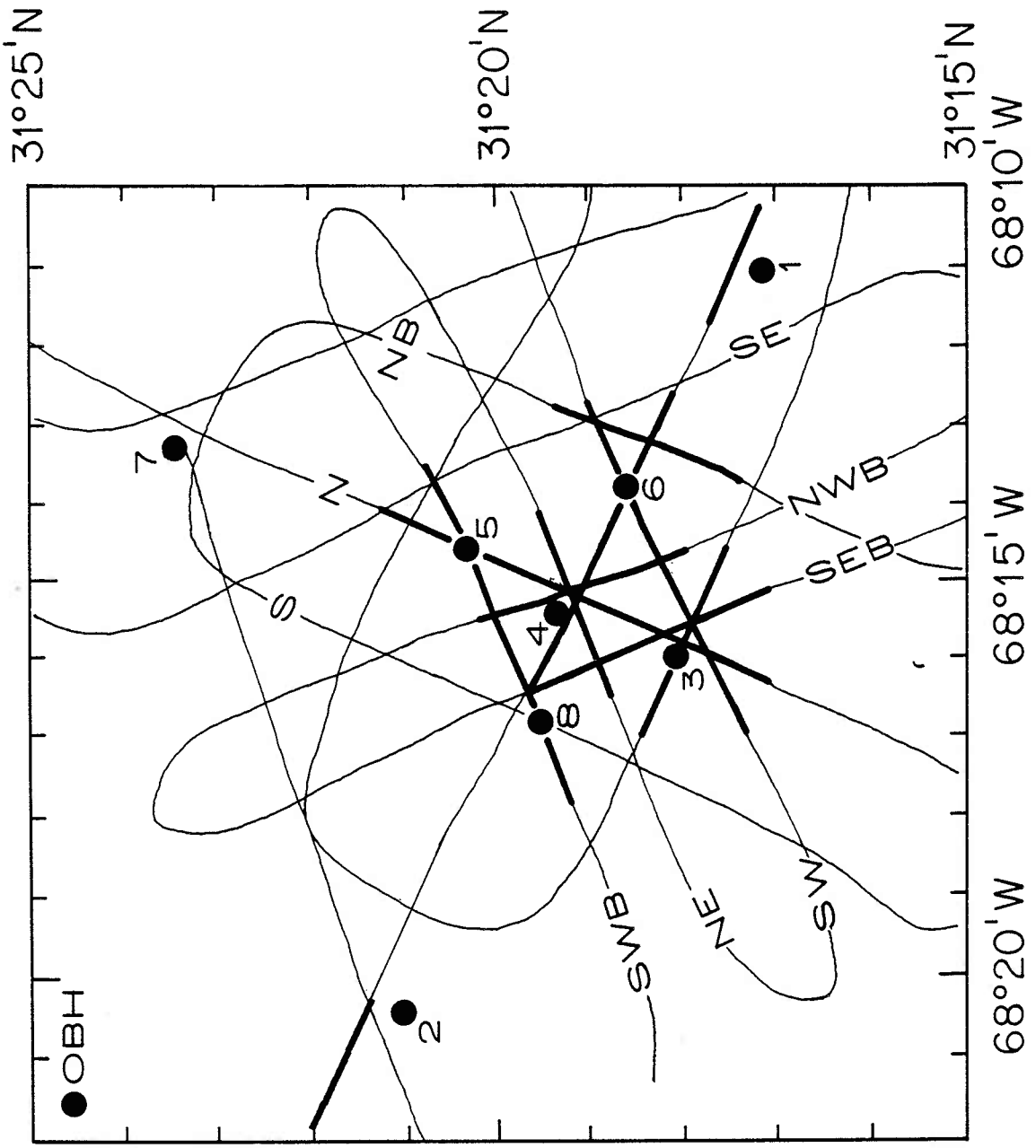
31°25'N
31°20'N
31°15'N
68°10'W
68°15'W
68°20'W
OBH
1
2
3
4
5
6
7
8
NB
SE
N
NWB
S
SEB
SWB
NE
SW

Figure 4. 0.66L ($40in^3$) airgun data Line 4N, received by OBH 4 shot while steaming north. Heavy line indicates compressional basement reflector. Note large increase in amplitude of the basement reflection at critical point, ~3.5 km horizontal range.

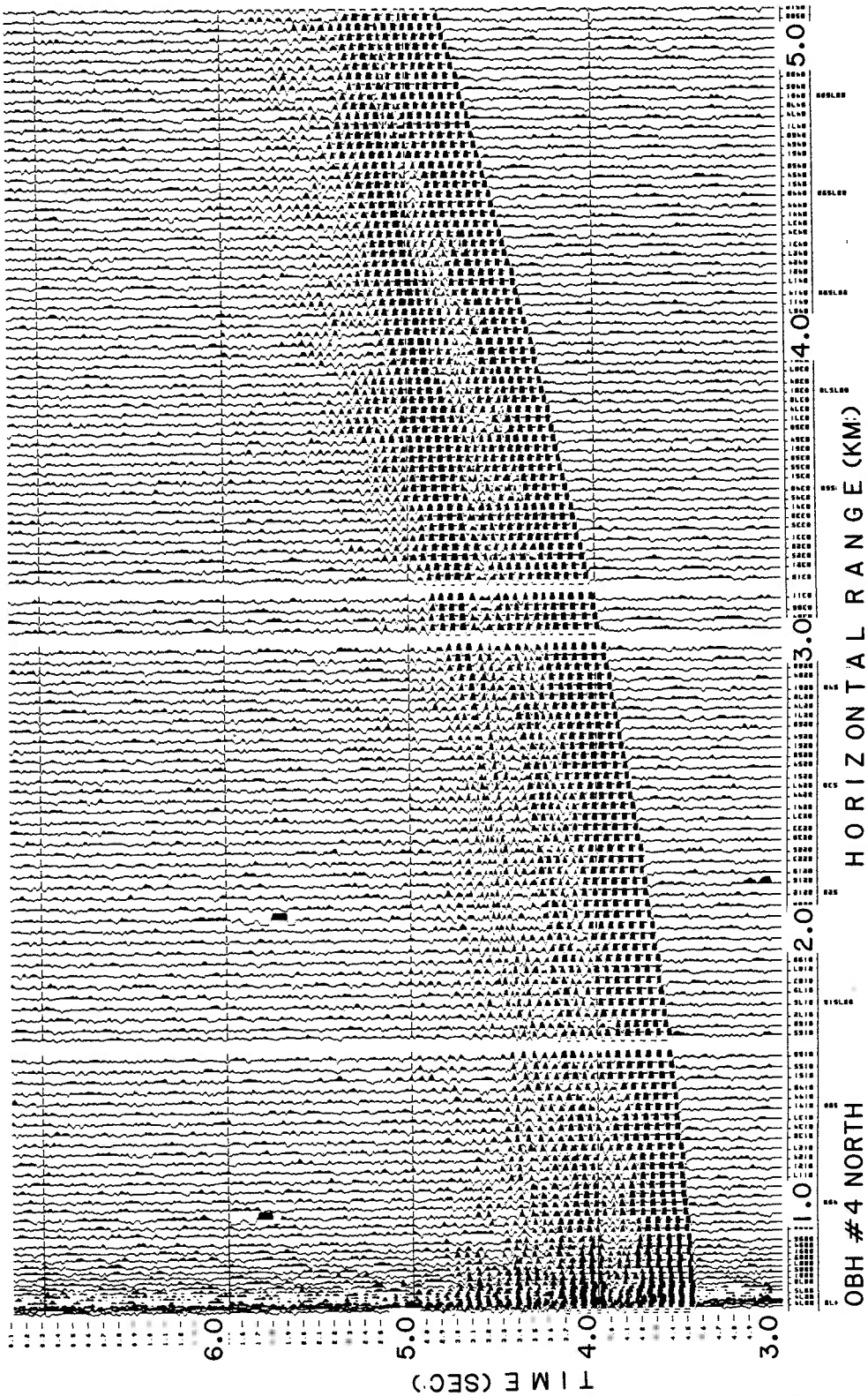
OBH #4 NORTH
HORIZONTAL RANGE (KM)
1.0
2.0
3.0
4.0
5.0
TIME (SEC)
6.0
5.0
4.0
3.0

Figure 5. Amplitude vs ray phase velocity calculated from the Zoeppritz equations for reflections from a flat lying interface between semi-consolidated limestones (Poisson's ratio=0.4, P-wave velocity=3.1 km/s) overlying basement of Poisson's ratio=0.3 and P-wave velocities equal to A) 5.3 km/s, B) 4 km/s and C) 3.5 km/s.

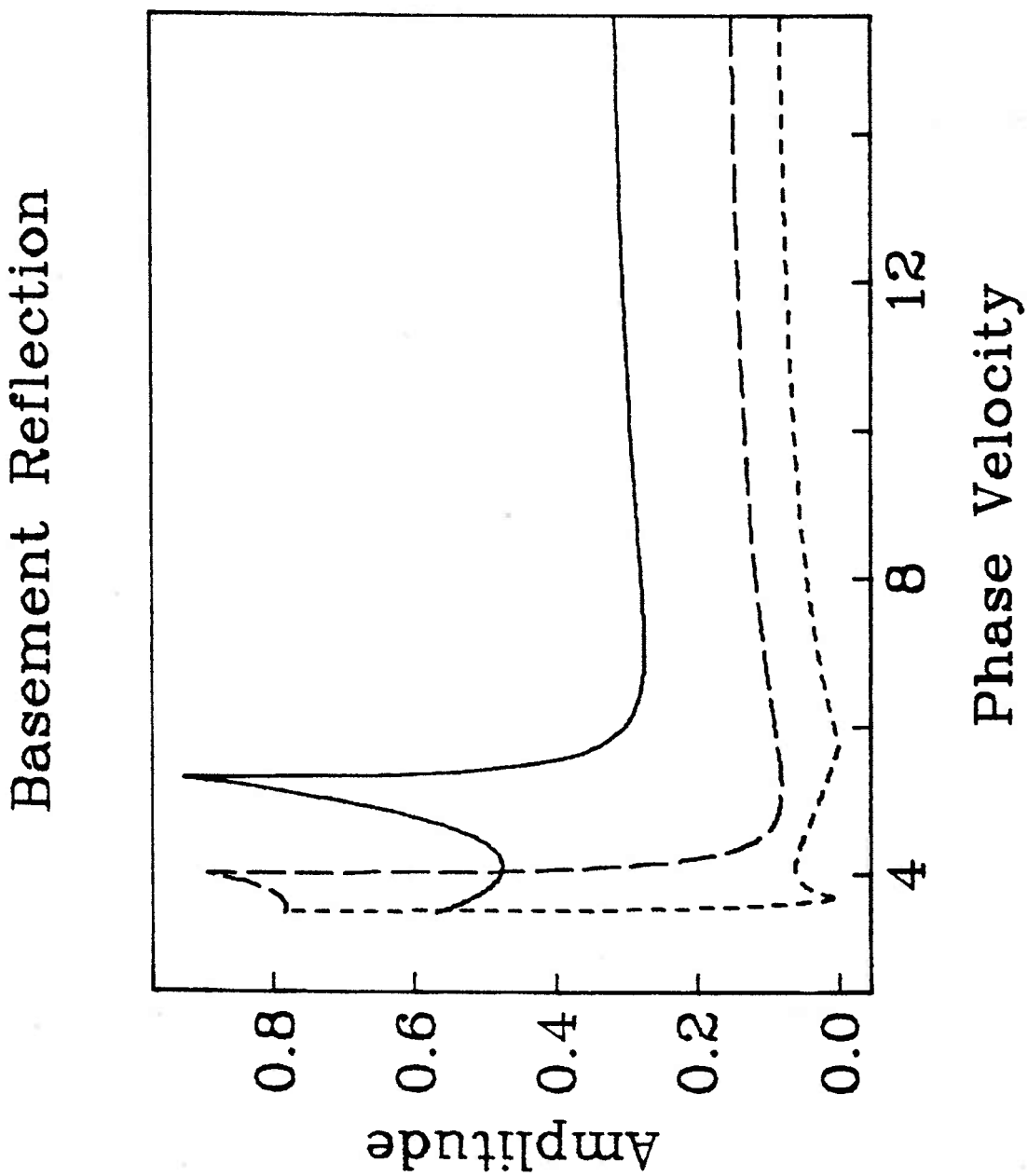
Basement Reflection
Amplitude
0.0
0.2
0.4
0.6
0.8
4
8
12
Phase Velocity

5.

Figure 6. 0.66L (40in^3) airgun data Line 4W shot while steaming west. Data have been filtered 0-10 Hz. Note break in basement reflector at 2 km horizontal range with basement reappering earlier at 2.5 km horizontal range. Heavy lines indicate compressional basement reflections.

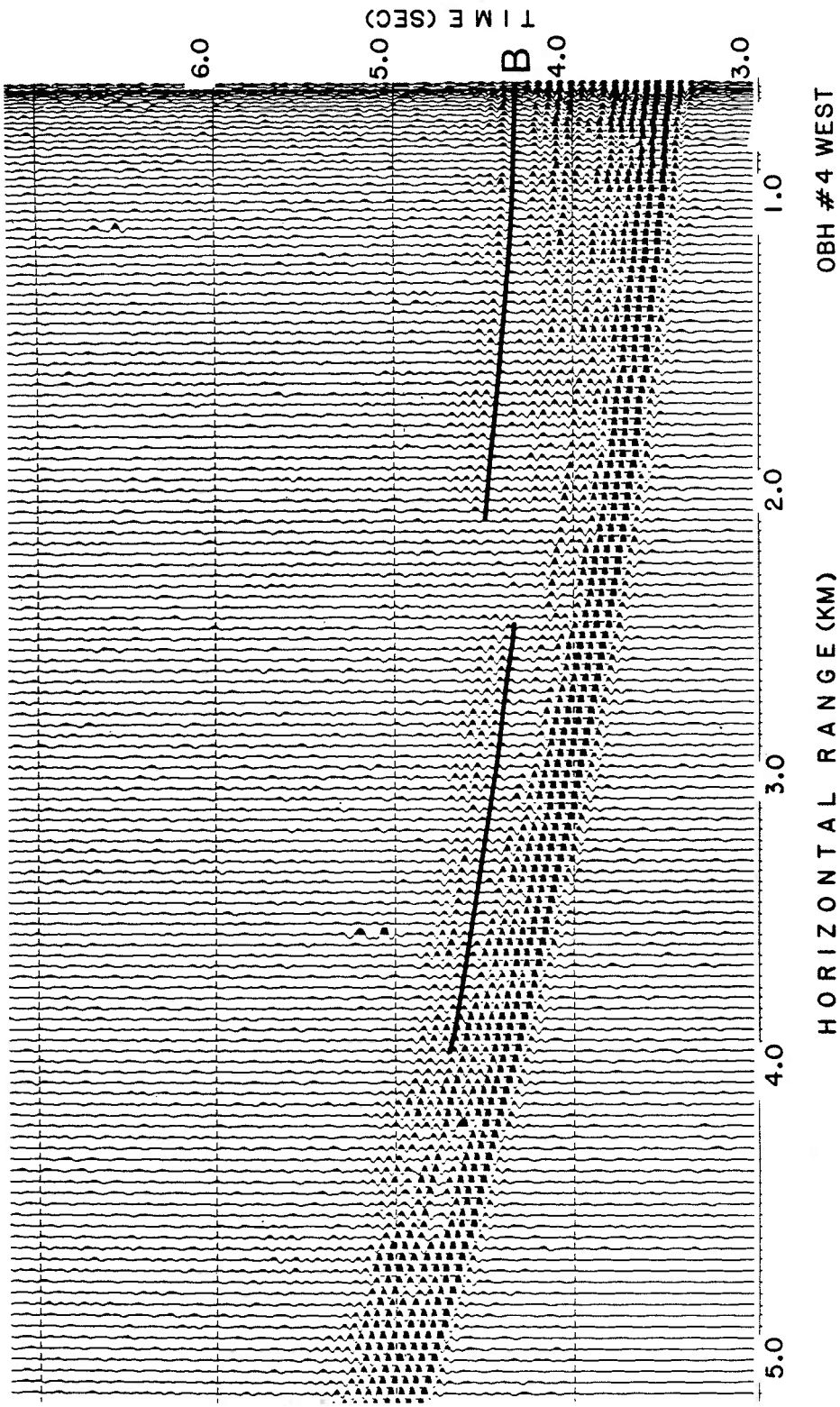
TIME (SEC)
6.0
5.0
B
4.0
3.0
1.0
2.0
3.0
4.0
5.0
HORIZONTAL RANGE (KM)
OBH #4 WEST

Figure 7. 0.66L (40in^3) airgun data Line 3NE, OBH 3 shot while steaming northeast. Note lack of basement reflection; this is caused by topographic roughness on the scale of a seismic wavelength (150m).

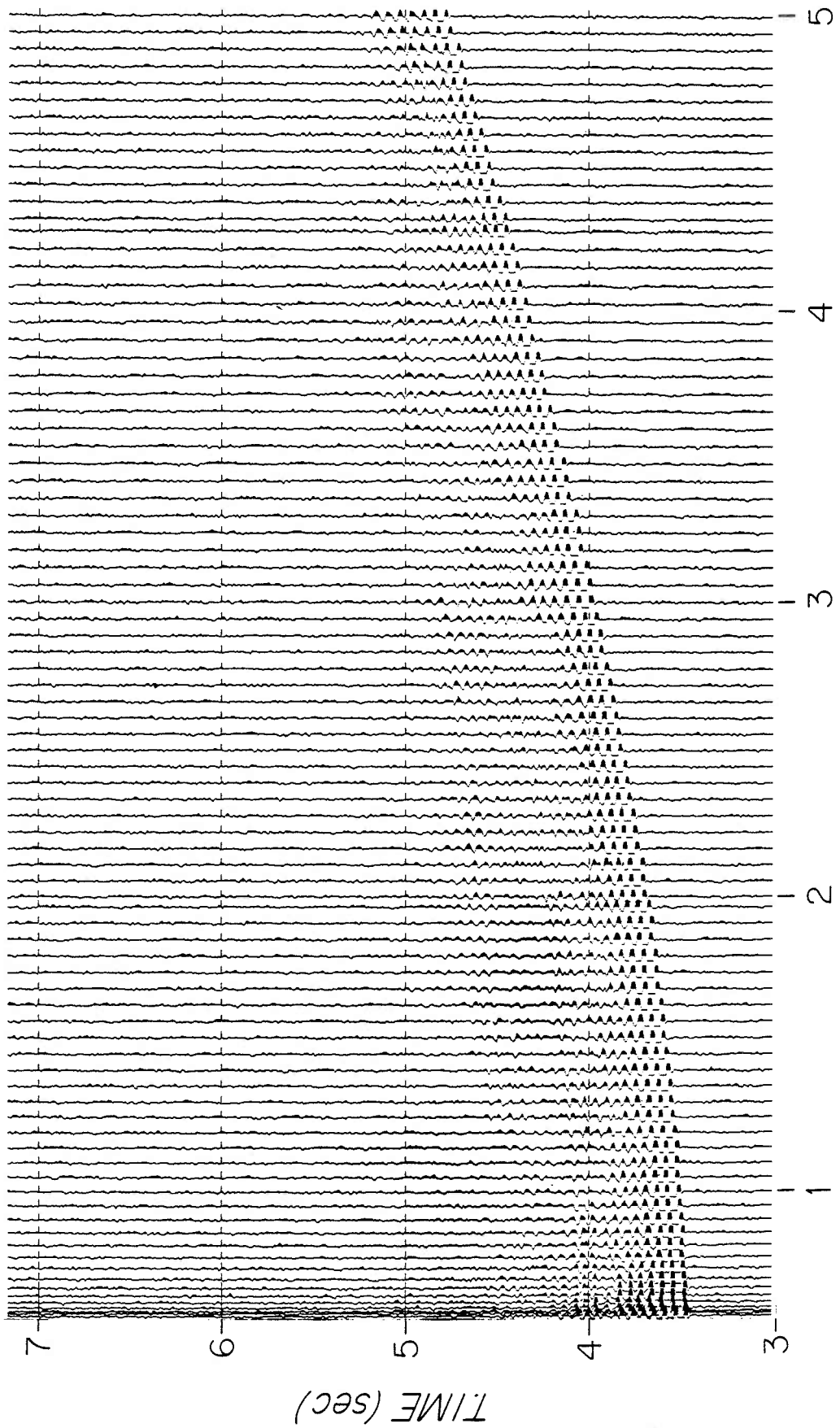

7.

Figure 8. Energy vs range for basement reflections recorded on seven lines by OBH 4. Energy for each shot was calculated by squaring and summing the amplitudes of the digitised data within a 0.1 s window. The position of the window was calculated from the coefficients of the best fitting hyperbola to the basement reflection. These energy values then had a ten point running average applied to them to average out short term variations caused by compressor cycling sea state etc. Lines 4 South, South-southeast, East-southeast, East, Northeast, North-Northeast, and North are shown on one axis.

Basement Reflection

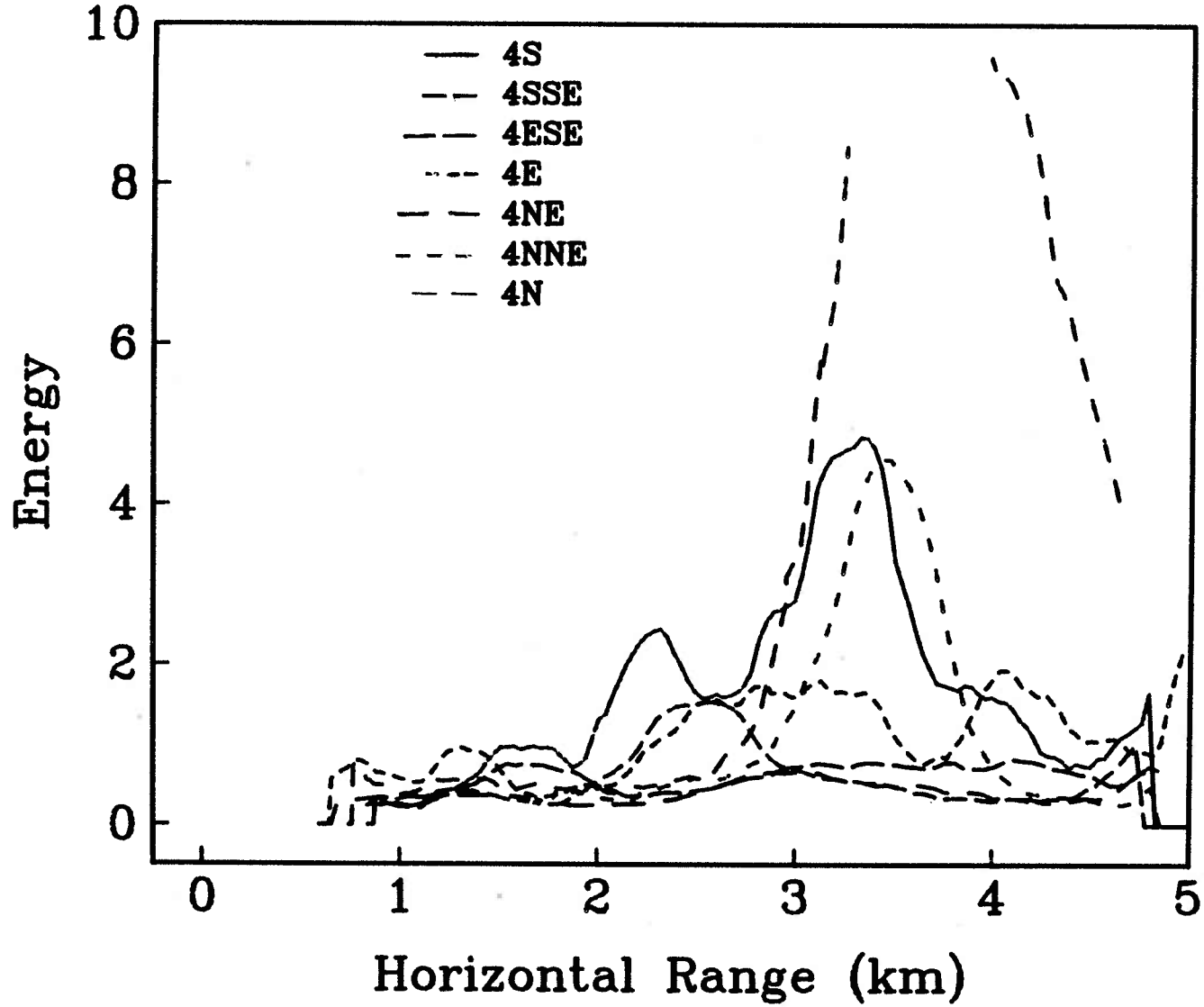

Figure 9. Energy vs range of lines 4 South, South-southeast, East-southeast, East, Northeast, North-Northeast, and North are plotted individually. Note difference in scale for line 4N.

Basement Reflection

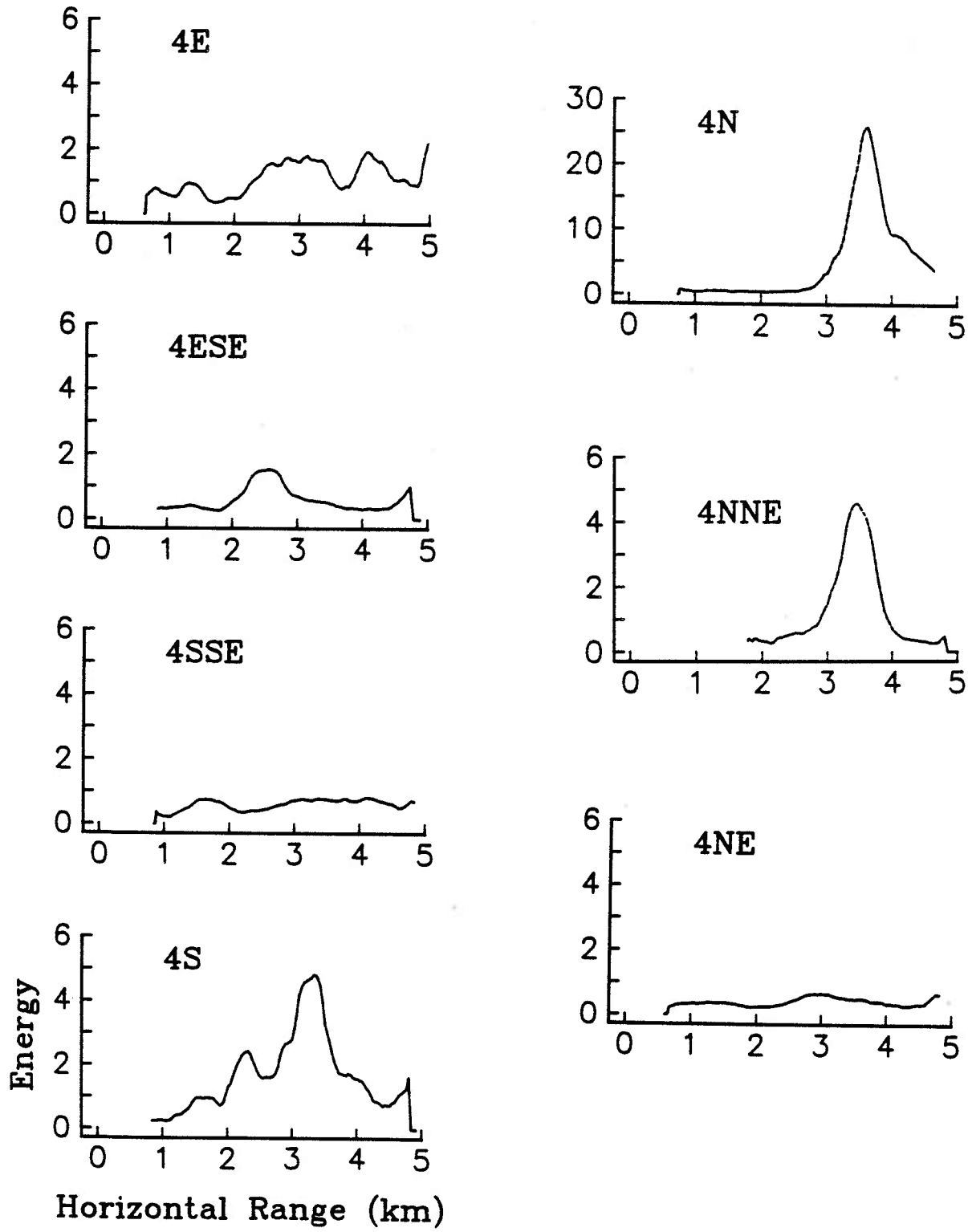

Figure 10. Two-dimensional ray tracing for inward facing fault scarp underneath sediment velocity structure in Table 1. The fault topography was taken from a deep towed hydrophone profile (Purdy and Gove, 1982) east of OBH 4. Rays are shot from the instrument to the sea surface. A) defocussing at ranges greater than 3.0 km from the instrument, B) focussing of energy at ~2.0 km from the instrument.

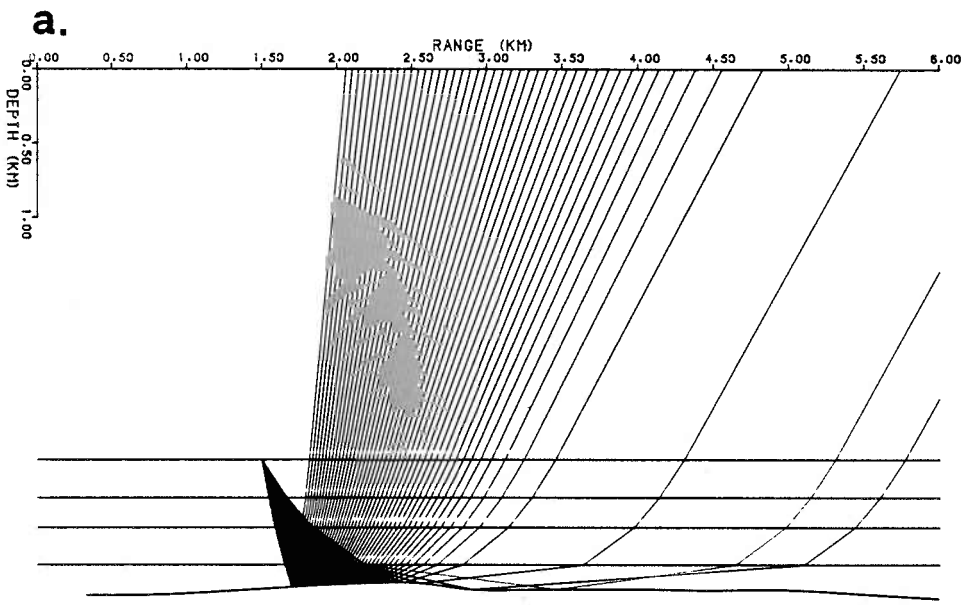
a.
RANGE (KM)
0.00 0.50 1.00 1.50 2.00 2.50 3.00 3.50 4.00 4.50 5.00 5.50 6.00
DEPTH (KM)
0.00
0.50
1.00

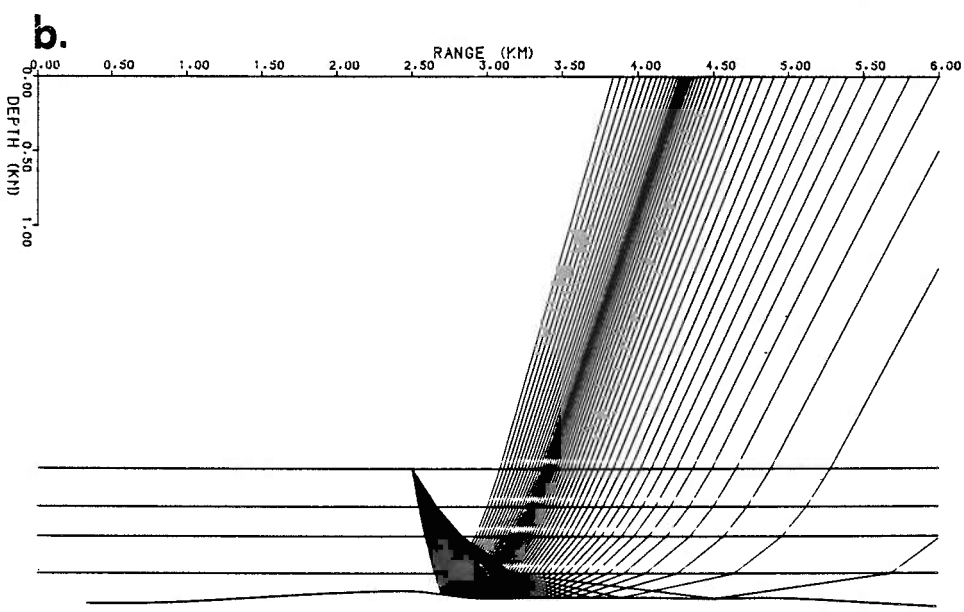
b.
RANGE (KM)
0.00 0.50 1.00 1.50 2.00 2.50 3.00 3.50 4.00 4.50 5.00 5.50 6.00
DEPTH (KM)
0.00
0.50
1.00

Figure 11. 0.66L ($40in^3$) airgun data Line 3SE, OBH 3 shot while steaming at a 45^o south-east. Note increase in the amplitude of the basement reflection at 4.0 km after a short zone of interference between the basement reflection and the refraction.

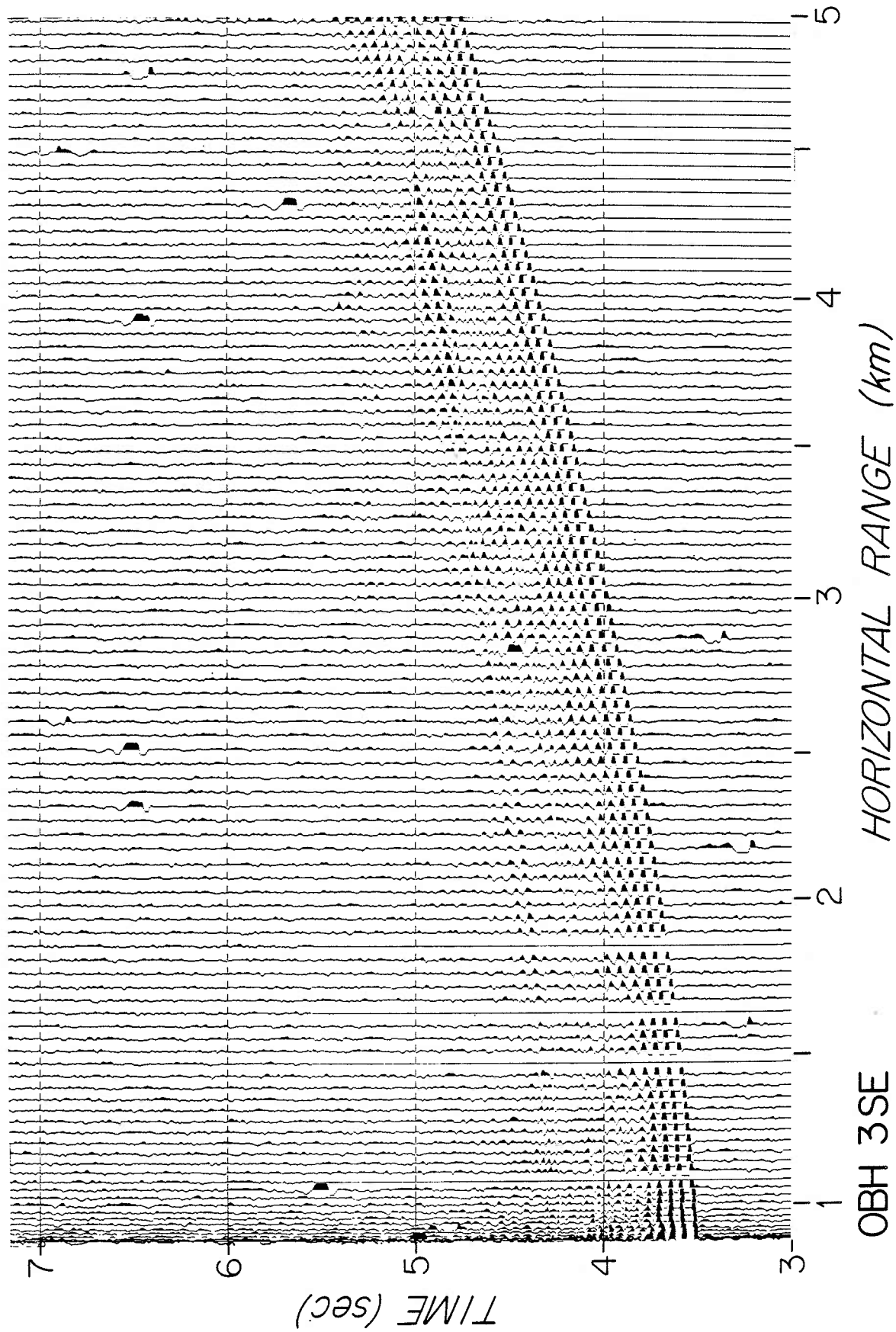

11.

Figure 12. 0.66L (40in^3) airgun data Line 2W, OBH 2 shot while steaming west. Note increase in the amplitude of the basement reflection at 3.0 km after a short zone of interference between the basement reflection and the refraction.

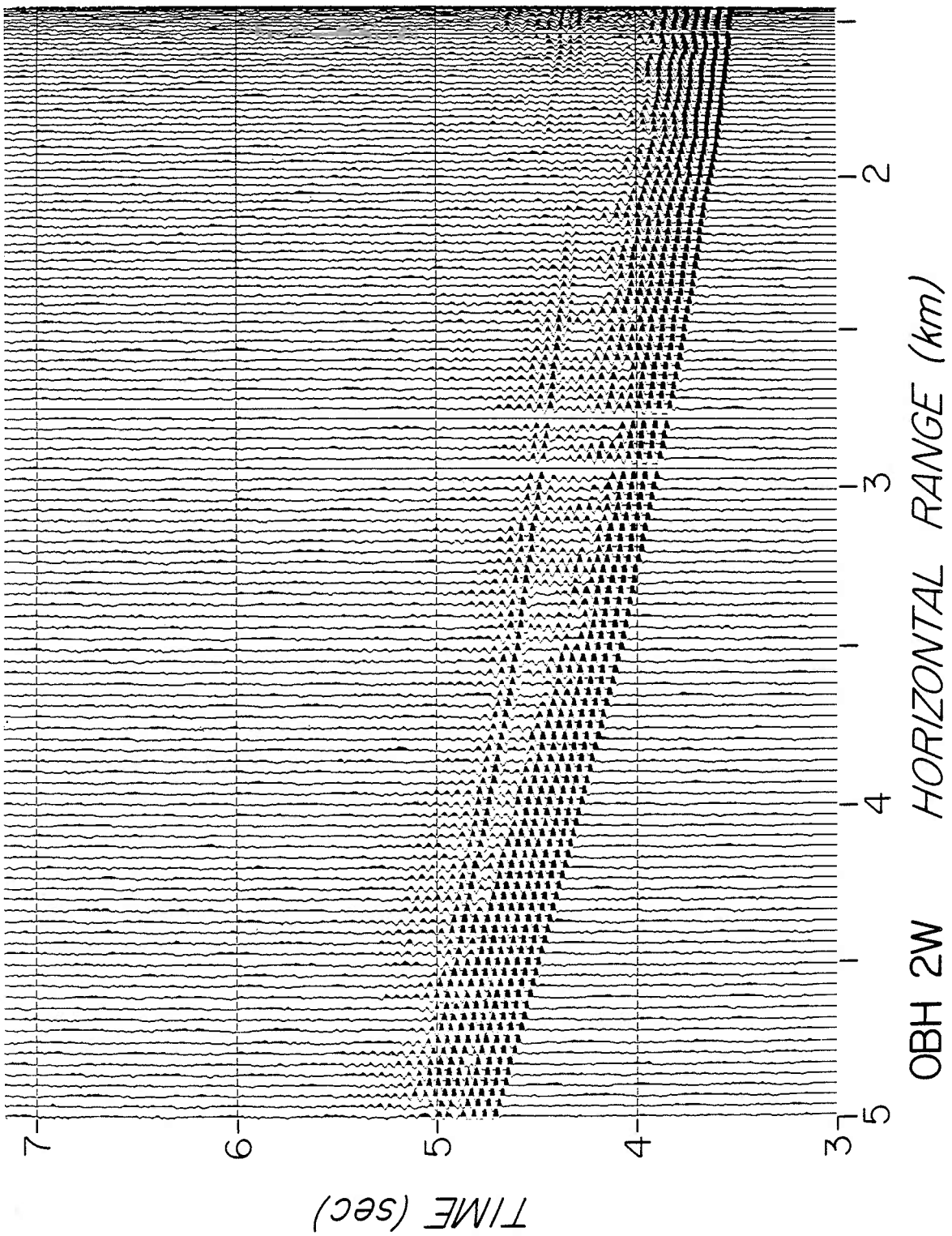

12.

Figure 13 A.) Velocity-depth profile used to calculate synthetic seismograms by the Fuchs-Muller reflectivity algorithm; there is a 150m transition zone between the sediments and basalt. B.) Energy vs range for basement reflections modelled by velocity profiles described in Fig. 13a and line 4N. Note the increase in the energy of the basement reflections at 3.5 km. The energy values of the synthetic seismograms have been normalised to the peak energy value in the data.

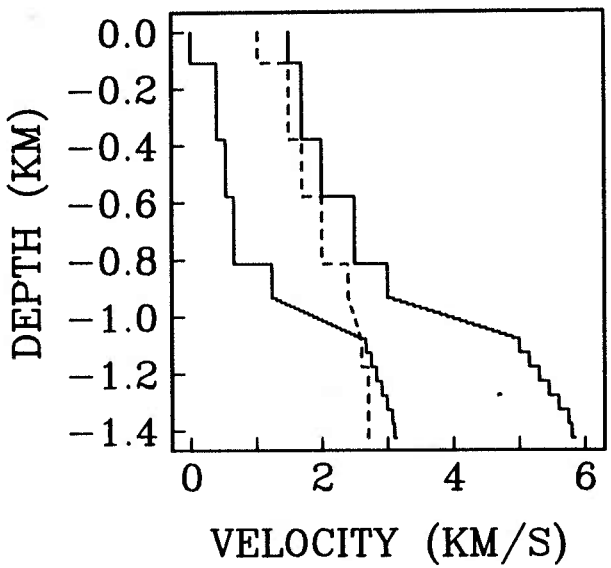
DEPTH (KM)
0.0
−0.2
−0.4
−0.6
−0.8
−1.0
−1.2
−1.4
0
2
4
6
VELOCITY (KM/S)

13a.

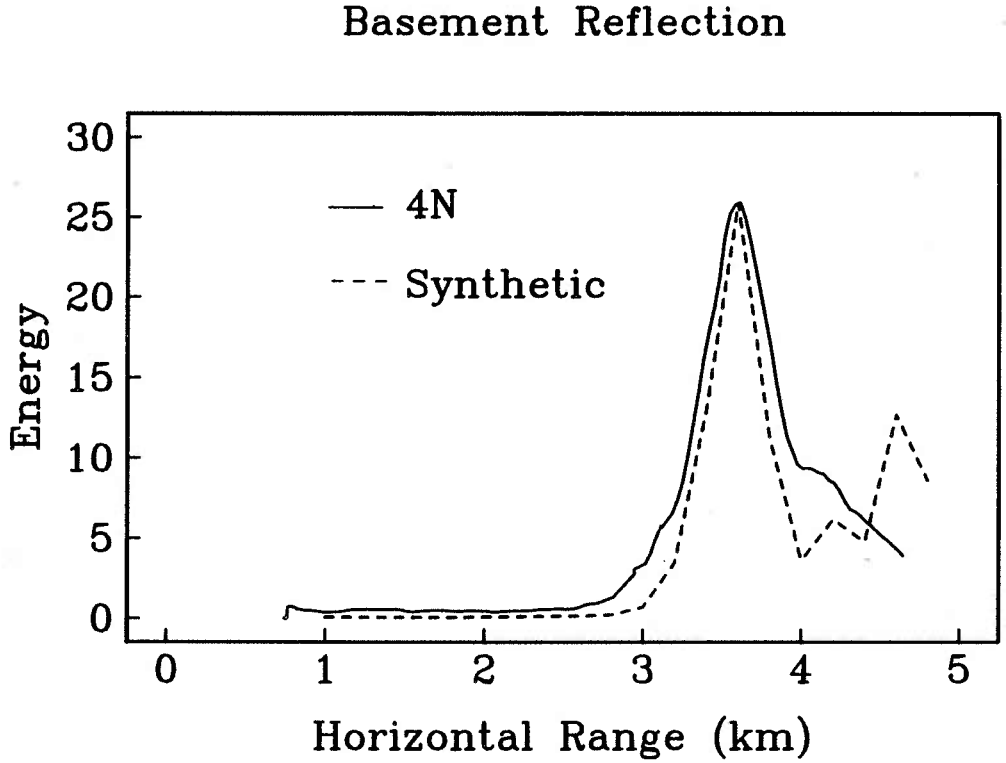
Basement Reflection
Energy
30
25
20
15
10
5
0
4N
Synthetic
0
1
2
3
4
5
Horizontal Range (km)

13b.

Figure 14. Synthetic seismograms from velocity-depth function B in (Fig. 13. Note the high amplitude basement reflections at approximately 3.5 km; this pattern is similar to that observed on line 4N.

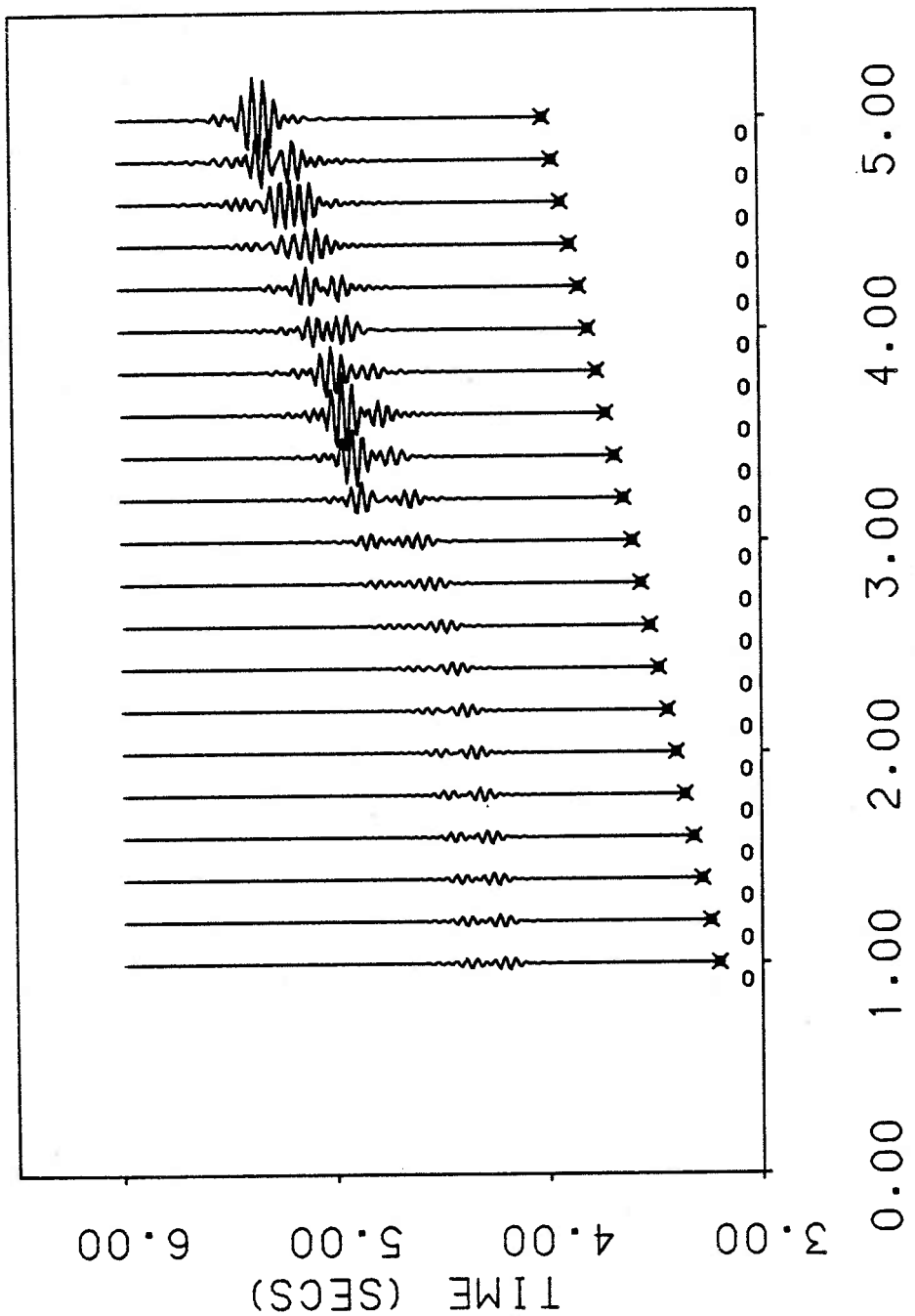

14.

Figure 15. A.) Velocity-depth profile used to calculate synthetic seismograms by the Fuchs-Muller reflectivity algorithm; there is a 300m transition zone between the sediments and basalt. B.) Energy vs range for basement reflections modelled by velocity profiles described in (Fig. 13a) and line 3SE. Note the increase in the energy of the basement reflections at 4.0 km.

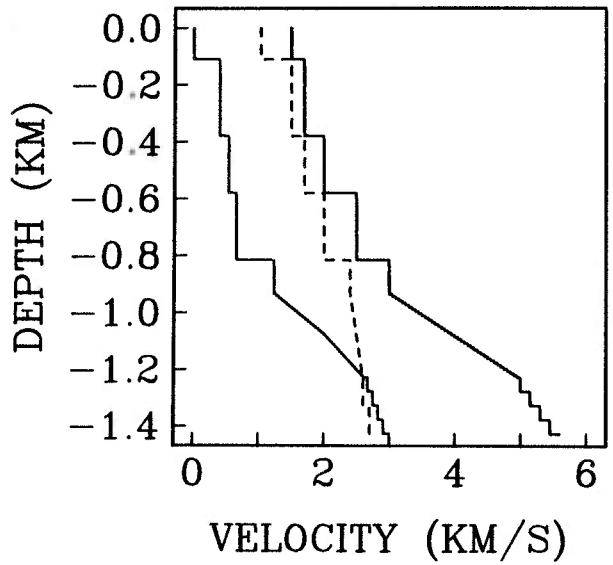
0.0
−0.2
−0.4
−0.6
−0.8
−1.0
−1.2
−1.4
DEPTH (KM)
0
2
4
6
VELOCITY (KM/S)

15a.

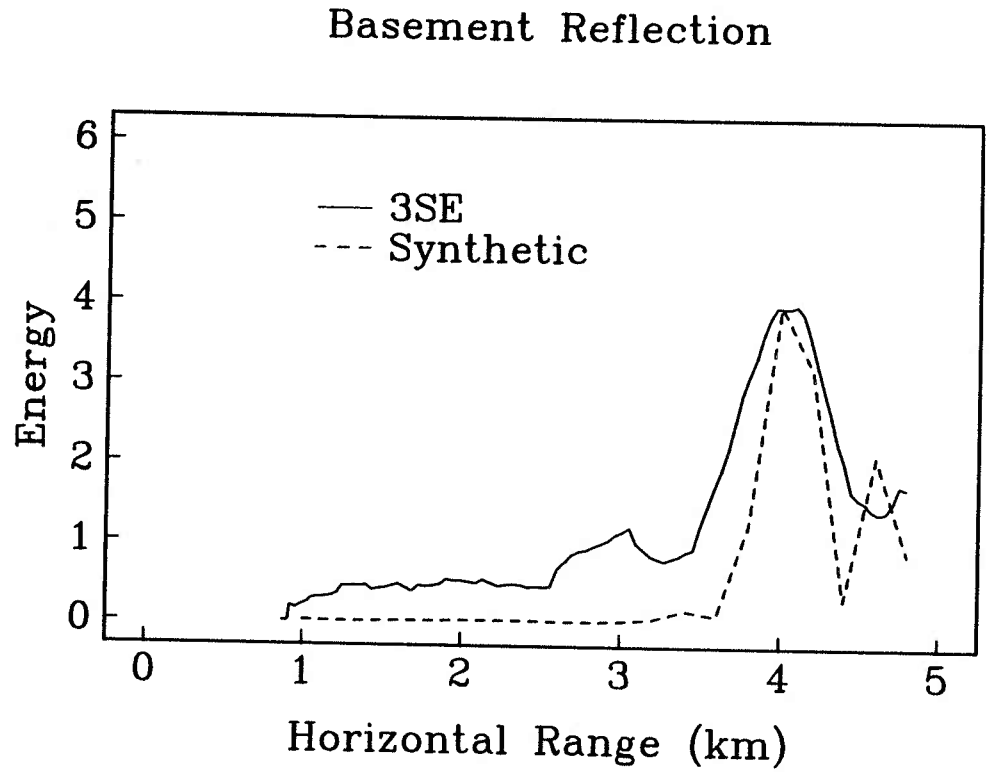
Basement Reflection
3SE
Synthetic
Energy
0
1
2
3
4
5
6
Horizontal Range (km)

15b.

Figure 16. A.) Velocity-depth profile used to calculate synthetic seismograms by the Fuchs-Muller reflectivity algorithm; there is no transition zone between the sediments and basalt. B.) Energy vs range for basement reflections modelled by velocity profiles described in Fig. 13a and line 3SE. Note the increase in the energy of the basement reflections at 3.0 km. The energy values of the synthetic seismograms have been normalised to the peak energy value in the data.

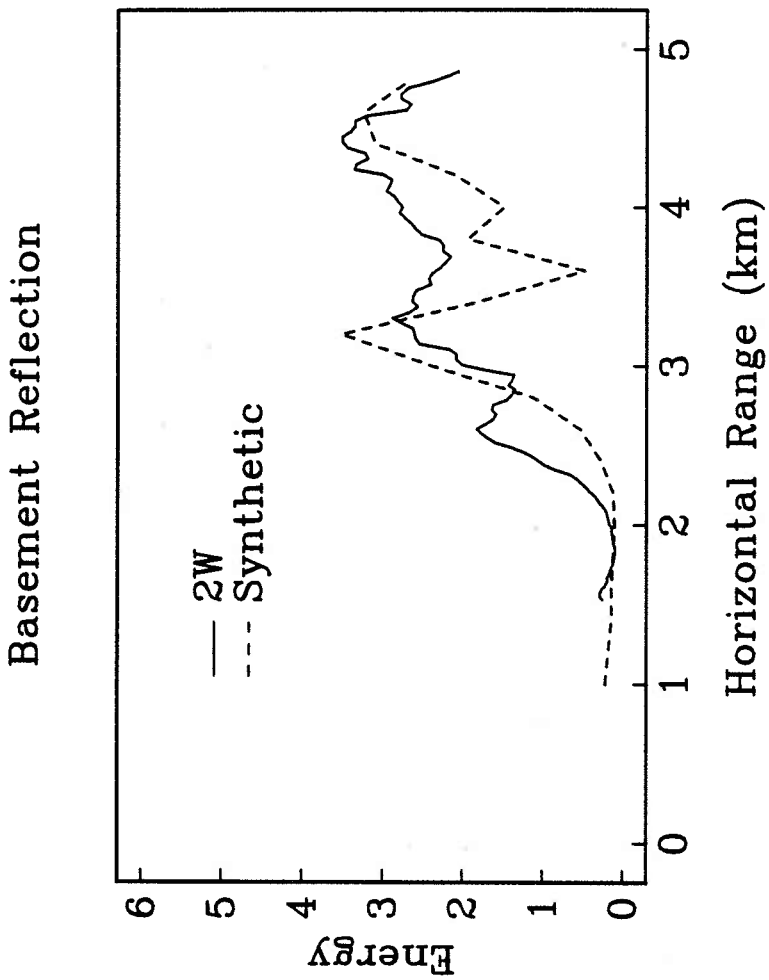
Basement Reflection
2W
Synthetic
Energy
Horizontal Range (km)
0
1
2
3
4
5
6

16b.

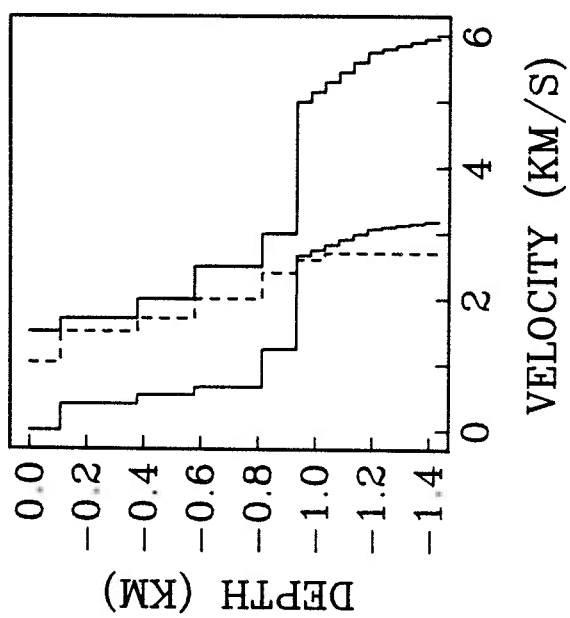
DEPTH (KM)
0.0
-0.2
-0.4
-0.6
-0.8
-1.0
-1.2
-1.4
VELOCITY (KM/S)
0
2
4
6

16a.

Figure 17. Deep towed hydrophone record (Purdy and Gove, 1982) in area of study shot while steaming east. The data have been filterd 80-155 Hz, stacked five-fold and deconvolved. The arrival skirting the very top of the figure is the direct water wave received by the deep towed hydrophone; the signal's variability in arrival time is due to the hydrophone's variable height above the sea floor. Line 2W was shot while steaming parallel to the plane of this profile over relatively smooth topography. Line 4N was shot perpendicular to the plane of this profile.

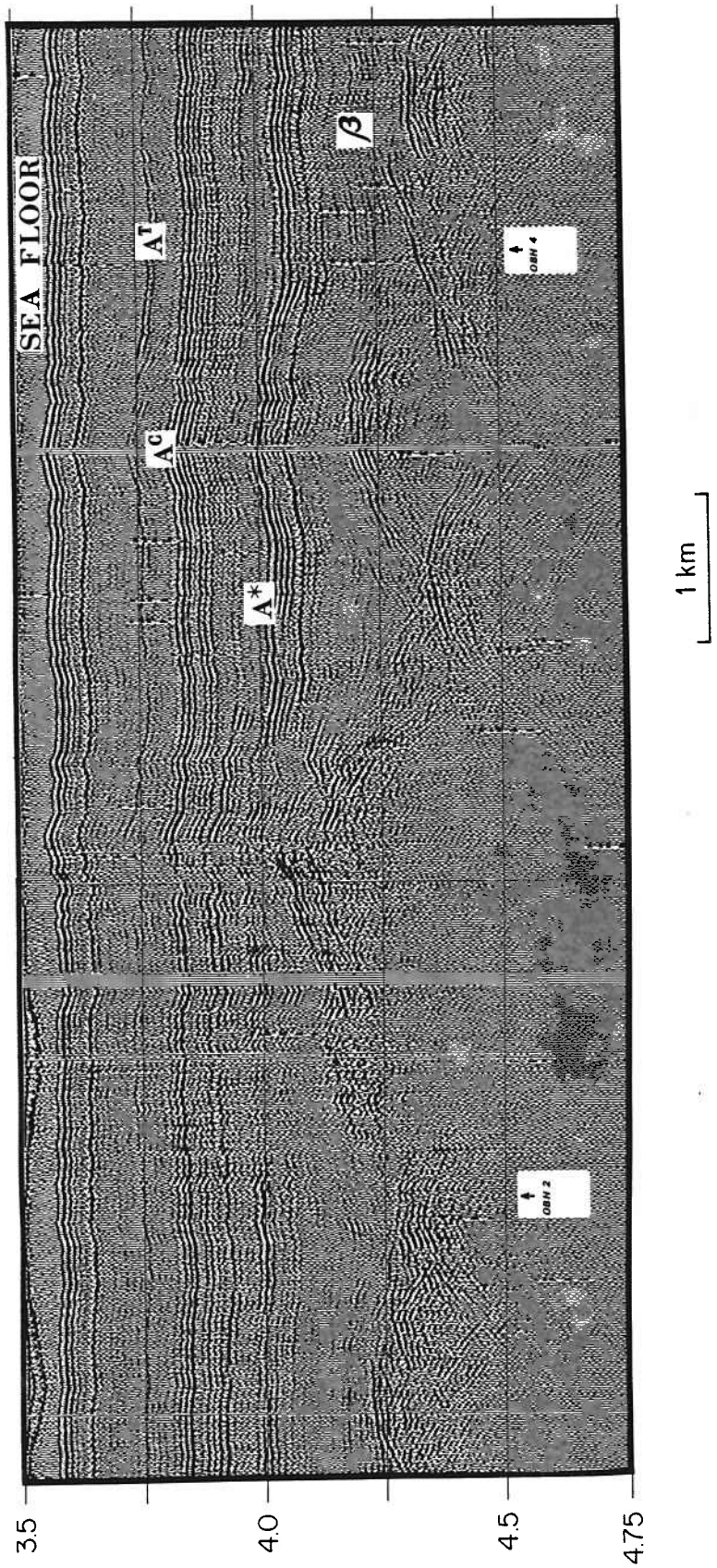

17.

REFERENCES

Cerveny, V., The amplitude-distance curves for waves reflected at a plane interface for different frequency ranges, Geophys. J. R. astr. Soc., 13, 187-196, 1967.

Christensen, N.I. and M.H. Salisbury, Velocities, elastic moduli and weathering-age relations for Pacific Layer 2 basalts, Earth and Plan. Sci. Lett., 19, 461-470, 1973.

Christensen, N.I., S.C. Blair, R.H. Wilkens, and M.H. Salisbury, Compressional wave velocities, densities, and porosities of basalts from holes 417A 417D and 418A, Deep Sea Drilling Project Legs 51 through 53, in Donnelly,T., Francheteau, J., Bryan, W.B., Robinson, P., Flower, M., Salisbury, M. et al., 1979, Initial Reports of the Deep Sea Drilling Project, v.51,52,53 Part 2: Washington (U.S. Government Printing Office), p.1467-1473.

Donnelly,T., Francheteau, J., Bryan, W.B., Robinson, P., Flower, M., Salisbury, M. et al., 1979a, Initial Reports of the Deep Sea Drilling Project, v.51,52,53: Washington (U.S. Government Printing Office).

Donnelly, T., R.S. Pritchard, R. Emmerman, and H. Puchelt, The aging of oceanic crust: synthesis of the mineralogical and chemical results of Deep Sea Drilling Project Legs 51 through 53, in Donnelly,T., Francheteau, J., Bryan, W.B., Robinson, P., Flower, M., Salisbury, M. et al., 1979b, Initial Reports of the Deep Sea Drilling Project, v.51,52,53 Part 2: Washington (U.S. Government Printing Office), p.1563-1577.

Elthon, D., Metamorphism in oceanic spreading centers, in Emiliani, C. (ed.), The Sea, v. 7, John Wiley and Sons, New York, 1982, p. 285-304.

Ewing, J. and M. Ewing, Seismic refraction measurements in the Atlantic Ocean basins, in the Mediterranean Sea, on the Mid-Atlantic ridge and in the Norwegian Sea, Geol. Soc. Amer. Bull., 70,291-318, 1959.

Ewing, J. and R. Houtz, Acoustic stratigraphy and structure of the oceanic crust, in Deep Drilling Results in the Atlantic Ocean: Ocean Crust, Maurice Ewing Ser., v.2, editd by M. Talwani, C.G. Harrison, and D.E. Hayes, pp1-14, AGU, Washington, D.C., 1979.

Ewing, J. and G.M. Purdy, Upper crustal velocity structure in the ROSE area of the East Pacific Rise, J. Geophys. Res., 1982.

Fuchs, K. and G. Muller, Computation of synthetic seismograms with the reflectivity method and comparison with observations, Geophys. J. Roy. Astr. Soc., 23, 417-433, 1971.

Hamano, Y., Physical properties of basalts from holes 417D and 418A, in Donnelly,T., Francheteau, J., Bryan, W.B., Robinson, P., Flower, M., Salisbury, M. et al., 1979, Initial Reports of the Deep Sea Drilling Project, v.51,52,53, Part 2: Washington (U.S. Government Printing Office), p. 1457-1466.

Hashin, Z. and S. Shtrickman, A variational approach to the elastic behavior of multiphase meterials, J. Mech. Phys. Solids, 11, 127-140, 1963.

Helmberger, D.V. and G.B. Morris, A travel time and amplitude

interpretaition of a marine refraction profile: transformed shear waves, Bull. Seism. Soc. Amer., 68, 593-600, 1970.

Honnorez, J., The aging of the oceanic crust at low temperature, in Emiliani, C. (ed.), The Sea, v. 7, John Wiley and Sons, New York, 1982, p.525-588.

Houtz, R. and J. Ewing, Upper crustal structure as a function of plate age, J. Geophys. Res., 81, 2490-2498, 1976.

Hyndman, R.D. and M.J. Drury, The physical properties of oceanic basement rocks from deep drilling on the Mid-Atlantic Ridge, J. Geophys. Res., 81, 4042-4060, 1976.

Kennett, B.L.N., Towards a more detailed seismic picture of the oceanic crust and mantle, Mar. Geophys. Res., 3, 7-42, 1977.

Kirkpatrick, R.J., The physical state of the oceanic crust: Results of downhole geophysical logging in the Mid-Atlantic ridge at 23^{o} N, J. Geophys. Res., 84, 179-188, 1979.

Koelsch, D.E. and G.M. Purdy, An ocean bottom hydrophone instrument for seismic refraction experiments on the deep ocean, Mar. Geophys. Res., 4, 115-125, 1979.

Larson, R.L. et al., 1981, Initial Reports of the Deep Sea Drilling Project, v.61: Washington (U.S. Government Printing Office).

Ostrander, W. J., Plane wave reflection coefficients for gas sands at nonnormal angles of incidence, at Fifty-second anual meeting and exposition of the Society of Exploration Geophysics, Dallas, 1982.

Purdy, G.M., The variability in seismic structure of Layer 2

near the East Pacific Rise at 12° N, J. Geophys. Res., 87, 8403-8416, 1982a.

Purdy, G.M., The seismic structure of 140 my old crust in the western central North Atlantic Ocean, subm. to Geophys. J. Roy. Astr. Soc., 1982b.

Purdy, G. M. and L.A. Gove, Reflection profiling in the deep ocean using a near bottom hydrophone, Mar. Geophys. Res., 5, 301-314, 1982.

Purdy, G.M., L.A. Gove, D. E. Koelsch, G. Power, and M.D. Allison, The Woods Hole Oceanographic Institution system for reduction and handling of marine seismic refraction data, Unpub. WHOI Tech. Rep., 1982.

Rohr, K., Hyperbolic stacking of wide-angle reflections from deep-sea sediments, subm. to J. Geophys. Res., 1982.

Spudich, P.K.P. and D.V. Helmberger, Synthetic Seismograms from Model Ocean Bottoms, J. Geophys. Res., 84, 189-204, 1979.

Spudich P. and J. Orcutt, Petrology and porosity of an oceanic crustal site: results from wave form modelling of seismic refraction data, J. Geophys. Res., 85, 1409-1433, 1980a.

Spudich P. and J. Orcutt, A new look at the seismic velocity structure of the oceanic crust, Rev. Geophys. Space Phys., 18, 627-645, 1980b.

Stephen, R.A, Travel time curves for a simple sea floor model, Mar. Geophys. Res., 5, 315-326, 1982.

Stephen. R.A., K.E. Louden, and D.H. Matthews, The oblique

seismic experiment on DSDP Leg 52, Geophys. J. Roy. Astr. Soc., 60, 289-300, 1980.

Tucholke, B.E., Relation between acoustic stratigraphy and lithostratigraphy in the western North Atlantic Basin, in Tucholke, B.E., Vogt, P.R., et al., 1979, Initial Reports of the Deep Sea Drilling Project, v.43: Washington (U.S. Govt. Printing Office), p.827-846.

White, R.S., Oceanic upper crustal structure from variable angle seismic reflection-refraction profiles, Geophys. J. Roy. Astr. Soc., v.20, p.683-726, 1979.

White, R.S. and R.A. Stephen, Compressional to shear conversion in oceanic crust, Geophys. J. Roy. Astr. Soc., 63, 547-565, 1980.

Chapter 5: CONCLUSIONS

In the previous three chapters wide-angle reflections from Layers 1 and 2 of oceanic crust ~140 my old in the western North Atlantic Ocean basin have been interpreted for a detailed velocity structure of Layer 1 and the velocity structure of the uppermost Layer 2. Previous work with sonobuoys had been unable to detail the sediments' velocities on the Bermuda Rise while seismic refraction work is rarely capable of measuring the velocity structure of the upper basaltic crust. Stacking wide-angle reflections from sedimentary reflectors and basement resolved the interval velocities and thicknesses of four layers; stacking should be able to provide similar resolution on data recorded digitally by a sonobuoy. A tau-p mapping of the data failed to measure the velocity gradient in the upper Layer 2, in spite of a very careful mapping procedure. The topography of the sediment-basement interface and a low signal-to-noise ratio made it impossible to resolve energy refracted from the upper Layer 2. A study of the amplitudes of the wide-angle reflections from the sediment-basement interface, however, measured the velocity structure of the top few hundred meters of Layer 2 near three OBH's. The differences in the amplitude vs range patterns observed at each instrument were interpreted to indicate lateral heterogeneity in the upper crust on the scale of the instrument separation, 3 to 8 km.

*

In chapter 2 the application of hyperbolic stacking (Taner and Koehler, 1969) to wide-angle reflections from Layers 1 and 2

resolves four layers within Layer 1 and their interval velocities and thicknesses. Stacking provides more detail in the sediments' velocity structure than picking travel-times. Previous work on sonobuoys could yielded only an average value of the sediments' velocity in this region of the North Atlantic Ocean (Houtz, 1980). Measuring the velocity structure of the sediments in detail is of importance to the study of the sediments and their evolution, to the mapping of the depth to basement and to the interpretation of the amplitudes of seismic refraction data.

In most of the western North Atlantic Ocean basin the sedimentary structure is characterised by only an average value of the seismic velocities. Houtz (1980) has summarised the results of sonobuoy studies; stippling has been added to his map (Fig. 5.1) to highlight the areas in which only average velocities are known. The experiment described here took place in area 'M' where the sediments have an average velocity of 2.00 +/- 0.20 km/s. Seismic reflectors A^t, A^c, A* and β have been mapped in this area (Tucholke, 1981) and elsewhere are associated with velocity increases (Houtz, LePichon and Ewing, 1968). The figure shows that twenty-seven stations have been shot in this area, but the sediments are too thin (<0.1s) to be able to resolve their structure by picking travel-times from sonobuoy records. Ten sonobuoys were deployed by Naini and Ewing (unpubl.) ~40km from the experiment described here (Fig, 5.2); data from eight yielded average velocities for the sediments of 1.9-2.3 km/s and from only two were two sedimentary

layers resolved. The uppermost layer had a velocity of 1.81-2.07 km/s and the lowermost had a velocity of 2.36-2.8 km/s.

In chapter 2 the application of hyperbolic stacking to wide-angle reflections from deep-sea sediments is shown to result in a more detailed picture of the velocity structure of the sediments than was previously available from sonobuoy records. The results of the stacking procedure correlate with the sedimentary reflectors, A^c, A* and β, which are visible on the normal incidence reflection records. It is also shown that the stacking velocity-two way normal incidence travel-time values can be interpreted either by modelling or inversion, and that the results of the two methods are remarkably similar (Table 2.2). Thus, the interval velocities and thicknesses of four layers have been interpreted instead of the one or two layers interpreted by picking travel-times.

The high interval velocities measured between β and basement are generally considered to indicate a high degree of lithification. Houtz, Ewing and LePichon (1968) note a "profound change in velocity" at reflector β, and Tucholke, Houtz and Ludwig (1982) claim that the velocities beneath β increase by 0.25 km/s for each kilometer of overburden. Reflector β is thin on the Bermuda Rise and few measurements of its velocity have been made. In chapter 2 the seismic velocity beneath β is measured as 3.12 +/- 0.32 km/s and its Poisson's ratio as 0.4; this latter value was obtained from the two-way normal incidence travel-times to β, basement and a low phase velocity event. The Poisson's ratio of 0.4 shows that the Neocomian

to late Jurassic limestones on the Bermuda Rise are indeed consolidated as in deeper areas of the western North Atlantic Ocean basin and not 75^{o}/o "clayey low-velocity interbeds" (Tucholke et al., 1979) as inferred at DSDP Site 387. Such measurements of this layer's velocity and Poisson's ratio are a key to understanding the mechanisms of sediment consolidation and lithification operating in the deep-sea environment.

The depth to basement is a fundamental parameter of marine geophysical investigations; in sedimented areas its measure depends on knowledge of the sedimentary velocity structure. As Tucholke, Houtz and Ludwig (1982) have noted "The preparation of realistic regional maps of sediment thickness and depth to basement therefore requires a detailed knowledge of the speed of sound in sediments." The topography of oceanic basement is frequently interpreted from time sections of normal incidence seismic data. Basement topography appears differently in these records according to whether water (1.5km/s), unconsolidated sediments (2.0km/s) or consolidated sediments (3.0km/s) are above the basement. Topography underneath β is apparently smooth yet when migrated it is similar in roughness to topography found near the mid-ocean ridge (Purdy and Gove, 1982) (Fig. 5.3). This is an important effect to take into consideration when studying such problems as the rough-smooth boundary in the western North Atlantic.

Hyperbolic stacking could equally well be applied to sonobuoy data in order to measure the sedimentary structure. Since sonobuoys

are more easily deployed than ocean-bottom hydrophones, simply recording the data digitally and stacking the data along hyperbolae would improve the resolution of the sediments' velocity structure. A set of programs developed for the mapping of data into stacking velocity-two-way normal incidence travel-time space and the interpretation of the results is listed in Appendix I.

The velocity of the sediments immediately overlying basement affect the amplitudes of both compressional and shear seismic refractions from oceanic crust. Figure 5.4 shows the transmission coefficients of compressional and shear energy for two models of a sediment-basement interface. The sediments' velocity and Poisson's ratio varied from 2.0km/s and 0.48 to 3.1km/s and 0.4, respectively, while the basement remained fixed at 5.0km/s and 0.3. For phase velocities appropriate to Layer 2, Layer 3 and mantle (5.0-8.0 km/s) the interface beneath the high velocity (consolidated) sediment allows ~ 30^{0}/o more compressional energy through than the low velocity (unconsolidated) sediment. The interface beneath the consolidated sediments, however, converts only half as much shear energy as does the interface beneath unconsolidated sediments for phase velocities of 3.0-4.5 km/s which are appropriate for Layer 3 and Moho shear refractions. Thus, refraction studies over oceanic crust with consolidated sediments would have higher amplitude compressional refractions and lower amplitude shear refractions than would refraction studies over the same igneous crust overlain by unconsolidated sediments.

Velocity-depth functions used for modelling synthetic seismograms, therefore, must include as detailed a knowledge as possible of the sediments' velocity structure. Purdy (1982c), when modelling the refraction data in the experiment described here, used an average sediment velocity of 2.0 km/s; he finds that he must include a sediment-basement transition zone (a zone of high Poisson's ratio) in his velocity-depth function in order to model the low amplitude shear refractions from Layer 3. In fact, the consolidated limestones which have a high Poisson's ratio could be the cause of the low amplitude shear refractions. The lack of shear refractions recorded from oceanic crust with sediments of compressional veolocities >3.0 km/s was first noted by Houtz, Ewing, and LePichon (1968).

These differences in the properties of the sediment-basement interface also indicate that studies comparing the amplitudes of seismic refraction data from different ocean basins must be conducted very carefully to include the effect of the sediments. For example, DSDP drilling at Site 307 (Larson et al., 1975) found ~300m of cherts and clay with an interval velocity of 2.3 km/s overlying basement ~140 my old west of Hawaii. Refraction data shot over such crust would appear very different from refracton data collected over the crust studied in this thesis simply because of the differing sedimentary layers.

*

Chapter 3 shows that tau-p mapping does not provide much

information on data with a low signal-to-noise ratio and in which the reflectors' topography varies. The tau-p mapping was modified from the procedure outlined by Stoffa et al. (1980) in order to identify postcritical arrivals and to use the tau-p events in each subarray for the velocity-depth inversion. The noise in the data as well as the closeness in time of the sedimentary reflectors made it virtually impossible to resolve reflectors A^C and β in the tau-p map. Reflector A* and basement were visible, but the topography of the basement reflector made inversion of the data for the velocity gradient in the top of Layer 2 impossible. By comparison, the hyperbolic stacking of the same data discussed in chapter 2 resolved three sedimentary reflectors and basement, and the results were easily interpreted for interval velocities and thicknesses.

Tau-p mapping is best applied to high signal-to-noise data containing many postcritical arrivals and refractions, i.e. travel-time curves which are nearly linear. Since amplitudes can be preserved in the final map, the postcritical energy can be identified by its high amplitudes and the p-values used to constrain the inversion for a velcoity-depth function. This technique would be most useful for data collected in areas of smooth topography, such as oceanic crust which had been formed by fast spreading.

*

In chapter 4 the amplitudes of wide-angle reflections from the sediment-basement interface are interpreted to indicate the existence of lateral heterogeneity in the uppermost portion of Layer

2 on the scale of 3 to 8 km. Thirty lines were studied but only three appeared free from topographic disturbance. These lines were modelled by computing synthetic seismograms from velocity-depth functions with a transition zone between the sediments and basement. Transition zones with thicknesses of 0, 150, and 300m reproduced the amplitude patterns observed in the three lines. The transition zone is interpreted as a mixture of fractured, altered basalt and sediments, and its variability in thickness indicates that weathering and hydrothermal alteration of upper Layer 2 are spatially heterogeneous processes.

This study is interpreted to indicate that weathering and hydrothermal alteration of oceanic crust occur preferentially in highly faulted zones. Preferential water flow through highly fractured material is a well-known phenomenon (Elthon, 1982; Honnorez, 1982), but whether it significantly affected the structure and evolution of oceanic crust or whether the effects averaged out with time were not known. At DSDP Sites 417A, 417D and 418A (Donnelly et al., 1980) basalts which had been altered to very different degrees within 10 my of their formation were drilled within 1km of each other. The lateral extent of the heterogeneity, however, could not be determined by drilling. The heterogeneity in the old oceanic crust studied here is on the scale of a few km in the top few hundred meters of oceanic crust; this variability should be taken into account by geochemists calculating mass fluxes and balances for the oceans and oceanic crust (Humphris et al., 1979).

Since wide-angle reflections measure the velocity structure at the sediment-basement interface, such measurements on young oceanic crust could provide information on the hydrothermal evolution of oceanic crust. Seismic velocities are very suseptible to the degree of fracturing. One could then map the presence of open or sealed fractures at the top of Layer 2. These values could be compared to refraction data in order to measure when fractures in the lower crust seal.

The scale of the wide-angle reflection experiment descibed here is of potential use in correlating the small-scale measurements of oceanic crust made from drill holes ~6cm in diameter and seismic refraction measurements which are made on the scale of 0.5-1.0 km. A wide-angle reflection study of the oceanic crust affords greater resolution than seismic refraction experiments because higher frequencies can be used and the horizontal scale is on the order of 1 km instead of 10 to 100 km. Also, since DSDP holes rarely penetrate beyond the top few hundred meters of oceanic crust, this scale experiment is suited to measure seismic structure locally about the drill site. To further refine the experimental technique, energy of frequencies greater than 20 Hz could be used, and if the source function were impulsive (as produced by a water gun, for instance, rather than an airgun), the phases of the reflections could be interpreted as well as the amplitudes.

Wide-angle reflections can also be used to study the nature of the Mohorovicic discontinuity. Wide-angle reflections from the Moho

have been observed in seismic refraction data (Helmberger, 1977; Purdy, 1982c), but experiments with closer shot spacing designed to examine the amplitude vs range patterns of the reflections would provide more information. In places the Moho has been modelled as a velocity gradient and in others as a sharp interface (Helmberger and Morris, 1969; Helmberger, 1977; Spudich and Orcutt, 1980a; Purdy, 1982c). Multichannel seismic reflection lines have obtained reflections from the Moho on continental shelf off Scotland (Smythe et al., 1982), old Mesozoic oceanic crust (Grow and Markel, 1977), and young Pacific crust (Herron et al., 1978), but the reflections vary in both their amplitudes and travel-times over distances of a few tens of kilometers. The variability of these reflections could indicate variability of the velocity structure at the Moho, or topography on the Moho could be focussing and defocussing the reflected energy. Casey et al. (1982) have geologically mapped undulations of the ancient oceanic Moho in the Bay of Islands ophiolite on the scale of several kilometers relief over tens of kilometers distance. This topography would affect the reflections observed from energy with a wavelength of 1km. In these areas a study of the amplitudes of the wide-angle reflections would provide more information on the velocity structure at the interface.

This study of the amplitudes of wide-angle reflections also shows that the sediment-basement interface is an important boundary from the point of view of the transfer of seismic energy. Travel-times can be readily corrected for differences in sediment

thickness, i.e. the basement topography (Purdy, 1982a; Orcutt et al., 1976), but amplitudes are not so easily corrected. Focussing and scattering are difficult processes to model and an extremely detailed knowledge of the morphology of the interface must exist. Deep-towed seismic reflection systems (Purdy et al., 1980) map basement topography well, but are slow and difficult to guide over features of interest. The study of the amplitudes of seismic arrivals has yielded much information about the oceanic crust; as interpetations become more detailed care must be taken to include topographic effects in the analysis.

*

Thus methods of analysing wide-angle reflections discussed above provide more information on the oceanic crust than does picking travel-times. Increased resolution of the sediments' velocity structure was obtained by stacking the data along hyperbolae and the analysis of the postcritical reflections' amplitudes provide information on the velocity structure at the sediment-basement interface. These methods were applied to wide-angle reflections from the upper oceanic crust, but could equally well be applied to reflections from the Moho or from reflections from continental crust.

Figure 5.1. Location of sonobuoy stations in the western North Atlantic Ocean. Areas in which only an average value of the sediments velocity are known have been stippled. The experiment described in this thesis took place in area 'M'. Twenty-seven stations exist in this region, but could not define the velocity structure associated with sedimentary reflectors A^C, A* and β. Stacking wide-angle reflections from these reflectors resolved the interval velocities and thicknesses of four layers.

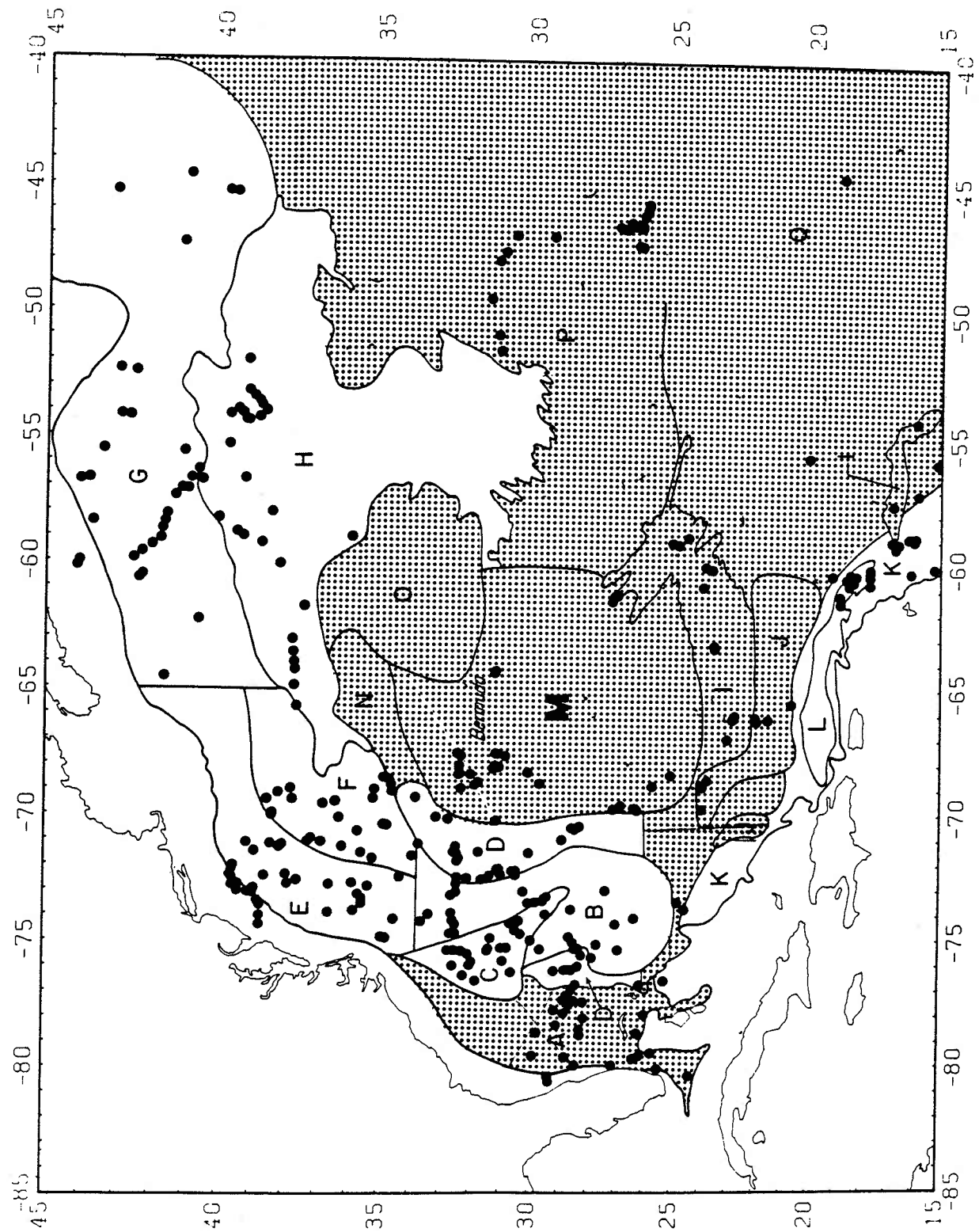
A
B
C
D
E
F
G
H
I
J
K
L
M
N
O
P
Q
Bermuda
45
40
35
30
25
20
15
-85
-80
-75
-70
-65
-60
-55
-50
-45
-40

5.1

Figure 5.2. Sonobuoy locations and velocity-depth solutions from Naini and Ewing (unpubl.). Note the apparent variability in the sediments' velocity structure measured by the sonobuoys within a 15 x 15 km area. Average velocities range from 1.8-2.3 km/s and only two sonobuoys could resolve two layers in the sediments.

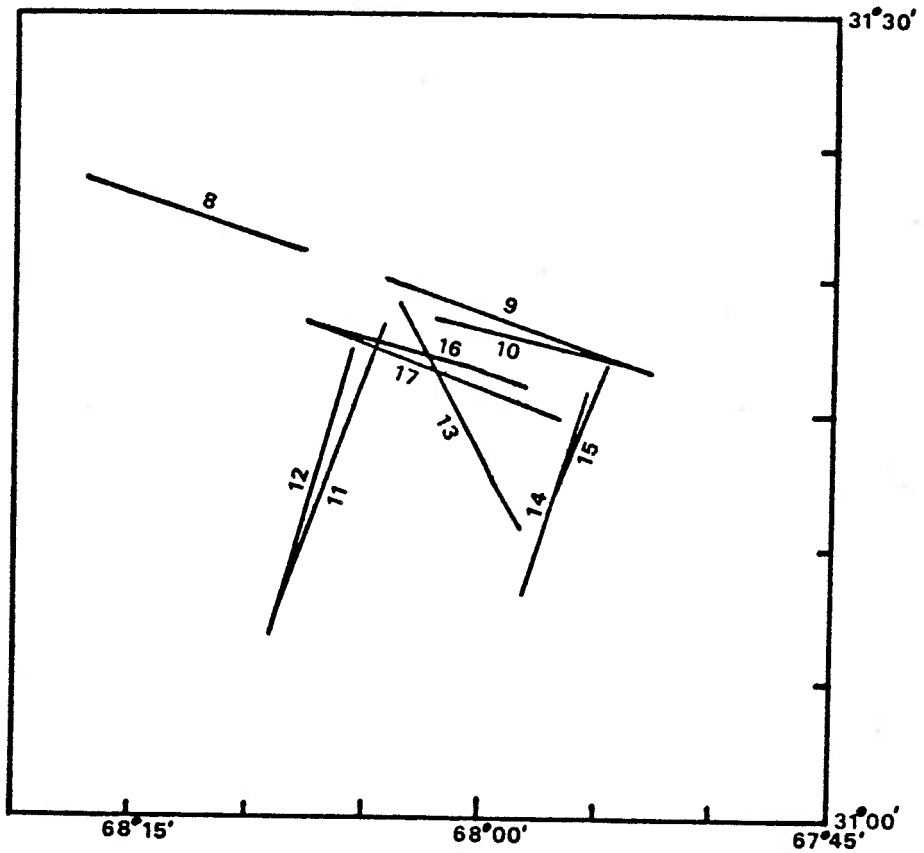
31°30'
8
9
16
10
17
13
12
11
14
15
31°00'
68°15'
68°00'
67°45'

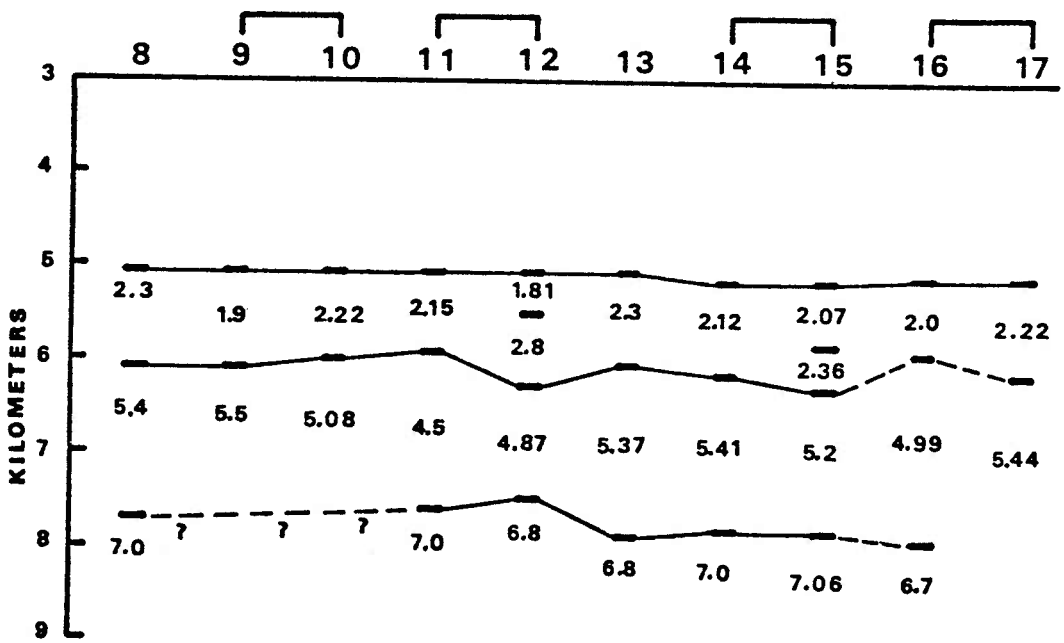
8
9
10
11
12
13
14
15
16
17
KILOMETERS
3
4
5
6
7
8
9
2.3
1.9
2.22
2.15
1.81
2.3
2.12
2.07
2.0
2.22
2.8
2.36
5.4
5.5
5.08
4.5
4.87
5.37
5.41
5.2
4.99
5.44
7.0
?
?
?
7.0
6.8
6.8
7.0
7.06
6.7

5.2

Figure 5.3. Basement topography interpreted from the deep towed hydrophone line shot along a flowline in the study area of this experiment (Purdy and Gove, 1982) using sediment velocities of 2.0 and 3.0 km/s. Below is a bathymetry profile of oceanic basement near the Mid-Atlantic Ridge measured by Scripps deep tow instrument (Shih, 1979).

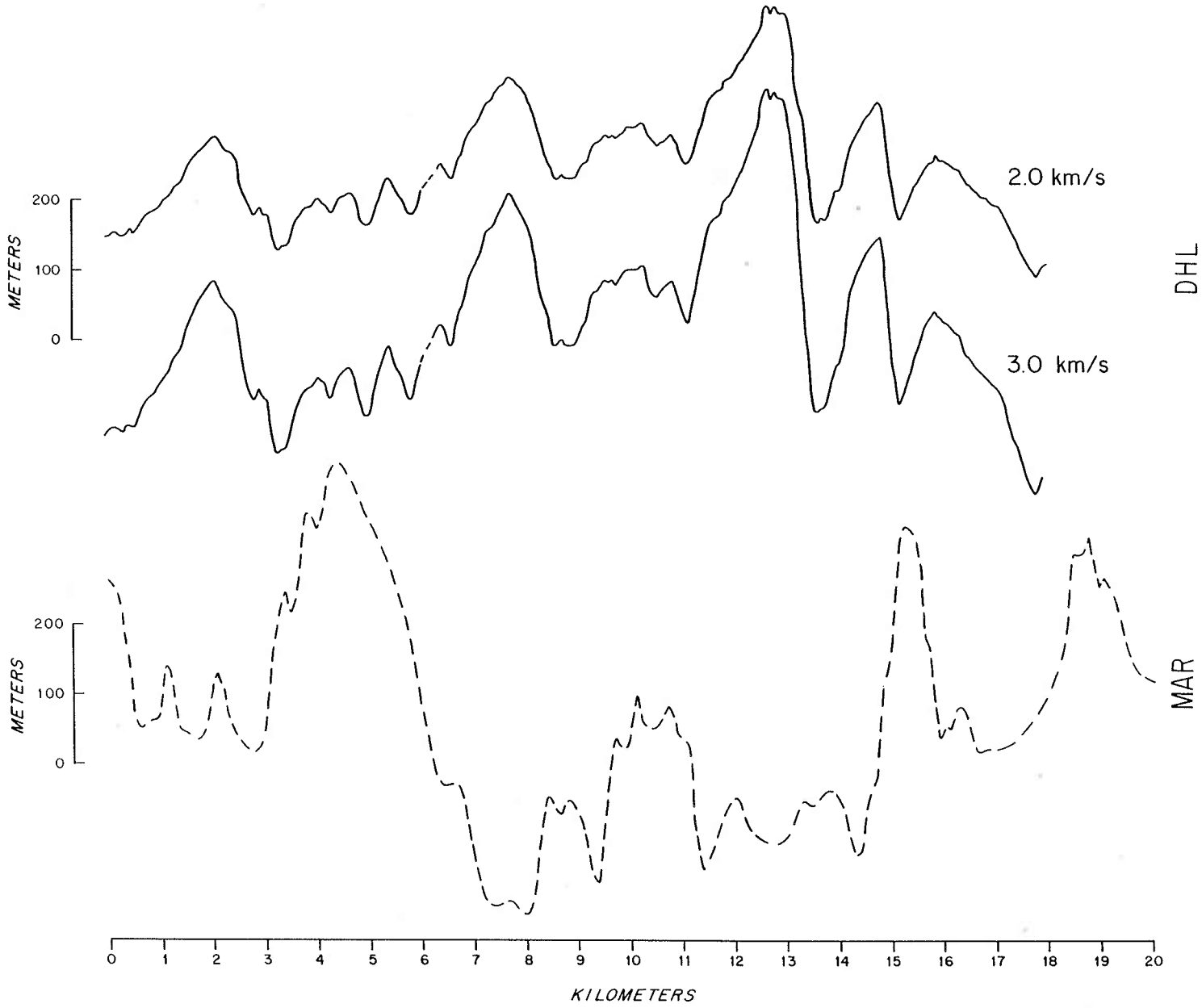
2.0 km/s
3.0 km/s
DHL
MAR
METERS
200
100
0
KILOMETERS
0 1 2 3 4 5 6 7 8 9 10 11 12 13 14 15 16 17 18 19 20

Figure 5.4. Transmission energy for a) compressional energy and b) shear energy for compressional energy incident at a sediment-basement interface at which the basement compressional velocity is 5.0 km/s and the Poisson's ratio is 0.3. Two cases are studied in the first unconsolidated sediments have a compressional velocity of 2.0km/s and Poisson's ratio of 0.48 overlying basement and in the second consolidated sediments have a compressional velocity of 3.1km/s and Poisson's ratio of 0.4. The consolidated sediments allow more compressional energy through the interface, whereas the unconsolidated sediments convert more incident compressional energy to transformed shear.

Compressional Transmission

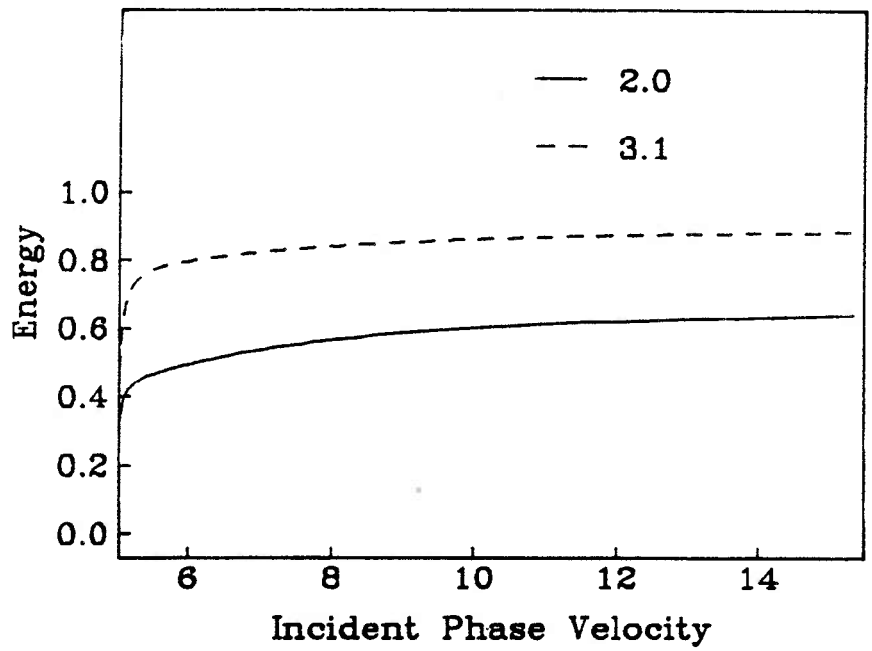

Shear Transmission

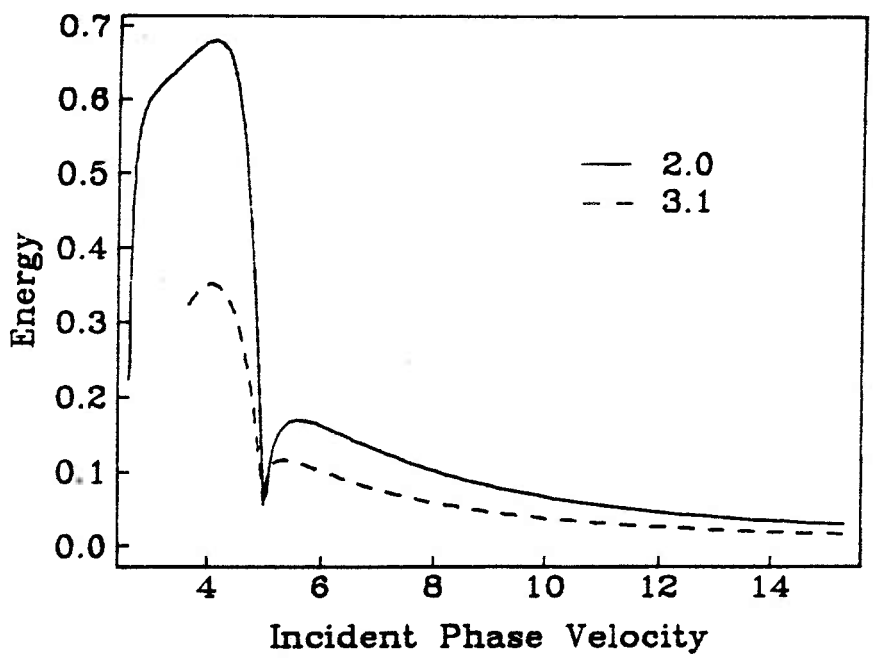

5.4b

REFERENCES

Casey, J.F., J.F. Dewey, P.J. Fox, J.A. Karson, and E. Rosencrantz, Heterogeneuous nature of oceanic crust and upper mantle: a perspective from the bay of islands ophiolite complex, in The Sea, v. 7, John Wiley and Sons, N.Y., 1982.

Donnelly,T., Francheteau, J., Bryan, W.B., Robinson, P., Flower, M., Salisbury, M. et al., 1979, Initial Reports of the Deep Sea Drilling Project, v.51,52,53: Washington (U.S. Government Printing Office).

Elthon, D., Metamorphism in oceanic spreading centers, in Emiliani, C. (ed.), The Sea, v. 7, New York, 1982, p. 285-304.

Ewing, J.I. and G.M. Purdy, Upper crustal velocity structure in the ROSE area of the East Pacific Rise, J. Geophys. Res., 87, 8397-8402, 1982.

Grow, J.A. and R. Markel, IPOD-USGS multichannel seismic reflection profile from Cape Hatteras to Mid-Atlantic Ridge, Geology, 5, 625-630, 1977.

Helmberger, D.V. and G.B. Morris, A travel time and amplitude interpretatio of a marine refraction profil: primary waves, J. Geophys. Res. 74, 483-494.

Helmberger, D.V., Fine structure of an Aleutian crustal section, Geophys. J. R. astr. Soc., 47, 257-284.

Herron, T.J., W.J. Ludwig, P.L. Stoffa, T.K. Kan, and P. Buhl, The structure of the East Pacific Rise Crest, J. Geophys. Res., 83, 798-817, 1980.

Honnorez, J., The aging of the oceanic crust at low temperature, in Emiliani, C. (ed.), The Sea, v. 7, John Wiley and Sons, New York, 1982, p.525-588.

Houtz, R.E., Comparison of velocity characteristics in western North Atlantic and Norwegian Sea sediments, J. Acoust. Soc. Amer., 68, 1409-1414, 1980.

Houtz, R.E., J. Ewing, and X. LePichon, Velocity of Deep Sea Sediments from Sonobuoy Data, J. Geophys. Res., 73, 2615-2641, 1968.

Humphris, S., R.N. Thompson, and G.F. Marriner, The mineralogy and geochemistry of basalt weathering, Holes 417A and 418A, in Donnelly,T., Francheteau, J., Bryan, W.B., Robinson, P., Flower, M., Salisbury, M. et al., Initial Reports of the Deep Sea Drilling Project, v.51,52,53: Washington (U.S. Government Printing Office), 1201-1218, 1979.

Kennett, B.L.N., Towards a more detailed seismic picture of the oceanic crust and mantle, Mar. Geophys. Res., 3, 7-42, 1977.

Larson, R.L., R. Moberly, et al., 1975, Initial Reports of the Deep Sea Drilling Project, v.32: Washington (U.S. Govt. Printing Office).

Orcutt, J.A., B.L.N. Kennett, and L.M. Dorman, Structure of the East Pacific Rise from an ocean-bottom seismometer survey, Geophys. J. R. astr. Soc., 45, 305-320, 1976.

Purdy, G.M., The correction for the travel time effects of seafloor topography in the interperetation of marine seismic data, J. Geophys. Res., 87, 8389-8396, 1982a.

Purdy, G.M., The variability in seismic structure of Layer 2 near the East Pacific Rise at 12° N, J. Geophys. Res., 86, 1982b.

Purdy, G.M., The seismic structure of 140 my old crust in the western central North Atlantic Ocean, subm. to Geophys. J. Roy. Astr. Soc., 1982c.

Purdy, G. M. and L.A. Gove, Reflection profiling in the deep ocean using a near bottom hydrophone, Mar. Geophys. Res., 5, 301-314, 1982.

Purdy, G.M., J.I. Ewing amd G.B. Bryan, A deep towed hydrophone seismic reflection survey around IPOD Sites 417 and 418, Mar. Geol., 35, 1-19.

Raitt, R.W., The crustal rocks, in M.N. Hill (ed.), The Sea, v.3, Interscience, N.Y., 1963.

Shih, J.S., The nature and origin of fine-scale sea-floor relief, Ph.D. thesis, W.H.O.I.-M.I.T. Joint Program.

Smythe, D.K., A. Dobinson, R. McQuillin, J.A. Brewer, D.H. Matthews, D.J. Blundell, and B. Kelk, Deep structure of the Scottish Caledonides revealed by the MOIST reflection profile, Nature, 299, 338-340, 1982.

Spudich, P.K.P. and D.V. Helmberger, Synthetic Seismograms from Model Ocean Bottoms, J. Geophys. Res., 84, 189-204, 1979.

Spudich P. and J. Orcutt, Petrology and porosity of an oceanic crustal site: results from wave form modelling of seismic refraction data, J. Geophys. Res., 85, 1409-1433, 1980a.

Stoffa, P.L., P. Buhl, J.B. Diebold, and F. Wenzel, Direct

mapping of seismic data to the domain of intercept time and ray parameter - a plane wave decomposition, Geophys., 46, 255-267, 1980.

Taner, M.T. and F. Koehler, Velocity Spectra - digital computer derivation and application of velocity functions, Geophys., 34, 859-881, 1969.

Tucholke, B.E., Geologic Significance of seismic reflectors in the deep western North Atlantic Ocean basin, SEPM Special Publication No. 32, 23-37, 1981.

Tucholke, B.E., Vogt, P.R., et al., Site 387, in Tucholke, B.E., Vogt, P.R., et al., 1979, Initial Reports of the Deep Sea Drilling Project, v.43: Washington (U.S. Govt. Printing Office), 323-391.

Tucholke, B.E., R.E. Houtz and Ludwig, Maps of sediment thickness and depth to basement in the western North Atlantic Ocean Basin, Am. Assoc. Petr. Geol., Tulsa, OK, 1982.

APPENDIX

PROGRAMS FOR HYPERBOLIC STACKING

The computer programs listed below are written in FORTRAN and were used on a VAX 11/780. They are available on tape with user's instructions from the author.

VANAL3 maps ROSE format data into stacking velocity, two-way normal incidence travel-time space. It computes the stack and the semblance of the data for specified stacking velocity values and two-way normal incidence travel-times. The stack is normalised and the semblance is bandpassed filtered and has a threshold value set; the stack and semblance are multiplied together and plotted.

TPCONT contours the output of VANAL3 using an NCAR package. The output of VANAL3 is averaged over a specified number of samples in the two-way normal incidence travel-time dimension.

SUMTPCONT sums and contours several outputs of VANAL3.

DIXER solves for layer interval thicknesses and velocities from values of stacking velocity and two-way normal incidence travel-times using the Dix approximation.

WIDANG solves for layer interval thicknesses and velocities from values of horizontal range and travel-time using the Dix approximation.

PCON solves for layer interval thicknesses and velocities from values of stacking velocity and two-way normal incidence travel-times using the reduced time reduced distance method of Dix (1955).

PCONPOLY solves for layer interval thicknesses and velocities from values of horizontal range and travel-time using the reduced

time reduced distance method of Dix (1955).

PENTEX models horizontal range and travel-time data given a starting model. Models are iteratively calculated until the horizontal range and travel-time values of the model fit the observed values.

BOUNCE traces rays through a stack of isovelocity layers. It calculates the horizontal range of the reflection point at the base of the layers and a point on the surface of one of the layers.

HYPCURV calculates the slope and curvature of an hyperbola over a specified horizontal range and at specified intervals.

DOCUMENT SUMMARY

Document Id: 8169A
Document Name: Hyper Chapt.2
Operator: Rohr
Author: Rohr

Comments: SciGoth/Cont 12/28

STATISTICS

OPERATION	DATE	TIME	WORKTIME	KEYSTROKES
Created	11/18/81	16:54	:52	3679
Last Revised	01/11/83	10:09	:11	152
Last Printed	01/29/83	11:06		
Last Archived	12/21/82	16:34	onto Diskette 1095A	

Total Pages: 60 Total Worktime: 45:31
Total Lines: 884 Total Keystrokes: 126260

Pages to be printed: 60